

การปรับปรุง โทเทเนียที่มีขนาดผลึกต่างกันและการประยุกต์ใช้เป็นตัวรองรับสำหรับ
ตัวเร่งปฏิกิริยาโคบอลต์



นางสาวกิติมา ปิ่นแก้ว

ศูนย์วิทยทรัพยากร
วิทยานิพนธ์นี้เป็นส่วนหนึ่งของการศึกษาตามหลักสูตรปริญญาวิศวกรรมศาสตรมหาบัณฑิต
สาขาวิชาวิศวกรรมเคมี ภาควิชาวิศวกรรมเคมี
คณะวิศวกรรมศาสตร์ จุฬาลงกรณ์มหาวิทยาลัย
ปีการศึกษา 2551
ลิขสิทธิ์ของจุฬาลงกรณ์มหาวิทยาลัย

MODIFICATION OF TITANIA HAVING DIFFERENT CRYSTALLITE SIZES
AND THEIR APPLICATIONS AS SUPPORTS FOR COBALT CATALYSTS



Miss Kitima Pinkaew

A Thesis Submitted in Partial Fulfillment of the Requirements
for the Degree of Master of Engineering Program in Chemical Engineering

Department of Chemical Engineering

Faculty of Engineering

Chulalongkorn University

Academic Year 2008

Copyright of Chulalongkorn University

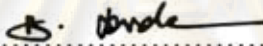
Thesis Title MODIFICATION OF TITANIA HAVING DIFFERENT
CRYSTALLITE SIZES AND THEIR APPLICATIONS AS
SUPPORTS FOR COBALT CATALYSTS

By Miss. Kitima Pinkaew

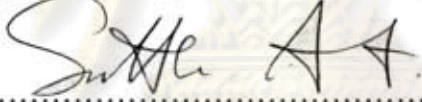
Field of study Chemical Engineering

Advisor Assistant Professor Bunjerd Jongsomjit, Ph.D.


Accepted by the Faculty of Engineering, Chulalongkorn University in Partial
Fulfillment of the Requirements for the Master's Degree


..... Dean of the Faculty of Engineering
(Associate Professor Boonsom Lerthirunwong, Dr.Ing)

THESIS COMMITTEE


..... Chairman
(Professor Suttichai Assabumrungrat, Ph.D.)


..... Advisor
(Assistant Professor Bunjerd Jongsomjit, Ph.D.)


..... Examiner
(Assistant Professor Joongjai Panpranot, Ph.D.)


..... External Examiner
(Assistant Professor Okorn Mekasuwandumrong, D.Eng.)

กิตติมา ปิ่นแก้ว: การปรับปรุงไทเทเนียมที่มีขนาดผลึกต่างกันและการประยุกต์ใช้เป็นตัวรองรับสำหรับตัวเร่งปฏิกิริยาโคบอลต์ (MODIFICATION OF TITANIA HAVING DIFFERENT CRYSTALLITE SIZES AND THEIR APPLICATIONS AS SUPPORTS FOR COBALT CATALYSTS) อ.ที่ปรึกษาวิทยานิพนธ์หลัก: ผศ. ดร. บรรเจิด จงสมจิตร, 100 หน้า

งานวิจัยนี้ศึกษาคุณลักษณะและสมบัติของตัวเร่งปฏิกิริยาโคบอลต์บนไทเทเนียมไดออกไซด์ขนาดนาโนที่ปรับปรุงด้วยรูเทเนียมและเซอร์โคเนีย และขนาดไทเทเนียมไดออกไซด์ต่างๆ กัน ในช่วง 11-16 นาโนเมตร โดยเตรียมไทเทเนียมไดออกไซด์ที่ได้รับการปรับปรุงโดยวิธีการเคลือบฝัง หลังจากนั้นจึงนำไปเคลือบฝังอีกครั้งด้วยโคบอลต์ จากการศึกษาวิเคราะห์ด้วยเครื่องการกระเจิงรังสีเอ็กซ์ การดูดซับทางกายภาพด้วยไนโตรเจน กระเจิงรังสีเอ็กซ์ การส่องด้วยกล้องจุลทรรศน์อิเล็กตรอน การวัดการกระจายตัวของโลหะ กล้องจุลทรรศน์อิเล็กตรอนแบบส่องผ่าน การรีดักชันแบบโปรแกรมอุณหภูมิ การดูดซับด้วยแก๊สคาร์บอนมอนอกไซด์ และเอ็กซ์เรย์โฟโตอิเล็กตรอนสเปกโทรสโกปี พบว่าขนาดของโคบอลต์ออกไซด์ใหญ่ขึ้นเมื่อขนาดของไทเทเนียมไดออกไซด์เพิ่มขึ้นจาก 11 เป็น 16 นาโนเมตร ผลจากการทำรีดักชันแบบโปรแกรมอุณหภูมิพบว่า การปรับปรุงไทเทเนียมไดออกไซด์ด้วยรูเทเนียมหรือเซอร์โคเนียมีผลต่อการรีดักชันของตัวเร่งปฏิกิริยาโคบอลต์ การปรับปรุงด้วยรูเทเนียมส่งผลให้อุณหภูมิในการรีดิวซ์ลดลงเนื่องมาจากการเกิดไฮโดรเจนสปีวโอเวอร์ขึ้น ในขณะที่การปรับปรุงด้วยเซอร์โคเนียส่งผลให้อุณหภูมิในการรีดิวซ์สูงขึ้นซึ่งอาจเกิดการฟอร์มตัวกันระหว่างโคบอลต์ออกไซด์และตัวรองรับ และยังพบว่าตัวไทเทเนียมไดออกไซด์ที่มีขนาดเล็กจะเกิดการกระจายตัวของโคบอลต์ที่ต่ำกว่าบนขนาดใหญ่ และผลจากการทำเอ็กซ์เรย์โฟโตอิเล็กตรอนสเปกโทรสโกปี ไม่พบการเปลี่ยนแปลงของค่าพลังงานการเกิดพันธะ อย่างไรก็ตามเมื่อนำไปทดสอบในปฏิกิริยาไฮโดรจิเนชันของคาร์บอนมอนอกไซด์ภายใต้สภาวะของการทำให้เกิดเป็นมีเทน พบว่าที่ตัวเร่งปฏิกิริยาโคบอลต์บนไทเทเนียมไดออกไซด์ขนาดเล็ก (11 นาโนเมตร) ให้ค่าความว่องไวสูงกว่าทั้งตัวที่ได้รับการปรับปรุงและไม่ได้รับการปรับปรุง โดยมีความแตกต่างของค่าการเลือกเกิดเป็นไฮโดรคาร์บอนที่ยาวขึ้น (C_2-C_4) ต่ำกว่าในเร่งปฏิกิริยาโคบอลต์บนไทเทเนียมไดออกไซด์ที่ได้รับการปรับปรุง ทั้งนี้แสดงว่า ตัวเร่งปฏิกิริยาโคบอลต์บนไทเทเนียมไดออกไซด์ที่ได้รับการปรับปรุงด้วยรูเทเนียมและเซอร์โคเนียทำให้สมบัติในการเร่งปฏิกิริยาของตัวเร่งปฏิกิริยาโคบอลต์เปลี่ยนแปลงไปโดยมีค่าสูงขึ้น โดยจะส่งผลกระทบต่อผลึกไทเทเนียมไดออกไซด์ขนาดใหญ่

จุฬาลงกรณ์มหาวิทยาลัย

ภาควิชา.....วิศวกรรมเคมี..... ลายมือชื่อนิสิต *ปิยน ปิ่นแก้ว*
 สาขาวิชา.....วิศวกรรมเคมี..... ลายมือชื่อ อ.ที่ปรึกษาวิทยานิพนธ์หลัก..... *ปิ่นแก้ว*
 ปีการศึกษา2551.....

5070221221: MAJOR CHEMICAL ENGINEERING

KEYWORDS: TITANIA SUPPORTED COBALT CATALYSTS / RUTHENIUM
MODIFICATION / ZIRCONIUM MODIFICATION / DIFFERENT CRYSTALLITE
SIZE TITANIA / CARBON MONOXIDE HYDROGENATION

KITIMA PINKAEW: MODIFICATION OF TITANIA HAVING DIFFERENT
CRYSTALLITE SIZES AND THEIR APPLICATIONS AS SUPPORTS FOR
COBALT CATALYSTS. ADVISOR: ASST. PROF. BUNJERD
JONGSOMJIT, Ph.D., 100 pp.

Ru-modified and Zr-modified titania supported cobalt catalysts with different crystallite sizes of TiO_2 (11-16 nm) were investigated in this study. The catalysts were prepared by impregnation of cobalt precursor onto the modified and unmodified titania. The catalysts were characterized by several techniques such as XRD, BET, SEM & EDX, TEM, TPR, CO chemisorption, and XPS. It was found that the size of cobalt oxides on the support was corresponding to the size of the support used. The TPR results showed that Ru and Zr caused changes in reduction behavior of the cobalt catalysts. The Ru modification on titania support resulted in lower reduction temperature due to the effect of H_2 spillover whereas in case of Zr modification, the reduction temperature was shifted to higher. It indicated that there were formation between cobalt oxides and the support, which was modified with Zr. The TiO_2 _11 nm support exhibited more dispersion of Co oxides than the TiO_2 _16 nm. It revealed on significant changes in binding energy for Ru-modified/ Zr-modified and unmodified catalysts from XPS results. Based on CO hydrogenation, it was found that the smaller crystallite size of TiO_2 (11 nm) exhibited the better catalytic activity than the larger crystallite size (16 nm) for both modified and unmodified supports. However, the modified supported catalysts resulted in lower C_2 - C_4 hydrocarbon product under methanation condition. Ru and Zr modification of the TiO_2 had a significant impact on the properties of Co/ TiO_2 catalysts, especially on the larger TiO_2 crystallite size.

DepartmentChemical.Engineering.. Student's signature Kitima Pinkaew.....

Field of Study ..Chemical.Engineering. Advisor's signature Bunjerd Jongsomjit.....

Academic year2008.....

ACKNOWLEDGEMENTS

The author would like to express his greatest gratitude to her advisor, Associate Professor Bunjerd Jongsomjit for his invaluable suggestion and guidance throughout this study. In addition, I would also grateful to thank to Professor Suttichai Assabumrungrat who has been the chairman of the committee for this thesis, Associate Professor Joongjai Panpranot and Assistant Professor Okorn Mekasuwandamrong, members of the thesis committee for their kind cooperation.

Most of all, the author would like to express her highest gratitude to her parents, Mr.sumruay and Mrs.Urai Pinkaew, and her family who always pay attention to her all the times for suggestion and encouragement. The most success of graduation is devoted to my parents.

Moreover, the author wishes to thank all my friends and members of the Center of Excellent on Catalysis & Catalytic Reaction Engineering (Petrochemical Engineering Research Laboratory), Department of Chemical Engineering, Chulalongkorn University for their assistance and friendly encouragement.

Finally, the author would like to thank the Thailand Research Fund (TRF), as well as the Graduate School of Chulalongkorn University for their financial supports.

ศูนย์วิทยุทรัพยากร
จุฬาลงกรณ์มหาวิทยาลัย

CONTENTS

	Page
ABSTRACT (THAI)	iv
ABSTRACT (ENGLISH)	v
ACKNOWLEDGMENTS	vi
CONTENTS	vii
LIST OF TABLES	x
LIST OF FIGURES	xi
CHAPTER	
I INTRODUCTION	1
II LITERATURE REVIEWS	4
2.1 Titania supported Co Catalysts.....	4
2.2 Nanocrystalline anatase titania.....	5
2.3 Addition of noble metal on Co catalysts	6
III THEORY	9
3.1 Fischer-Tropsch synthesis (FTS).....	9
3.1.1 The surface carbide mechanism.....	13
3.1.2 The hydroxycarbene mechanism.....	15
3.1.3 The CO insertion mechanism.....	16
3.2 Titanium (IV) Oxide.....	18
3.3 Cobalt	21
3.3.1 General.....	20
3.3.2 Physical Properties.....	21
3.3.3 Cobalt Oxides.....	24
3.4 Co-based Catalysts.....	25
3.5 Sol-gel method.....	26
IV EXPERIMENTAL	30
4.1 Catalyst Preparation	30
4.1.1 Chemicals	30
4.1.2 Preparation of the titania supports by sol- gel method.....	31

CHAPTER	Page
4.1.3 Preparation of the modified-titania support.....	31
4.1.4 Preparation of the supported cobalt catalysts.....	31
4.1.5 Catalyst Nomenclature.....	32
4.2 Catalyst characterization.....	32
4.2.1 BET surface area.....	32
4.2.2 X-ray diffraction (XRD).....	33
4.2.3 Scanning electron microscopy and energy dispersive X-ray spectroscopy (SEM/EDX).....	33
4.2.4 Transmission electron microscopy (TEM).....	33
4.2.5 Temperature-programmed reduction (TPR).....	33
4.2.6 CO-Pulse Chemisorption.....	34
4.2.7 X-ray photoelectron spectroscopy.....	34
4.3 Reaction study in CO hydrogenation.....	35
4.3.1 Materials.....	35
4.3.2 Apparatus.....	35
4.3.2.1 Reactor.....	35
4.3.2.2 Automation Temperature Controller.....	35
4.3.2.3 Electrical Furnace.....	35
4.3.2.4 Gas Controlling System.....	36
4.3.2.5 Gas Chromatography.....	36
4.3.3 Procedures.....	37
V RESULTS AND DISCUSSIONS	40
5.1 The Study of Ruthenium modified different TiO ₂ crystallite size	40
5.1.1 Characterization of the Catalysts	40
5.1.1.1 XRD	40
5.1.1.2 BET surface areas	44
5.1.1.3 SEM & EDX	46
5.1.1.4 TEM	49
5.1.1.5 TPR	51
5.1.1.6 CO-Pulse Chemisorption.....	53

CHAPTER	Page
5.1.1.7 XPS.....	54
5.1.2 Reaction study.....	58
5.2 The Study of Zirconium modified different TiO ₂ crystallite size	61
5.2.1 Characterization of the Catalysts	61
5.2.1.1 XRD	61
5.2.1.2 BET surface areas	62
5.2.1.3 SEM & EDX.....	63
5.2.1.4 TEM.....	66
5.2.1.5 TPR	68
5.2.1.6 CO-Pulse Chemisorption.....	70
5.2.1.7 XPS.....	71
5.2.2 Reaction Study	75
5.3 Comparison between Ru and Zr-modified TiO ₂ support in catalytic activity.....	77
VI CONCLUSIONS AND RECOMMENDATIONS	80
6.1 Conclusions	80
6.2 Recommendations	81
REFERENCES	82
APPENDICES	87
APPENDIX A: CALCULATION FOR CATALYST PREPARATION ..	88
APPENDIX B: CALCULATION FOR TOTAL CO CHEMISSORPTION AND DISPERSION	91
APPENDIX C: CALIBRATION CURVES.....	92
APPENDIX D: CALCULATION OF CO CONVERSION, REACTION RATE AND SELECTIVITY	97
APPENDIX E: CALCULATION OF TURNOVER OF FREQUENCY ..	98
APPENDIX F: LIST OF PUBICATIONS.....	99
VITA.....	100

LIST OF TABLES

Table		Page
3.1	Crystallographic properties of anatase, brookite, and rutile.	19
3.2	Physical properties of cobalt.....	23
4.1	Chemicals used in the preparation of catalysts.....	30
4.2	Operating condition for gas chromatograph.....	36
5.1	Water: alkoxide ratio, average crystallite size, and BET surface areas of titania supports.....	45
5.2	BET surface areas and crystallite size of Co_3O_4 of the catalysts.....	46
5.3	CO chemisorption results of cobalt catalysts.....	53
5.4	Binding energy and surface composition of Ru modified and unmodified Co catalysts.....	54
5.5	Activity and product selectivity of Ru modified and unmodified Co catalyst.....	59
5.6	BET surface areas and crystallite size of Co_3O_4 of the catalysts.....	63
5.7	CO chemisorption results of the cobalt catalysts.....	71
5.8	Binding energy and surface composition of Zr modified and unmodified Co catalysts.....	72
5.9	Activity and product selectivity of Zr modified and unmodified Co catalyst.....	77
5.10	Catalytic activity and product selectivity of modified and unmodified- TiO_2 cobalt catalysts.....	79
C.1	Conditions use in Shimadzu modal GC-8A and GC-14B.....	92

LIST OF FIGURES

Figure		Page
2.1	Crystal structures of anatase (a), rutile (b), and brookite.....	20
4.1	Flow diagram of CO hydrogenation system	39
5.1	XRD patterns of different crystallite size of TiO ₂ obtained from various water: alkoxide ratio	41
5.2	XRD patterns of Ru modified titania support	42
5.3	XRD patterns of Ru modified titania supported Co catalysts.....	43
5.4	XRD patterns of unmodified TiO ₂ supported Co catalysts	44
5.5	SEM micrographs for Ru modified and unmodified TiO ₂ supported Co catalysts with different crystallite size	47
5.6	EDX mapping for Co/TiO ₂ _16 nm catalyst granule.....	48
5.7	TEM micrographs of Ru modified and unmodified supported cobalt catalysts	50
5.8	TPR profiles of Ru modified and unmodified Co catalysts with different TiO ₂ crystallite size	52
5.9	The deconvolution of XPS spectra of Ru modified and unmodified supported cobalt catalyst (a) Co/TiO ₂ _11 nm_Ru (b) Co/TiO ₂ _11 nm	55
5.10	The deconvolution of XPS spectra of Ru modified and unmodified supported cobalt catalyst (a) Co/TiO ₂ _13 nm_Ru (b) Co/TiO ₂ _13 nm	56
5.11	The deconvolution of XPS spectra of Ru modified and unmodified supported cobalt catalyst (a) Co/TiO ₂ _16 nm_Ru (b) Co/TiO ₂ _16 nm	57
5.12	Reaction rate vs. time on stream of Ru modified and unmodified Co catalysts with different crystallite size of TiO ₂	60

Figure	Page
5.13 XRD patterns of Zr modified titania support.....	61
5.14 XRD patterns of Zr modified titania supported Co catalysts	62
5.15 SEM micrographs for Zr modified and unmodified TiO ₂ supported Co catalysts with different crystallite size	64
5.16 EDX mapping for Co/TiO ₂ _16 nm_Zr catalyst granule	65
5.17 TEM micrographs of Zr modified and unmodified supported cobalt catalysts	67
5.18 TPR profiles of Zr modified and unmodified Co catalysts with different TiO ₂ crystallite size	69
5.19 The deconvolution of XPS spectra of Zr modified and unmodified supported cobalt catalyst (a) Co/TiO ₂ _11 nm_Zr (b) Co/TiO ₂ _11 nm	73
5.20 The deconvolution of XPS spectra of Zr modified and unmodified supported cobalt catalyst (a) Co/TiO ₂ _13 nm_Zr (b) Co/TiO ₂ _13 nm	74
5.21 The deconvolution of XPS spectra of Zr modified and unmodified supported cobalt catalyst (a) Co/TiO ₂ _16 nm_Zr (b) Co/TiO ₂ _16 nm	75
5.22 Reaction rate vs. time on stream of Zr modified and unmodified Co catalysts with different crystallite size of TiO ₂	78
C.1 The calibration curve of methane	93
C.2 The calibration curve of ethylene	93
C.3 The calibration curve of propane	94
C.4 The calibration curve of propene	94
C.5 The calibration curve of butane	95
C.6 The calibration curve of butene	95
C.7 The chromatograms of catalyst sample from thermal conductivity detector, gas chromatography Shimadzu model 8A (Molecular sieve 5A column)	96

Figure**Page**

- C.8 The chromatograms of catalyst sample from flame ionization detector, gas chromatography Shimadzu model 14B (VZ10 column)..... 96



ศูนย์วิทยทรัพยากร
จุฬาลงกรณ์มหาวิทยาลัย

CHAPTER I

INTRODUCTION

The Fischer-Tropsch (FT) synthesis was successfully carried out for future alternative resource instead of coal or crude oil. There are many active metals that can be used for hydrogenation of carbon monoxide (CO) to hydrocarbon such as ruthenium (Ru), iron (Fe), cobalt (Co), palladium (Pd), and etc. For example, cobalt and iron are the metals which used in the industry for hydrocarbon synthesis. Even though the cobalt catalysts are more expensive, but they are more resistant to deactivation than iron metals [1]. Supported cobalt catalysts have been extensively investigated with many inorganic supports for years, such as SiO₂ [2], Al₂O₃ [3], TiO₂ [4]. Supported cobalt catalysts, which are the most popular FT catalysts, have been used as catalyst for FT synthesis for many years as results of their high catalytic activity and selectivity, low water-gas shift (WGS) activity, and comparatively low price [5, 6]. CO and H₂ (syngas) have been converted to paraffinic or long chain hydrocarbon through hydrogenation reaction. In fact, the interaction between cobalt oxide species and supports has an important role on dispersion of cobalt oxide species [7]. Addition of small amount of noble metals resulted in better performance of supported cobalt catalysts [7-9]. Noble metal with being easily reducible used as promoters, such as Pt, Pd, Re, and Ru have been investigated for the supported cobalt catalysts in order to shift the reduction temperatures of cobalt oxide species interacting with the support to lower temperatures [8-9]. The presence of Ru in supported cobalt catalysts also enhanced the turnover rate and Co site density during reaction, which was described by Iglesia et al. [10].

As known, the catalytic performance is usually enhanced by addition a promoter such as noble metal. Promotion with oxides has been one of the methods to improve the activity and hydrocarbon selectivity of FT catalysts. Among the oxide promoters, ZrO₂, La₂O₃, MnO, and CeO₂ have been most often employed. Addition of

oxide promoters could modify the catalyst texture and porosity, increase cobalt dispersion, reducibility, and fraction of different cobalt metal crystalline phases, enhance mechanical and attrition resistance of cobalt FT catalysts, and improve the chemical stability of the support [1]. They also found that promotion with zirconia results in higher activity in FT reaction rates [1, 8]. Besides the catalytic phase and promoter, a support could play an important role on the catalytic performance.

TiO₂ is a great material because it can use in many applications such as photocatalysis, support, pigment, UV absorber, O₂ sensor and coating films. In this study, titania was used as a support of Co catalyst for CO hydrogenation. Titania-supported Co catalysts have been reported to be more active for CO hydrogenation than cobalt catalysts supported on other supports i.e. Al₂O₃, SiO₂, etc [11].

On account of a significant development in nanotechnology in the recent years, many inorganic nanomaterials have brought much attention to the research in this field. These inorganic nanomaterials can be potentially used as outstanding catalytic supports due to their unique properties, great thermal and mechanical stability.

In the present work, the properties of cobalt as a catalytic phase for CO hydrogenation reaction dispersed on Ru-modified and Zr-modified nano-TiO₂ were investigated. The samples were prepared and characterized by several techniques, such as BET, XRD, SEM/EDX, TEM, TPR, CO chemisorption, and XPS. The reaction study of CO hydrogenation was carried out in order to measure activity and product selectivity under methanation condition.

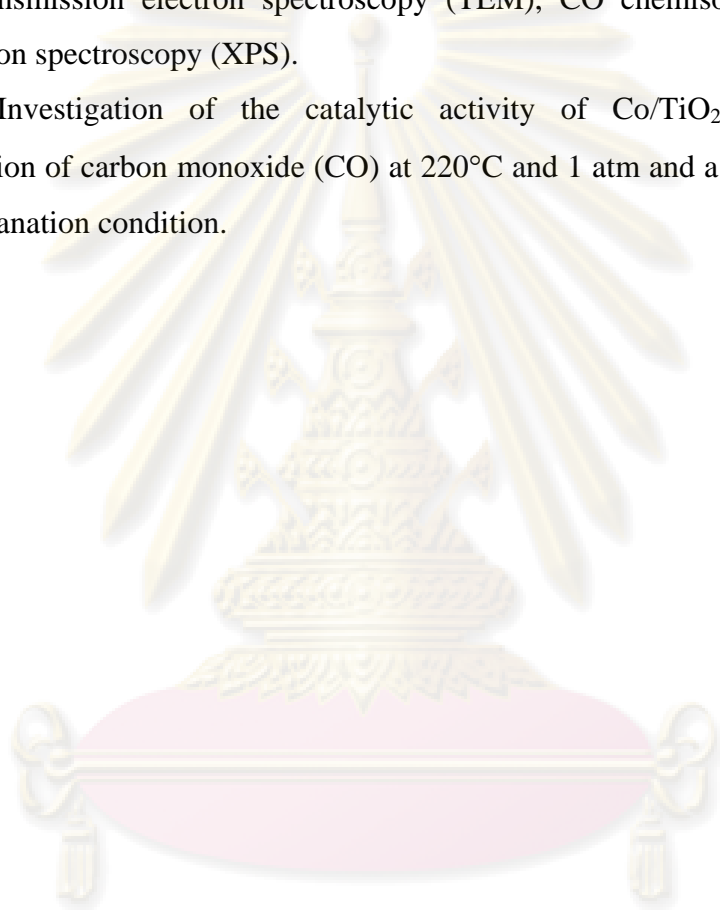
The study was scoped as follows:

1. Preparation of the TiO₂ supports via sol-gel method (water: alkoxide molar ratio in the range of 4-165).
2. Characterization of the crystallite size of TiO₂ supports by using X-ray diffraction (XRD), BET surface area.
3. Preparation of modified-TiO₂ supports with 0.02 wt% Ru or 0.3 wt% Zr using the incipient wetness impregnation method.

4. Preparation of supported Co catalyst on the modified-TiO₂ supports (20 wt% Co) using the incipient wetness impregnation method.

5. Characterization of the catalyst samples using BET surface area, X-ray diffraction (XRD), temperature programmed reduction (TPR), CO chemisorption, scanning electron microscopy (SEM) and energy dispersive X-ray spectroscopy (EDX), transmission electron spectroscopy (TEM), CO chemisorption and X-ray photoelectron spectroscopy (XPS).

6. Investigation of the catalytic activity of Co/TiO₂ catalyst in the hydrogenation of carbon monoxide (CO) at 220°C and 1 atm and a H₂/CO ratio of 10 under methanation condition.



ศูนย์วิจัยทรัพยากร
จุฬาลงกรณ์มหาวิทยาลัย

CHAPTER II

LITERATURE REVIEWS

This chapter reviews the work about titania supported Co catalyst that is also of great interest in the field of heterogeneous catalysis while it has been used for catalytic application. The last section of this review shows a few research investigations about the addition of noble metal on supported cobalt catalyst.

2.1. Titania supported Co Catalysts

The strong metal support interaction (SMSI) between the titania support and Co metal is used to determine the cobalt dispersion and reduction behavior of Co/TiO₂ catalyst. The synthesis of highly dispersed cobalt on TiO₂ support requires the strong interaction between cobalt and support. However, too strong interaction can produce the Co-support compound as a suboxide at an interface that is high resistant to reduction. Active sites in Cobalt catalyst were found in many directions such as unsupported metallic cobalt and cobalt monocrystals were active, for large cobalt metal particles the reaction rate is proportional to the number of cobalt surface sites [7]. In addition, the active cobalt metallic phases, a working FT catalyst, could contain several other cobalt species: cobalt carbide, cobalt oxides, cobalt support mixed compounds, etc. These species are probably not directly involved in FT synthesis. Cobalt carbide formation seems to be related to a deactivation process. Oxidized cobalt species (Co₃O₄, CoO, etc.) do not catalyze FT synthesis either. Oxidation of cobalt metallic species during the reaction leads to catalyst deactivation and reduces FT reaction rates. At the same time, cobalt oxidized species could probably affect the rate of several side and secondary reactions, such as water-gas shift, olefin isomerization, reinsertion, and hydrogenolysis [1].

In many recent years, titania-supported Co catalysts have been widely studied by many authors, especially for the application of FT in a continuous stirred tank reactor (CSTR) [12]. The anatase:rutile phase of titania can affect to the catalytic activity of Co/TiO₂ catalyst. The formerly study reported that both activity and selectivity of CO hydrogenation reaction were altered by changing the rutile:anatase ratios in the titania support (B. Jongsomjit et al., 2005). The activity of a Co/ γ -Al₂O₃ catalyst could affect by addition of CO during H₂ reduction results in increasing both Co reducibility and dispersion (B. Jongsomjit and J.G. Goodwin, 2002).

Co support compound formation (Co-SCF) was found to lower activity of the Co catalyst. In addition, Co-SCF was found during standard reduction resulting in a lower reducibility of the Co catalyst and it is non-reducible at temperature < 800°C during TRP difference from CoTiO₃ [13].

Type of supported also affect to the phase composition and interaction of cobalt with support. The study of type of supported cobalt catalyst (CoO_x/SiO₂, CoO_x/TiO₂ and CoO_x/Al₂O₃) has been studied. From the result, it showed that the interaction of cobalt oxide with supports was much stronger in the kinds of Al₂O₃ and TiO₂, while no conclusive evidence of any interaction was found for SiO₂ [14]. The support interactions on the reduction of cobalt oxide species were observed in the order Al₂O₃ > TiO₂ > SiO₂. Besides, the amounts of cobalt metal loading also affect the reducibility by decreasing interactions with the support [9]

Co/TiO₂ also use as catalyst for dry reforming of methane for generating synthesis gas and is related to the generation of fuel for fuel cells [15].

2.2. Nanocrystalline anatase titania

Sol-gel method is widely used to prepare nanosized TiO₂, the precipitated powders obtained are amorphous in nature and further change to crystallization by heat treatment. Nanocrystalline anatase titania can be produced by changing the chemical of the system. The crystal structure, size, shape, and organisation of TiO₂ nanocrystals can be controlled by adjusting the relative concentrations of TTIP (titanium tetraisopropoxide) and Me₄NOH (tetramethylammonium hydroxide), the

reaction temperature, and the pressure. They found that anatase-TiO₂ nanocrystals with 12 nm particle size were produced by using TTIP: Me₄NOH = 1.14:0.82 molar ratio. It has been reported that the TiO₂ particle size depends on the peptisation temperature. The higher peptisation temperature results in breaking the agglomerates during peptisation [16]. Besides, the crystallite size of TiO₂ obtained from other method such as solvothermal method could be controlled by regulating precursor composition, reaction temperature, solvent property, and aging time. There are many studies about the effect of crystallite size of TiO₂. The larger TiO₂ crystallite size, the increasing surface defect (Ti³⁺) which that resulted in higher photocatalytic activity [17]. The crystal size of TiO₂ increased from 4 to 35 nm as the calcination temperature was increased to 700 °C [18]. The amount of surface defect (Ti³⁺) found to increase with increasing crystallite size of TiO₂. The photocatalytic activity also increases too [19].

2.3. Addition of noble metal on Co catalysts

Numerous studies have shown that introduction of a noble metal (Ru, Rh, Pt, and Pd) has a strong impact on the structure and dispersion of cobalt species, FT reaction rates, and selectivities. The promoting metal is typically introduced via co-impregnation or subsequent impregnation. Introduction of noble metals could result in the following phenomena: much easier reduction of cobalt oxide particles, formation of bimetallic particles and alloys, a lower fraction of barely reducible mixed oxides, enhancement in cobalt dispersion, inhibition of catalyst deactivation, appearance of additional sites of hydrogen activation, and an increase in the intrinsic reactivity of surface sites [1].

Many authors have observed much easier reduction of cobalt oxides to active metal cobalt phases in the presence of noble metals. H.F.J. Van't Blik et al. [20] showed that co-impregnation of silica with solutions of cobalt nitrate and ruthenium chloride resulted in bimetallic particles, which could be reduced at much lower temperatures than the parent Co/SiO₂. K. Takeuchi et al. [21] showed that modification with ruthenium of cobalt silica-supported catalysts prepared from cobalt

acetate considerably increased the extent of cobalt reduction and its activity in the synthesis of C_2 -oxygenates from syngas. The positive effect of ruthenium on cobalt reducibility was also observed by M. Reinikainen et al. [22]. K. Okabe et al. [2] showed that addition of iridium considerably increased cobalt reducibility.

A significant effect of promotion with noble metals on the number of cobalt metal sites was observed on alumina-supported catalysts. In fact, significant shifts of cobalt oxide reduction temperature to lower values have been observed with Pt and Ru addition [3, 23]. It was suggested that Pt was situated on the edge of the cluster and that reduction occurred on Pt first, allowing hydrogen to spill over to cobalt oxide and nucleate cobalt metal sites [24]. N. Tsubaki et al. [8] found that addition of small amount of Ru to cobalt catalysts remarkably increased the extent of cobalt reduction, whereas modification with Pt and Pd did not have any effect on cobalt reducibility. Pt and Pd were found to promote mostly cobalt dispersion. The cobalt catalysts promoted with noble metals displayed the following order of FT catalytic activity: $CoRu > CoPd > CoPt > Co$. Pd- and Pt-containing samples also showed higher methane selectivity than Co and CoRu samples. The effect of promotion with Re on cobalt reducibility is usually less significant than with platinum and ruthenium. It is known that reduction of Co_3O_4 to metallic cobalt proceeds via intermediate formation of CoO. It was suggested that Re affected only the second reduction step: CoO to Co [9, 25]. This was attributed to the fact that reduction of Re occurred above the temperature of Co_3O_4 to CoO reduction.

E. Iglesia et al. [10] have reported that addition of small amounts of Ru to a Co/TiO₂ FT catalyst led to an increase in Co site density during reaction without modifying the chemical reactivity of the exposed Co surface atoms. The addition of promoters such as rhenium, hafnium, cerium, or zirconium to the Co/TiO₂ catalyst could prevent the formation of titanate (CoTiO₃). Titanate, which occurs from cobalt oxide (Co_3O_4) react with TiO₂, has been reported that is very stable and does not have any FT activity. The presence of Ru caused an increased reduction of surface Co in a Co/TiO₂ catalyst. They also found that the CoRu catalyst was more active for the FT reaction than the Co catalyst. It has also been reported that the addition of Re or Ru to a Co/TiO₂ system improved the catalyst activity and selectivity for the FT reaction. The noble metal promoted the reduction of Co oxide in the Co/TiO₂ catalyst

[26]. Jongsomjit et al. [27] have reported that Co-support compound formation (Co-SCF) in Co/TiO₂ was found during standard reduction resulting in a lower reducibility of the catalyst. Co-FSP is considered to be non-reducible at temperature < 800°C during TPR and difference from CoTiO₃. It was also reported Co-SCF in SiO₂ [28] and in Al₂O₃ [5-6,29]. The Co-SCF in Al₂O₃ could occur during standard reduction and resulted in a lower degree of reduction. There also another study in addition of water has significant effect on the CO conversion on Pt promoted Co/TiO₂ catalyst (10 wt %) in CSTR [30].

Promotion with zirconia usually results in higher FT reaction rates; an increase in C⁵⁺ selectivity has been also reported. It was claimed that zirconium could enhance the activity and hydrocarbon selectivity of Co/SiO₂ catalysts. Preimpregnated zirconia could constitute a protecting layer, preventing a chemical reaction between silica and cobalt and thus formation of hardly reducible cobalt silicates. It was claimed that zirconium could enhance the activity and hydrocarbon selectivity of Co/SiO₂ catalysts. Preimpregnated zirconia could constitute a protecting layer, preventing a chemical reaction between silica and cobalt and thus formation of hardly reducible cobalt silicates [31]. A. Feller et al. [32] showed that modification with zirconia facilitated reduction of cobalt species. An increase in zirconia content resulted in larger and easily reducible cobalt particles. The reaction rate also increased with higher zirconia contents, which was attributed to a larger concentration of cobalt metal sites in the catalysts with a higher extent of reduction. G. Jacobs et al. [9] found that zirconia addition increased the cobalt dispersion and decreased the reducibility of cobalt species in alumina-supported FT catalysts. Other study about zirconia-modified titania consisting of difference phase have been studied by T. Wongsalee et al. [33], it showed that modification on the pure anatase TiO₂ resulted in decreased activities. In contrary, the modification on mixed phase TiO₂ resulted in increased activities without effects on selectivity.

CHAPTER III

THEORY

This chapter focuses on the fundamental theory of the Fischer-Tropsch Synthesis (FTS) which is well known as one type of carbon monoxide (CO) hydrogenation using Co-based catalysts. The chapter consists of the basic details of Fischer-Tropsch Synthesis (FTS), titanium oxides properties, cobalt properties, details of Co-based catalysts and cobalt-support compound formation (Co-SCF), and sol-gel method synthesis.

3.1 Fischer-Tropsch synthesis (FTS)

Fischer-Tropsch synthesis (FTS) that discovered by Fischer and Tropsch over 80 years ago, as an alternate process, can convert the synthesis gas (H_2/CO) derived from carbon sources such as coal, peat, biomass and natural gas, into hydrocarbons and oxygenates. During the past decades, FTS has been developed continuously by many researchers, although the rise and fall in research intensity on this process has been highly related to the demands for liquid fuels and relative economics. This synthesis is basically the reductive polymerization (oligomerization) of carbon monoxide by hydrogen to form organic products containing mainly hydrocarbons and some oxygenated products in lesser amounts.

A. Y. Khodakov et al. [1] say that all group VIII metals have noticeable activity in the hydrogenation of carbon monoxide to hydrocarbons. Ruthenium followed by iron, nickel, and cobalt are the most active metals for the hydrogenation of carbon monoxide. Many studies showed that the molecular average weight of hydrocarbons produced by FT synthesis decreased in the following sequence: $Ru > Fe > Co > Rh > Ni > Ir > Pt > Pd$. Thus, only ruthenium, iron, cobalt, and nickel have

catalytic characteristics which allow considering them for commercial production. Nickel catalysts under practical conditions produce too much methane. Ruthenium is too expensive; moreover, its worldwide reserves are insufficient for large-scale industry. Cobalt and iron are the metals which were proposed by Fischer and Tropsch as the first catalysts for syngas conversion. Both cobalt and iron catalysts have been used in the industry for hydrocarbon synthesis. Cobalt catalysts are more expensive, but they are more resistant to deactivation. Although the activity at low conversion of two metals is comparable, the productivity at higher conversion is more significant with cobalt catalysts. Water generated by FT synthesis slows the reaction rate on iron to a greater extent than on cobalt catalysts. At relatively low temperatures (473-523 K), chain growth probabilities of about 0.94 have been reported for cobalt-based catalysts and about 0.95 for iron catalysts. The water-gas shift reaction is more significant on iron than on cobalt catalysts. Iron catalysts usually produce more olefins. Both iron and cobalt catalysts are very sensitive to sulfur, which could readily contaminate them. For iron-based catalysts, the syngas should not contain more than 0.2 ppm of sulfur. For Co catalysts, the amount of sulfur in the feed should be much less than 0.1 ppm. Cobalt catalysts supported on oxide supports are generally more resistant to attrition than iron coprecipitated counterparts; they are more suitable for use in slurry-type reactors. Iron catalysts produce hydrocarbons and oxygenated compounds under different pressures, H_2/CO ratios, and temperatures (up to 613 K). Cobalt catalysts operate at a very narrow range of temperatures and pressures; an increase in temperature leads to a spectacular increase in methane selectivity. Iron catalysts seem to be more appropriate for conversion of biomass-derived syngas to hydrocarbons than cobalt systems because they can operate at lower H_2/CO ratios.

By manipulation of the reaction conditions, the process may be designed to produce heavier saturated hydrocarbons or lower olefins or oxygenated hydrocarbons as we shall see in the following discussion.

Metals that have significant activity for Fischer-Tropsch synthesis include iron, cobalt, nickel and ruthenium. Iron has proved so far to be the best. It is superior to cobalt with respect to conversion rate, selectivity and flexibility. Nickel has

disadvantage of producing appreciable amounts of methane. Ruthenium enhance the formation of high molecular weight alkanes and catalyzes polymerization to polymethane. Other group VIII metals are of low activity. Copper does not catalyze Fisher-Tropsch synthesis.

The catalyst is usually prepared by fusion or precipitation over a silica, alumina or kieselguhr support. Small amounts of promoters such as alkali metal or copper salts are included in the catalytic mix. Copper is believe to facilitate the reduction of the catalyst, alkali metal salt, particularly K_2O_2 enhance activity and olefins selectivity. The support increased the surface area of the catalyst metal thus extremely increasing in dispersion.

Sulfur compounds generally poison the catalyst and they must be removed from the synthesis gas feed stream. However, partial sulfur poisoning may have favorable effects. Thus, it has been found that deliberate slight sulfur poisoning of the iron/manganese catalyst enhances selectivity to shot chain olefins.

Three main types of reactors are currently in use in the Fischer-Tropsch processes: Fixed-bed, fluidized-bed and slurry bed reactors. Fixed-bed reactors are usually tubular, each tube having 50 mm ID and 12 m length. A single reactor may contain as many as 2000 such tubes. Fluidized-bed reactors provide for better heat transfer and continuous regeneration of the catalyst. The catalyst used in fluidized-bed reactors must have high physical stability. SASOL (in Sought Africa), uses fluidized-bed reactors 46 m high, 230 cm in diameter with reaction temperature of 320-360°C and pressure. In the slurry-bed reactors the feed gas is bubbled through a suspension of finely divided catalyst particles. It has the advantage of good temperature control thus providing greater flexibility of reaction conditions.

Each type of reactor is better suited for certain product composition. Fixed-bed reactors, for example, produce high boiling straight-chain hydrocarbons consisting, typically, of 33% gasoline hydrocarbons (C_5-C_{11}), 17% diesel and 40% heavy paraffins and higher waxes. The gasoline fraction is of low octane value and requires further treatment (isomerization or blending) before use. Fluidized-bed reactors are

the best when lighter hydrocarbons are desired. A typical product composition is 72% lower molecular weight gasoline-range hydrocarbons rich in olefins and 14% oxygenated hydrocarbons. However, the product is low in diesel. Thus two or more different reactors may be operated in parallel to provide an integrated fuel plant.

The demands on selectivity of Fischer-Tropsch reactions are ever-increasing. In the earlier days of the process the concern was to improve selectivity with respect to better gasoline grade and/or diesel oil chemicals. With the realization of feasible route of converting synthesis gas to industrial intermediates, more stringent conditions are being imposed on the reaction parameters to make the process more selective.

Selectivity improvement is sought with respect to product properties such as chain length, chain branching, olefin content, alcohol content and methane content. Reaction conditions that particularly eliminate or minimize carbon deposition are desirable. In order to achieve and improve product selectivity the optimization of the following reaction parameters has been investigated: reaction temperature and pressure, H_2/CO ratio, conversion, space velocity, amount and type of promoters, nature of the catalyst, size of catalyst particles and mode of its deposition, type of support, and type of reactor.

We have already seen examples of how the choice of the metal catalyst and support affects the product distribution. The effect of the choice of the reactor type on the nature of the reaction products has also been demonstrated.

Selectivity to olefins may be enhanced by addition of promoters such as K_2O , Ti, Mn or V. Selectivity of greater than 70% to C_2-C_4 olefins at high conversion rate has been achieved.

The search for selectivity to lower olefins by controlling the chain growth and inhibiting hydrogenation has been followed in three directions:

- (a) The use of highly dispersed catalyst either by improving the method of deposition or using special dispersing supports.

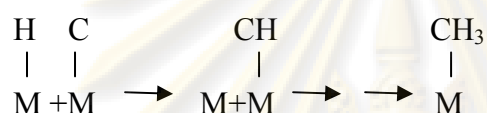
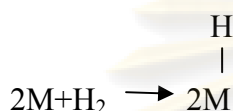
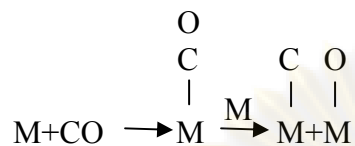
- (b) The use of bimetallic catalyst eg. With Mn/Fe ratio of 9:1 at 330 °C up to 90% olefin selectivity has been achieved. However, the activity of the catalyst and its life-time are low.
- (c) The use of shape-selective catalyst.

Since the Fischer-Tropsch process was originally intended for the production of hydrocarbons, little attention was paid in the early phases of the application of the process to the oxygenated products obtained as co-products. With the search for more economical sources of the oxygenated hydrocarbons, the possibility of tuning the Fischer-Tropsch process for the production such as oxygenates has been investigated. It has been found that with a nitrided iron catalyst, selectivity for alcohols may exceed 80%. A Rh/Hg/SiO₂ catalyst system gave 75% selectivity with respect to ethanol. The major side products are olefins.

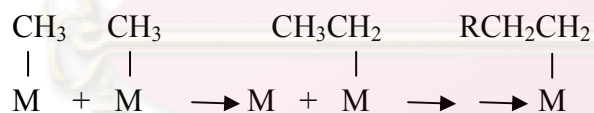
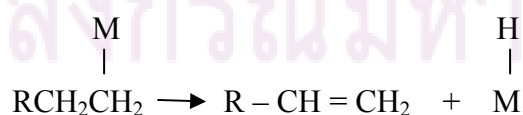
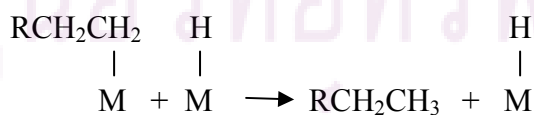
The Fischer-Tropsch process may be defined as being the hydrogenative oligomerization of CO over heterogeneous catalyst to produce alkanes, alkenes oxygenated hydrocarbons and water. A complete mechanism must account for the formation of all products observed. The first attempt at elucidating the mechanism of the process was made by the inventors of the process themselves, Fischer and Tropsch.

3.1.1 The surface carbide mechanism

Fischer and Tropsch apparently were trying to explain the formation of alkanes and alkenes rather than introduce a mechanism for whole line of the products that could be formed from the process. They observed that hydrocarbon formation occurred with heterogeneous metal catalysts (Ni, Fe, Co, Ru) that tend to absorb CO dissociatively to form surface carbide species. Their mechanism consists of the following steps:

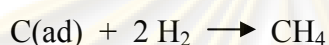
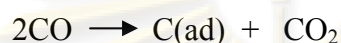
(i) Initiation:

Note: M-X means species X chemisorbed on the metal surface atom M. The hyphen has no implication with respect to the strength of the M-X interaction or the order of the bond. More recently it has been suggested, based spectroscopic evidence, that in order to for an absorbed CO to undergo dissociation it must be bonded side-on to the metal, not end-on.

(ii) Propagation:**(iii) Termination:**

The carbide mechanism has survived the several decades since its introduction. Several items of evidence arising from recent investigation support this mechanism e.g.

(a) In the hydrogenation of CO over clean Ni surface it has been observed that CO₂ evolution proceeds that CH₄ thus



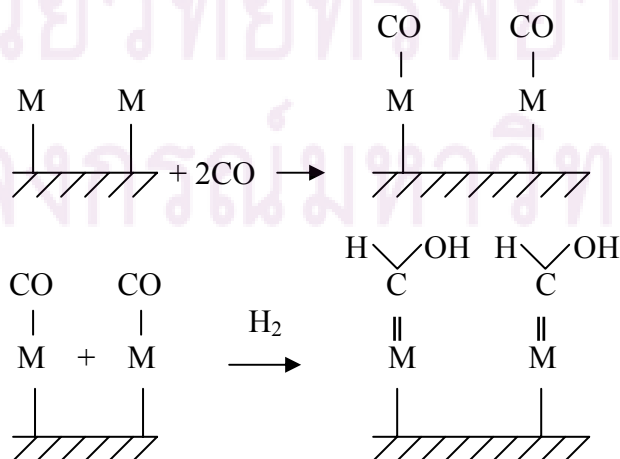
(b) Decomposition of diazomethane(CH₂N₂) at 200°C in the presence of H₂ over Co, Fe and Ru catalysts gives linear alkanes and olefins with distribution similar to that obtained from CO/H₂ reaction over the same catalyst.

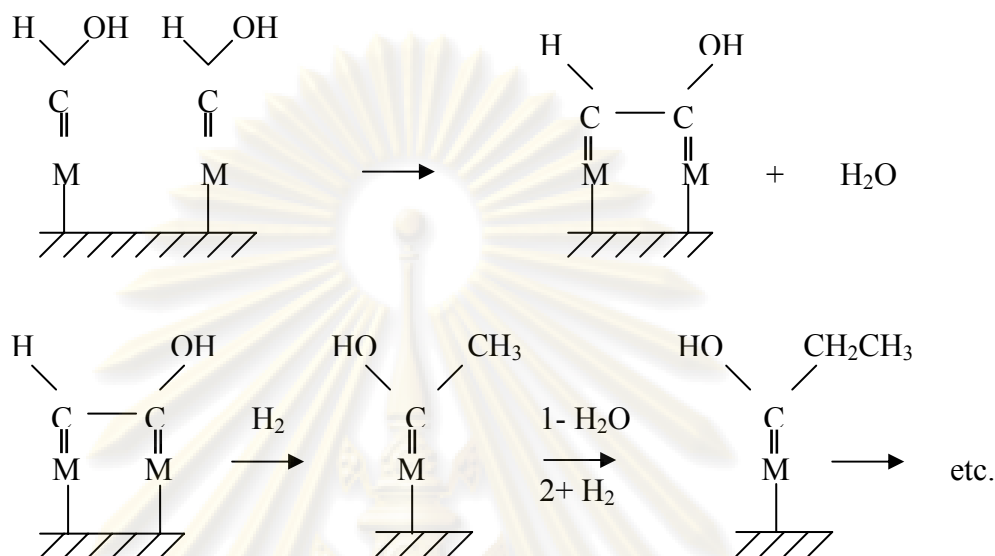
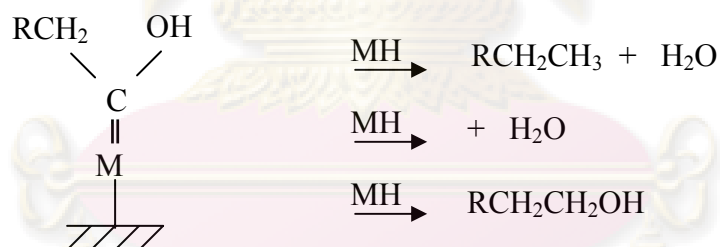
(c) Distribution of ¹³C in CH₂=CH formed when ¹³CO, H₂- and ¹²CH₂N₂ were reacted under Fischer-Tropsch conditions is consistent with the distribution predicted based on the carbided mechanism and inconsistent with other proposed mechanism.

However, a drawback of this mechanism is that it does not explain the formation of oxygenated products.

3.1.2 The hydroxycarbene mechanism

(i) Initiation:

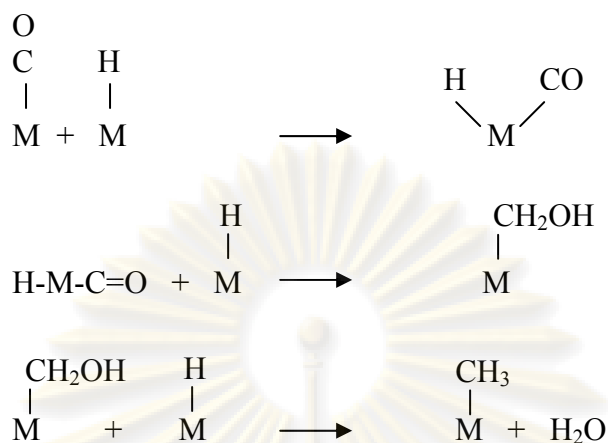


(ii) Propagation:**(iii) Termination:**

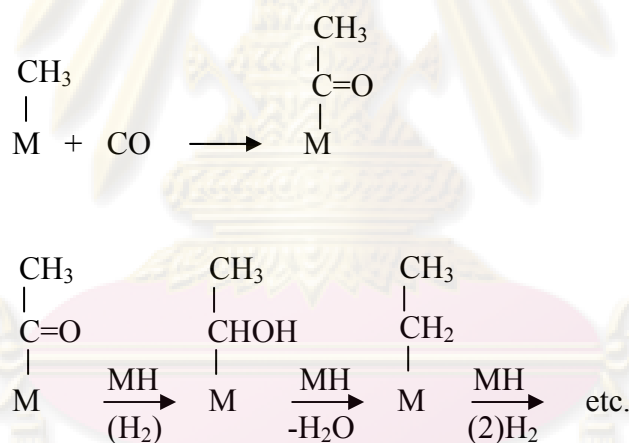
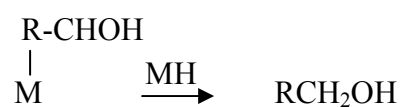
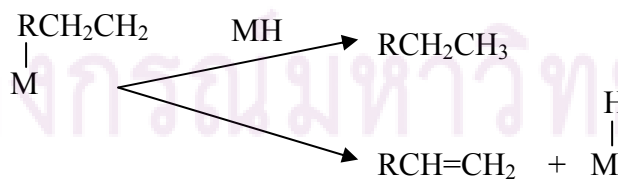
This mechanism explains the formation of alkanes, and olefins as well as oxygenated hydrocarbons. However, it precludes the dissociation of CO, which is not consistent with many experimental observations.

3.1.3 The CO insertion mechanism.**(i) initiation :**

The initiation of active species is similar to that of the carbide mechanism although the mechanism of its formation is different.

**(ii) Propagation:**

propagation proceeds via CO insertion rather than $-\text{CH}_2-$ insertion.

**(iii) Termination:**

Normally, catalysts used for FTS are group VIII metals. By nature, the hydrogenation activity increases in order of $\text{Fe} < \text{Co} < \text{Ni} < \text{Ru}$. Ru is the most active. Ni forms predominantly methane, while Co yields much higher ratios of paraffins to olefins and much less oxygenated products such as alcohols and aldehydes than Fe.

The current main goal in FTS is to obtain high molecular weight, straight chain hydrocarbons. However, methane and other light hydrocarbons are always present as less desirable products from the synthesis. According to the Anderson-Schulz-Flory (ASF) product distribution, typically 10 to 20% of products from the synthesis are usually light hydrocarbon ($\text{C}_1\text{-C}_4$). These light alkanes have low boiling points and exist in the gas phase at room temperature, which is inconvenient for transportation. Many attempts have been made to minimize these by-products and increase the yield of long chain liquid hydrocarbons by improving chain growth probability. It would be more efficient to be able to convert these less desirable products into more useful forms, rather than re-reforming them into syngas and recycling them. Depending upon the type of catalyst used, promoters, reaction conditions (pressure, temperature and H_2/CO ratios), and type of reactors, the distribution of the molecular weight of the hydrocarbon products can be noticeably varied.

3.2 Titanium (IV) Oxide [34]

Titanium (IV) oxide occurs naturally in three crystalline forms:

1. Rutile, which tends to be more stable at high temperatures. The application of almost rutile type is used in industrial products such as paints, cosmetics foodstuffs and sometimes found in igneous rocks.
2. Anatase, which tends to be more stable at lower temperatures. This type generally shows a higher photoactivity than other types of titanium dioxide.
3. Brookite, which is usually found only in minerals and has a structure belonging to orthorhombic crystal system.

Table 3.1 Crystallographic properties of anatase, brookite, and rutile.

Properties	Anatase	Brookite	Rutile
Crystal structure	Tetragonal	Orthorhombic	Tetragonal
Optical	Uniaxial, negative	Biaxial, positive	Uniaxial, negative
Density, g/cm ³	3.9	4.0	4.23
Hardness, Mohs scale	5 ¹ / ₂ – 6	5 ¹ / ₂ – 6	7 – 7 ¹ / ₂
Unit cell	D _{4h} ¹⁹ .4TiO ₂	D _{2h} ¹⁵ .8TiO ₂	D _{4h} ¹² .3TiO ₂
Dimension, nm			
a	0.3758	0.9166	0.4584
b		0.5436	
c	0.9514	0.5135	2.953

Both of rutile and anatase type have a structure belonging to tetragonal crystal system but they are not isomorphous (Figure 2.1). The two tetragonal crystal types are more common because they are easy to make. Anatase occurs usually in near-regular octahedral, and rutile forms slender prismatic crystal, which are frequently twinned. Rutile is the thermally stable form and is one of the two most important ores of titanium.

The three allotropic forms of titanium dioxide have been prepared artificially but only rutile, the thermally stable form, has been obtained in the form of transparent large single crystal. The transformation from anatase to rutile is accompanied by the evolution of ca. 12.6 kJ/mol (3.01 kcal/mol), but the rate of transformation is greatly affected by temperature and by the presence of other substance which may either catalyze or inhibit the reaction. The lowest temperature at which conversion of anatase to rutile takes place at a measurable rate is ca. 700°C, but this is not a transition temperature. The change is not reversible; ΔG for the change from anatase to rutile is always negative.

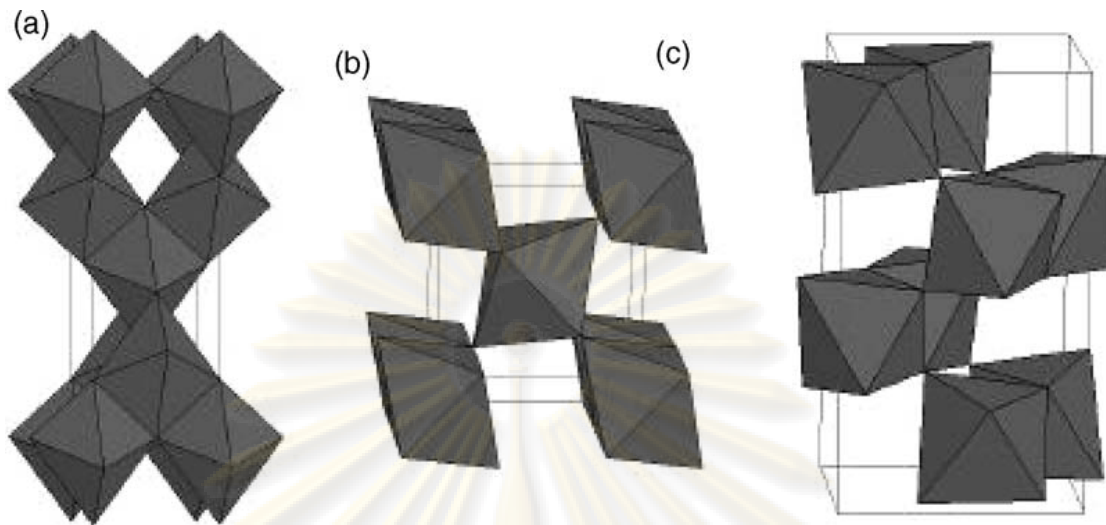


Figure 2.1 Crystal structures of anatase (a), rutile (b), and brookite (c) TiO_2 [35].

Brookite has been produced by heating amorphous titanium (IV) oxide, prepared from an alkyl titanates of sodium titanate with sodium or potassium hydroxide in an autoclave at 200 to 600 °C for several days. The important commercial forms of titanium (IV) oxide are anatase and rutile, and these can readily be distinguished by X-ray diffraction spectrometry.

Since both anatase and rutile are tetragonal, they are both anisotropic, and their physical properties, e.g. refractive index, vary according to the direction relative to the crystal axes. In most applications of these substances, the distinction between crystallographic direction is lost because of the random orientation of large numbers of small particles, and it is mean value of the property that is significant.

Measurement of physical properties, in which the crystallographic directions are taken into account, may be made of both natural and synthetic rutile, natural anatase crystals, and natural brookite crystals. Measurements of the refractive index of titanium dioxide must be made by using a crystal that is suitably orientated with respect to the crystallographic axis as a prism in a spectrometer. Crystals of suitable size of all three modifications occur naturally and have been studied. However, rutile is the only form that can be obtained in large artificial crystals from melts. The refractive index of rutile is 2.75. The dielectric constant of rutile varies with

direction in the crystal and with any variation from the stoichiometric formula, TiO_2 ; an average value for rutile in powder form is 114. The dielectric constant of anatase powder is 48.

Titanium dioxide is thermally stable (mp 1855°C) and very resistant to chemical attack. When it is heated strongly under vacuum, there is a slight loss of oxygen corresponding to a change in composition to $\text{TiO}_{1.97}$. The product is dark blue but reverts to the original white color when it is heated in air.

3.3 Cobalt [36,-37)

3.3.1 General

Cobalt, a transition series metallic element having atomic number 27, is similar to silver in appearance.

Cobalt and cobalt compounds have expanded from use colorants in glasses and ground coat frits for pottery to drying agents in paints and lacquers, animal and human nutrients, electroplating materials, high temperature alloys, hard facing alloys, high speed tools, magnetic alloys, alloys used for prosthetics, and used in radiology. Cobalt is also as a catalyst for hydrocarbon refining from crude oil for the synthesis of heating fuel.

3.3.2 Physical Properties

The electronic structure of cobalt is $[\text{Ar}] 3d^7 4s^2$. At room temperature the crystalline structure of the α (or ϵ) form, is close-packed hexagonal (cph) and lattice parameters are $a = 0.2501 \text{ nm}$ and $c = 0.4066 \text{ nm}$. Above approximately 417°C , a face-centered cubic (fcc) allotrope, the γ (or β) form, having a lattice parameter $a = 0.3544 \text{ nm}$, becomes the stable crystalline form. Physical properties of cobalt are listed in Table 3.2.

The scale formed on unalloyed cobalt during exposure to air or oxygen at high temperature is double-layered. In the range of 300 to 900°C, the scale consists of a thin layer of mixed cobalt oxide, Co_3O_4 , on the outside and cobalt (II) oxide, CoO , layer next to metal. Cobalt (III) oxide, Co_2O_3 , may be formed at temperatures below 300 °C. Above 900°C, Co_3O_4 decomposes and both layers, although of different appearance, are composed of CoO only. Scales formed below 600°C and above 750°C appear to be stable to cracking on cooling, whereas those produced at 600-750°C crack and flake off the surface.

Cobalt forms numerous compounds and complexes of industrial importance. Cobalt, atomic weight 58.933, is one of the three members of the first transition series of Group 9 (VIII B). There are thirteen known isotopes, but only three are significant: ^{59}Co is the only stable and naturally occurring isotope; ^{60}Co has a half-life of 5.3 years and is a common source of γ -radioactivity; and ^{57}Co has a 270-d half-life and provides the γ -source for Mössbauer spectroscopy.

Cobalt exists in the +2 or +3 valence states for the major of its compounds and complexes. A multitude of complexes of the cobalt (III) ion exists, but few stable simple salts are known. Octahedral stereochemistries are the most common for cobalt (II) ion as well as for cobalt (III). Cobalt (II) forms numerous simple compounds and complexes, most of which are octahedral or tetrahedral in nature; cobalt (II) forms more tetrahedral complex than other transition-metal ions. Because of the small stability difference between octahedral and tetrahedral complexes of cobalt (II), both can be found in equilibrium for a number of complexes. Typically, octahedral cobalt (II) salts and complexes are pink to brownish red; most of the tetrahedral Co (II) species are blue.

จุฬาลงกรณ์มหาวิทยาลัย

Table 3.2 Physical properties of cobalt [37]

Property	Value
atomic number	27
atomic weight	58.93
transformation temperature, °C	417
heat of transformation, J/g ^a	251
melting point, °C	1493
latent heat of fusion, ΔH_{fus} J/g ^a	395
boiling point, °C	3100
latent heat of vaporization at bp, ΔH_{vap} kJ/g ^a	6276
specific heat, J/(g·°C) ^a	
15-100°C	0.442
molten metal	0.560
coefficient of thermalexpansion, °C ⁻¹	
cph at room temperature	12.5
fcc at 417°C	14.2
thermal conductivity at 25 °C, W/(m·K)	69.16
thermal neutron absorption, Bohr atom	34.8
resistivity, at 20 °C ^b , 10 ⁻⁸ Ωm	6.24
Curie temperature, °C	1121
saturation induction, 4πI _s , T ^c	1.870
permeability, μ	
initial	68
max	245
residual induction, T ^c	0.490
coercive force, A/m	708
Young's modulus, Gpac	211

Table 3.2 Physical properties of cobalt (cont.)

Property	Value		
Hardness ^f , diamond pyramid, of %Co	99.9	99.98 ^e	
At 20 °C	225	253	
At 300 °C	141	145	
At 600 °C	62	43	
At 900 °C	22	17	
strength of 99.99 %cobalt, MPa ^g	as cast	annealed	sintered
tensile	237	588	679
tensile yield	138	193	302
compressive	841	808	
compressive yield	291	387	

^aTo convert J to cal, divided by 4.184.

^bconductivity = 27.6 % of International Annealed Copper Standard.

^cTo convert T to gauss, multiply by 10⁴.

^dTo convert GPa to psi , multiply by 145,000.

^eZone refined.

^fVickers.

^gTo convert MPa to psi , multiply by 145.

3.3.3 Cobalt Oxides

Cobalt has three well-known oxides:

Cobalt (II) oxide, CoO, is an olive green, cubic crystalline material. Cobalt (II) oxide is the final product formed when the carbonate or the other oxides are calcined to a sufficiently high temperature, preferably in a neutral or slightly reducing atmosphere. Pure cobalt (II) oxide is a difficult substance to prepare, since it readily takes up oxygen even at room temperature to re-form a higher oxide. Above

about 850°C, cobalt (II) oxide form is the stable oxide. The product of commerce is usually dark gray and contains 75-78 wt % cobalt. Cobalt (II) oxide is soluble in water, ammonia solution, and organic solvents, but dissolves in strong mineral acids. It is used in glass decorating and coloring and is a precursor for the production of cobalt chemical.

Cobalt (III) oxide, Co_2O_3 , is formed when cobalt compounds are heated at a low temperature in the presence of an excess of air. Some authorities told that cobalt (III) oxide exists only in the hydrate form. The lower hydrate may be made as a black powder by oxidizing neutral cobalt solutions with substances like sodium hypochlorite. Co_2O_3 or $\text{Co}_2\text{O}_3 \cdot \text{H}_2\text{O}$ is completely converted to Co_3O_4 at temperatures above 265°C. Co_3O_4 will absorb oxygen in a sufficient quantity to correspond to the higher oxide Co_2O_3 .

Cobalt oxide, Co_3O_4 , is formed when cobalt compounds, such as the carbonate or the hydrated sesquioxide, are heated in air at temperatures above approximately 265°C and not exceeding 800°C.

3.4 Co-based Catalysts

Supported cobalt (CO) catalysts are the preferred catalysts for the synthesis of heavy hydrocarbons from natural gas based syngas (CO and H_2) because of their high Fischer-Tropsch (FT) activity, high selectivity for linear hydrocarbons and low activity for the water-gas shift reaction. It is known that reduced cobalt metal, rather than its oxides or carbides, is the most active phase for CO hydrogenation in such catalysts. Investigations have been done to determine the nature of cobalt species on various supports such as alumina, silica, titania, magnesia, carbon, and zeolites. The influence of various types of cobalt precursors used was also investigated. It was found that the used of organic precursors such as CO (III) acetyl acetate resulting in an increase of CO conversion compared to that of cobalt nitrate [38].

3.5 Sol-gel method

Basically, the sol-gel process means the synthesis of an inorganic network by chemical reactions in solution at low temperature. The most obvious feature of this reaction is the transition from liquid (solution or colloidal solution) into solid (di-ormultiplasic gel) leading to the expression “sol-gel process”. Nevertheless, this type of reaction is not necessarily restricted to an aqueous system; although reactions in aqueous solution have been know for a very long time. Any precursor, which is able to form reactive “inorganic” monomers or oligomers can be used for sol-gel techniques. It is very difficult to foresight type of precursor to be used for a specific aim. The reactivity of the precursor does not only depend on its chemical nature but also on the applied reaction conditions. Even finely divided silica particles can be peptisized and used for preparation of sols. However, it is necessary to generate appropriate surface charges in order to prevent coagulation and precipitation. Most work in the sol-gel has been done by using alkoxides as precursors. Alkoxide provide a convenient source for “inorganic” monomers which in most cases are soluble in common solvents. Another advantage of the alkoxide route is possibility to control rate by controlling hydrolysis and condensation by chemical means, not by surface or colloid chemistry. In the case of a few metals, it might not be convenient to use alkoxides due to their unavailability and/or difficulties in synthesis, alternative precursors may have to be employed. Metal salts provide a viable alterative, because of the advantage in their solubity in organic solvents from the initial stage or during the sol-gel processing. However, care has to be exercised to choose such precursors since they can be converted easily to oxide by thermal or oxidative decomposition. Among the inorganic salts, metal nitrates are probably the best candidates as other salts such as sulfate or chloride are more thermally stable and therefore, it may be difficult to remove the anionic portion effectively from the final ceramic product.

Sol-gel preparation is widely used in glass and ceramic industries as well as in catalyst preparation [35]. There are many routes of sol-gel preparation starting with different precursors such as inorganic salt or metal alkoxide. Sol, which is suspension of nanosized or micron-sized solid particles in liquid, can be obtained by hydrolysis and partial condensation of the precursor. Further condensation of sol particles result

in three-dimensional network called gel, which is a diphasic material with solids encapsulating solvent. Alternatively, gel can be produced by destabilizing the solution of preformed sols. Operation at low temperature is the major advantage of this method. Furthermore, the obtained products are uniform. Sol-gel processing offers a number of advantages such as high purity, high degree of homogeneity, well-defined nanostructure, excellent chemical homogeneity and the possibility of deriving unique metastable structures at low reaction temperature [39].

These methods are used for the synthesis of thin films, powders, and membranes. Two types are known: the non-alkoxide and the alkoxide route. Depending on the synthetic approach used, oxides with different physical and chemical properties may be obtained. The sol-gel method has many advantages over other fabrication techniques such as purity, homogeneity, flexibility, and flexibility in introducing dopants in large concentrations, stoichiometry control, ease of processing, control over the composition, and the ability to coat large and complex areas. The non-alkoxide route uses inorganic salts (such as nitrates, chlorides, acetates, carbonates, acetylacetonates, etc.), which requires an additional removal of the inorganic anion; while the alkoxide route (the most employed) uses metal alkoxides as starting material. This method involves the formation of a TiO_2 sol or gel or precipitation by hydrolysis and condensation (with polymer formation) of titanium alkoxides. In order to exhibit better control over the evolution of the microstructure, it is desirable to separate and temper the steps of hydrolysis and condensation. In order to achieve this goal, several approaches were adopted. One of them is alkoxide modification by complexation with coordination agents such as carboxylates, or b-diketonates that hydrolyze slower than alkoxide ligands.

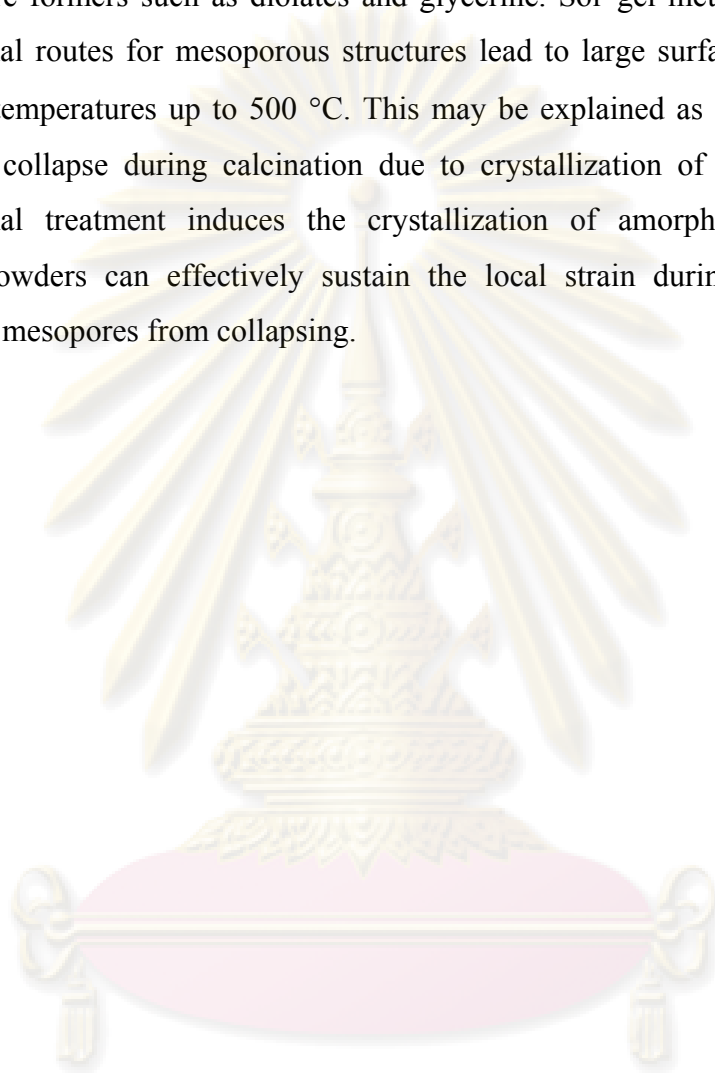
Additionally, the preferred coordination mode of these ligands can be exploited to control the evolution of the structure. In general, b-diketone ligands predominately form metal chelates which can cap the surface of the structure. Carboxylate ligands have a strong tendency to bridge metal centers, being likely to become trapped in the bulk of materials and on the surface of the particle. Acid-base catalysis can also be used to enable separation of hydrolysis and condensation steps. It

has been demonstrated that acid catalysis increases hydrolysis rates and ultimately crystalline powders are formed from fully hydrolyzed precursors. Base catalysis is thought to promote condensation with the result that amorphous powders are obtained containing unhydrolyzed alkoxide ligands. On the other hand, acetic acid may be used in order to initiate hydrolysis via an esterification reaction, and alcoholic sols prepared from titanium alkoxide using amino alcohols have been shown to stabilize the sol, reducing or preventing the condensation and the precipitation of titania. These reactions are followed by a thermal treatment (450–600 °C) to remove the organic part and to crystallize either anatase or rutile TiO₂. Recent variants of the sol–gel method lowered the necessary temperature to less than 100 °C. The calcinations process will inevitably cause a decline in surface area (due to sintering and crystal growth), loss of surface hydroxyl groups, and even induce phase transformation. Washing steps have been also reported to cause surface modifications. Cleaning of particles is usually achieved by washing the surface with a solvent, followed by centrifugation. The solvent can affect the chemical composition and crystallization. It was also reported that particle washing could affect the surface charge of the particles by bonding onto the surface. An alternative washing technique is to dialyze particles against double-distilled water, which could be an effective method of removing soluble impurities without introducing new species.

As titanium sources, Ti(O-E)₄, Ti(i-OP)₄, and Ti(O-nBu)₄ are most commonly used. The sol–gel method has been widely studied particularly for multicomponent oxides where intimate mixing is required to form a homogeneous phase at the molecular level. Thus, metal ions such as Ca²⁺, Sr²⁺, Ba²⁺, Cu²⁺, Fe³⁺, V⁵⁺, Cr³⁺, Mn²⁺, Pt⁴⁺, Co²⁺, Ni²⁺, Pb²⁺, W⁶⁺, Zn²⁺, Ag⁺, Au³⁺, Zr²⁺, La³⁺, and Eu³⁺ were introduced into TiO₂ powders and films by this method and the photocatalytic activity was improved to varying extent. Most nanocrystalline-TiO₂ (nc-TiO₂) particles that are commercially obtainable are synthesized using sol–gel methods.

Very recently, sol–gel and templating synthetic methods were applied to prepare very large surface area titania phases, which exhibit a mesoporous structure. Ionic and neutral surfactants have been successfully employed as templates to prepare

mesoporous TiO_2 . Block copolymers can also be used as templates to direct formation of mesoporous TiO_2 . In addition, many non-surfactant organic compounds have been used as pore formers such as diolates and glycerine. Sol-gel methods coupled with hydrothermal routes for mesoporous structures lead to large surface area even after heating at temperatures up to $500\text{ }^\circ\text{C}$. This may be explained as follows: generally, mesopores collapse during calcination due to crystallization of the wall. When a hydrothermal treatment induces the crystallization of amorphous powders, the obtained powders can effectively sustain the local strain during calcination and prevent the mesopores from collapsing.



ศูนย์วิทยทรัพยากร
จุฬาลงกรณ์มหาวิทยาลัย

CHAPTER IV

EXPERIMENTAL

This chapter consists of experimental systems and procedures used in this work which is divided into three parts including catalyst preparation, catalyst characterization and reaction study in CO hydrogenation.

The first part (section 4.1) is described catalyst preparation such as cobalt on Ru-modified, Zr-modified and unmodified titania with different crystallite sizes. The catalyst nomenclature is given in this section. The second part (section 4.2) is explained catalyst characterization by various techniques including of BET surface area, TPR, XRD, SEM/EDX, TEM, CO Chemisorption and XPS. Finally, the last part (section 4.3) is illustrated catalyst activity measurement in CO hydrogenation.

4.1 Catalyst preparation

4.1.1 Chemicals

The details of chemicals used in this experiment are shown in Table 4.1.

Table 4.1 Chemicals used in the preparation of catalysts.

Chemical	Supplier
Titanium(IV) isopropoxide 97%	Aldrich
Cobalt (II) nitrate hexahydrate 98%+	Aldrich
Ruthenium (III) nitrosyl nitrate, solution in dilute nitric acid, 1.5%	Aldrich
Zirconium (IV) <i>n</i> -propoxide 70wt% solution in 1-propanol	Aldrich
Ethanol	Merck

4.1.2 Preparation of the titania supports by sol- gel method [40-41]

Titania precursor will be dissolved in ethanol and then mixed with the solution of water: alkoxide which has molar ratio in the range of 4 – 165. Then the precursor solution will be added dropwise to the aqueous solution with stirring by ultrasonic at room temperature. White precipitates of hydrous oxides will be produced instantly and the mixture was stirred for at least 2 h. After that, the amorphous precipitates will be separated from the mother liquor by centrifugation and redispersed in ethanol five times to minimize particle agglomeration. The resulting materials will be dried and calcined at 450°C in air for 2 h.

4.1.3 Preparation of the modified-titania support

A Ruthenium/Zirconium supported cobalt catalyst was prepared by incipient wetness impregnation method. A designed amount of ruthenium (III) nitrosyl nitrate / zirconium (IV) *n*-propoxide was dissolved in deionized water and then impregnated into the titania support with 0.03 wt % Ru or 0.3 wt% Zr by calculating of the required amounts of Ru/Zr loading (see Appendix A). The catalyst was dried at 110°C for 12 h and calcined in air at 500 °C for 4 h for Ru modification and calcined at 350 °C for 2 h for Zr modification.

4.1.4 Preparation of the supported cobalt catalysts

The catalysts were prepared by incipient wetness impregnation with aqueous solution of cobalt (II) nitrate hexahydrate. The certain amount of cobalt (20 wt% loading) will be dissolved de-ionized water and then impregnated into the modified titania. The cobalt solution is dropped slowly to the modified-titania support and then the catalyst is dried in the oven at 110 °C for 12 h. The catalyst is calcined in air at 500 °C for 4 h.

4.1.5 Catalyst Nomenclature

The nomenclature used for the catalyst samples in this study is as follows:

- **Co/TiO₂_xx nm_Ru**
- **Co/TiO₂_xx nm_Zr**
- **Co/TiO₂_xx nm**

Co/TiO₂_xx nm refers to Co/TiO₂ catalyst using TiO₂ having **xx** nm of crystallite size.

Co/TiO₂_xx nm_Ru refers to the corresponding ruthenium modified-titania supported cobalt catalyst having different size of titania support.

Co/TiO₂_xx nm_Zr refers to the corresponding zirconium modified-titania supported cobalt catalyst having different size of titania support.

4.2 Catalyst characterization

Various characterization techniques were used in this studied in order to clarify the catalyst structure and morphology, and surface composition of catalysts.

4.2.1 BET surface area

Surface area measurements were carried out by low temperature nitrogen adsorption in a Micromeritic ChemiSorb 2750 system. Calculations were performed on the basis of the BET isotherm. 0.2 grams of sample was loaded into u-shape cell made from Pyrex and heated in helium to 200°C for 1 h in order to eliminate trace amount of water adsorbed on surface, then cooled down to room temperature. The analysis gas consist of 30%N₂ in helium was introduced to Pyrex cell. Sample adsorbed nitrogen at low temperature by dipped cell into liquid nitrogen dewar until it's surface was satuated with nitrogen and desorbed nitrogen at room temperature by moved away the dewar. The nitrogen that was desorbed from sample was measured by TCD detector.

4.2.2 X-ray diffraction (XRD)

XRD were performed to determine the bulk crystalline phases of catalyst. It was conducted using a SIEMENS D-5000 X-ray diffractometer connected with a computer with Diffract ZT version 3.3 program for fully control of the XRD analyzer. The experiments were carried out by using $\text{CuK}\alpha$ ($\lambda = 1.54439 \text{ \AA}$) radiation with Ni filter in the range $2\theta = 20\text{-}80^\circ$ resolution 0.04.

4.2.3 Scanning electron microscopy and energy dispersive X-ray spectroscopy (SEM/EDX)

SEM and EDX were used to determine the catalyst morphologies and elemental distribution throughout the catalyst granules, respectively. The SEM of JEOL mode JSM-5410LV was applied using the secondary electron mode at 15 kV. EDX was performed using Link Isis series 300 program.

4.2.4 Transmission electron microscopy (TEM)

The morphology and size of the catalysts were determined using a JEOL-TEM 200CX transmission electron spectroscopy operated at 160 kV at the Scientific and Technological Research Equipment Center (STREC), Chulalongkorn University.

4.2.5 Temperature-programmed reduction (TPR)

TPR was used to determine the reduction behaviors of the samples using a Micromeritics Chemisorb 2750.

1. The catalyst sample 0.1 g used in the sample cell.
2. Prior to operation, the catalysts were heated up to 200°C in flowing nitrogen and held at this temperature for 1 h.

3. After the catalyst sample was cooled down to room temperature, the carrier gas was 5% H₂ in Ar (30 CC/min) were ramping from 35 to 800 °C at 10 °C/min.
4. A cold trap was placed before the detector to remove water produced during the reaction.
5. A thermal conductivity detector (TCD) was used to determine the amount of hydrogen consumption during TPR.

4.2.6 CO-Pulse Chemisorption

The active sites and the relative percentages dispersion of cobalt catalyst was determined by CO-pulse chemisorption technique using Micromeritics ChemiSorb 2750 (pulse chemisorption system) and ASAP 2101C V.3.00 software. It was carried out using 20 mg of a sample and reduced in H₂ flow rate at 50 ml/min with heated from room temperature to 350°C at rate 10°C/min and held at this temperature for 3 h after the cooled down to room temperature in a He flow. Gas volumetric chemisorption at 100°C was performed. Desorbed CO was measured using thermal conductivity detector. Pulsing was continued until no further carbon monoxide adsorption was observed.

4.2.7 X-ray photoelectron spectroscopy

XPS was used to examine the binding energy and the surface composition of the catalysts by using an AMICUS spectrometer with a x-ray source as Mg K_α radiation operated at voltage of 20 kV, current of 10 mA. The computer controlled by using the AMICUS “VISION2” software.

จุฬาลงกรณ์มหาวิทยาลัย

4.3 Reaction study in CO hydrogenation

4.3.1 Materials

The reactant gas used for the reaction study was the carbon monoxide in hydrogen feed stream as supplied by Thai Industrial Gas Limited (TIG). The gas mixture contained 9.73 vol % CO in H₂ (22 CC/min). The total flow rate was 30 CC/min with the H₂/CO ratio of 10/1. Ultra high purity hydrogen (50 CC/min) and high purity argon (8 CC/min) manufactured by Thai Industrial Gas Limited (TIG) were used for reduction and balanced flow rate.

4.3.2 Apparatus

Flow diagram of CO hydrogenation system is shown in Figure 4.1. The system consists of a reactor, an automatic temperature controller, an electrical furnace and a gas controlling system.

4.3.2.1 Reactor

The reactor was made from a stainless steel tube (O.D. 3/8"). Two sampling points were provided above and below the catalyst bed. Catalyst was placed between two quartz wool layers.

4.3.2.2 Automation Temperature Controller

This unit consisted of a magnetic switch connected to a variable voltage transformer and a solid-state relay temperature controller model no. SS2425DZ connected to a thermocouple. Reactor temperature was measured at the bottom of the catalyst bed in the reactor. The temperature control set point is adjustable within the range of 0-800°C at the maximum voltage output of 220 volt.

4.3.2.3 Electrical Furnace

The furnace supplied heat to the reactor for CO hydrogenation. The reactor could be operated from temperature up to 800°C at the maximum voltage of 220 volt.

4.3.2.4 Gas Controlling System

Reactant for the system was each equipped with a pressure regulator and an on-off valve and the gas flow rates were adjusted by using metering valves.

4.3.2.5 Gas Chromatography

The composition of hydrocarbons in the product stream was analyzed by a Shimadzu GC14B (VZ10) gas chromatograph equipped with a flame ionization detector. A Shimadzu GC8A (molecular sieve 5A) gas chromatography equipped with a thermal conductivity detector was used to analyze CO and H₂ in the feed and product streams. The operating conditions for each instrument are shown in the Table 4.2.

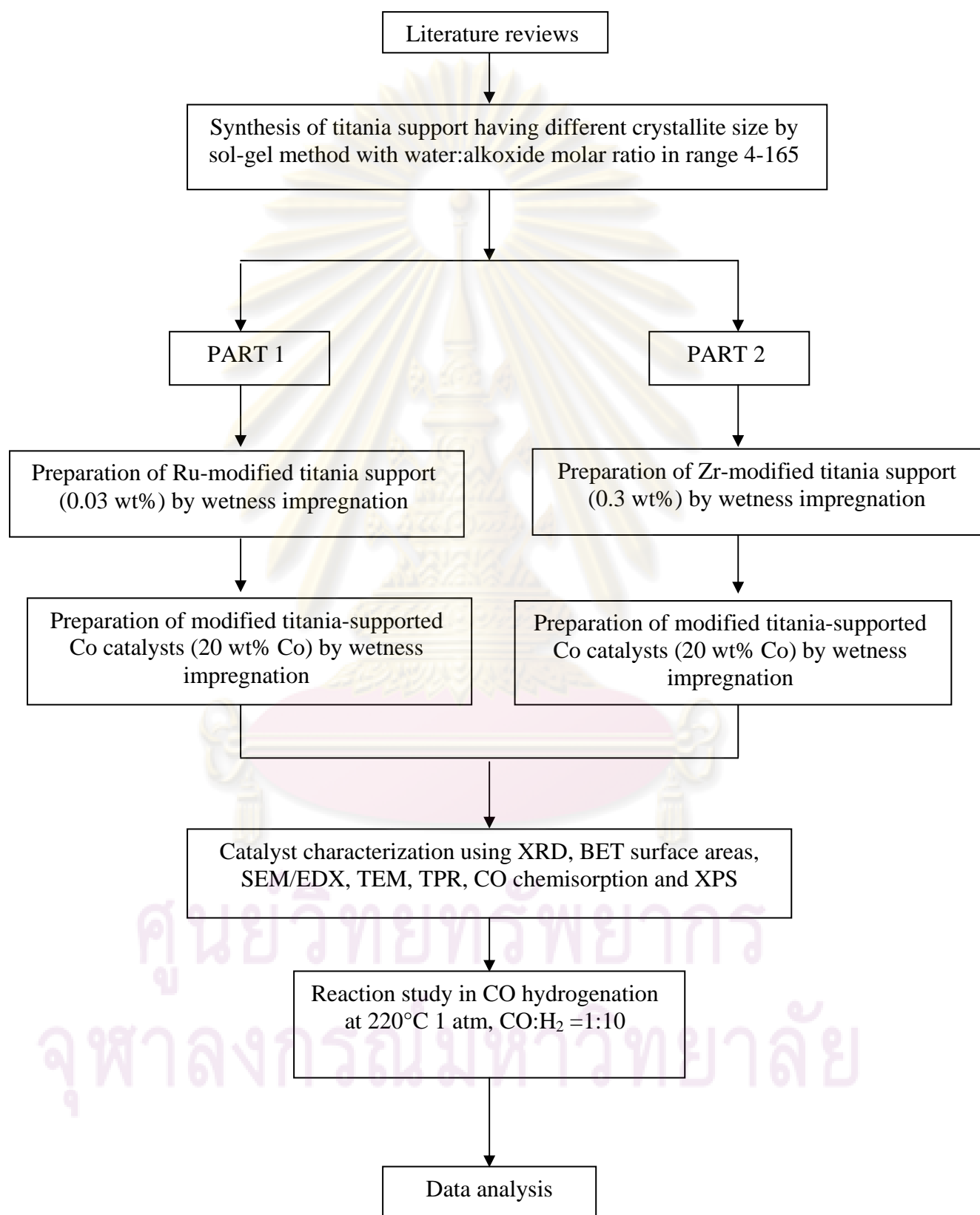
Table 4.2 Operating condition for gas chromatograph

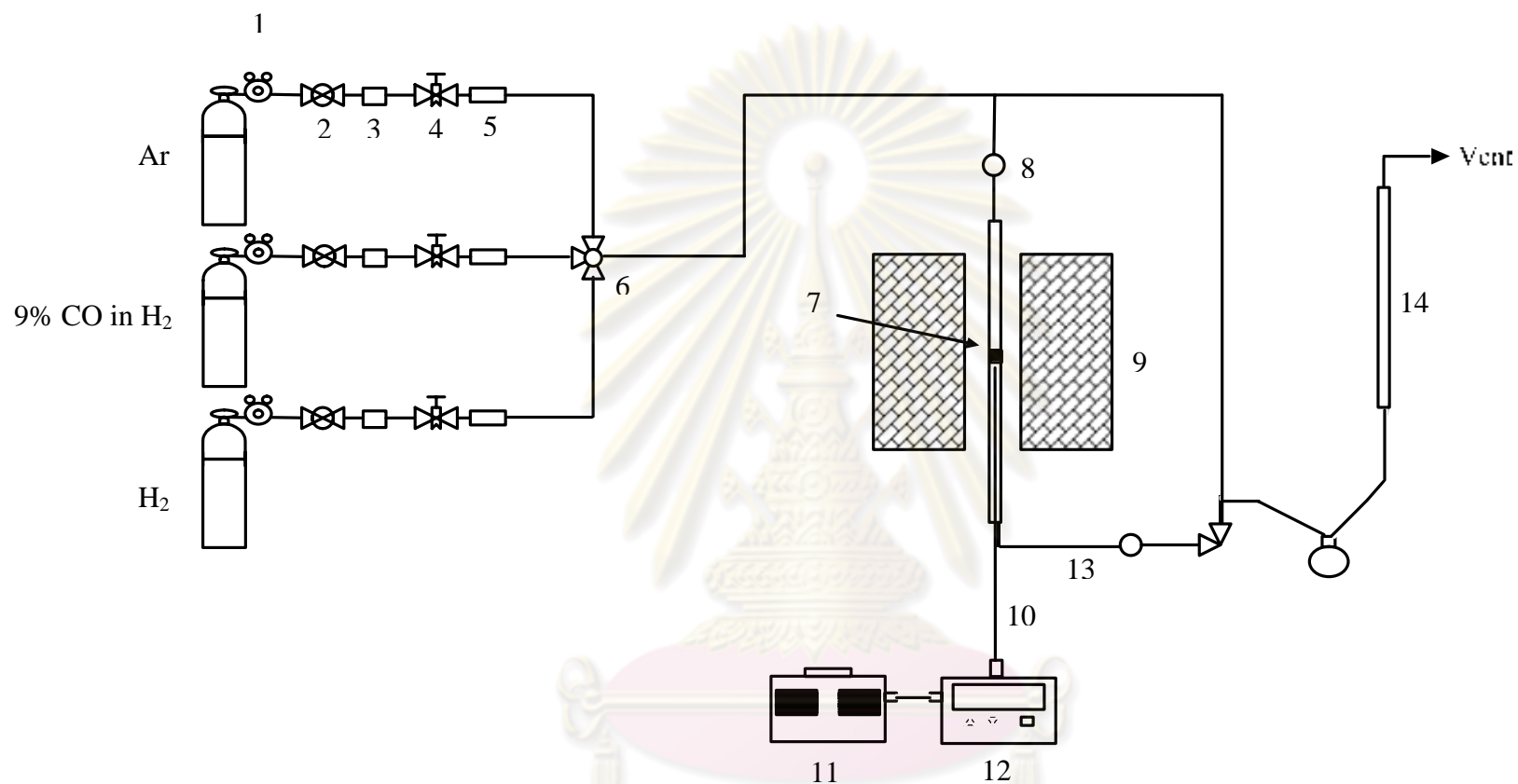
Gas Chromagraph	SHIMADZU GC-8A	SHIMADZU GC-14B
Detector	TCD	FID
Column	Molecular sieve 5A	VZ10
- Column material	SUS	-
- Length	2 m	-
- Outer diameter	4 mm	-
- Inner diameter	3 mm	-
- Mesh range	60/80	60/80
- Maximum temperature	350 °C	80 °C
Carrier gas	He (99.999%)	H ₂ (99.999%)
Carrier gas flow	40 cc/min	-
Column gas	He (99.999%)	Air, H ₂
Column gas flow	40 cc/min	-
Column temperature		
- initial (°C)	60	70
- final (°C)	60	70
Injector temperature (°C)	100	100
Detector temperature (°C)	100	150
Current (mA)	80	-
Analysed gas	Ar, CO, H ₂	Hydrocarbon C ₁ -C ₄

4.3.3 Procedures

1. Using 0.1 g of catalyst packed in the middle of the stainless steel microreactor, which is located in the electrical furnace.
2. A flow rate of Ar = 8 CC/min, 9% CO in H₂ = 22 CC/min and H₂ = 50 CC/min in a fixed-bed flow reactor. A relatively high H₂/CO ratio was used to minimize deactivation due to carbon deposition during reaction.
3. The catalyst sample was re-reduce *in situ* in flowing H₂ at 350 °C for 3 h prior to CO hydrogenation.
4. CO hydrogenation was carried out at 220 °C and 1 atm total pressure in flowing 9% CO in H₂.
5. The effluent was analyzed using gas chromatography technique. [Thermal conductivity detector (TDC) was used for separation of carbon monoxide (CO) and methane (CH₄) and flame ionization detector (FID) were used for separation of light hydrocarbon such as methane (CH₄), ethane (C₂H₆), propane (C₃H₈), etc.] In all cases, steady-state was reached within 6 h.

ศูนย์วิจัยทรัพยากร
จุฬาลงกรณ์มหาวิทยาลัย

RESEARCH METHODOLOGY



1. Pressure Regulator
 5. Back Pressure
 9. Furnace
 13. Heating Line

2. On-Off Valve
 6. 3-way Valve
 10. Thermocouple
 14. Bubble Flow Meter

3. Gas Filter
 7. Catalyst Bed
 11. Variable Voltage Transformer

4. Metering Valve
 8. Sampling point
 12. Temperature Controller

Figure 4.1 Flow diagram of CO hydrogenation system

CHAPTER V

RESULTS AND DISCUSSION

Supported Co catalysts are preferred for Fischer-Tropsch synthesis. The catalysts with 20 wt% Co loading were used in this study. This chapter is divided into three sections: 5.1) the study of ruthenium modified different TiO₂ crystallite size, 5.2) the study of zirconium modified different TiO₂ crystallite size. Each section consists of catalyst characterization and CO hydrogenation study and 5.3) Comparison between Ru and Zr-modified TiO₂ support in catalytic activity.

For catalyst characterization, the catalysts were characterized by several techniques such as XRD, BET, SEM, TEM, TPR, CO-pulse chemisorption, and XPS. For CO hydrogenation, the reaction was carried out at 220°C and 1 atm, CO/H₂/Ar = 20/2/8.

5.1 The Study of Ruthenium modified different TiO₂ crystallite size

5.1.1 Characterization of the Catalysts

5.1.1.1 X-ray Diffraction (XRD)

XRD patterns of titania support with different crystallite size are shown in **Figure 5.1**. They were collected at diffraction angle (2θ) between 20° and 80°, it was observed that all supports exhibited XRD peaks at 25°, 37°, 48°, 55°, 56°, 62°, 69°, 71°, and 75° assigning to anatase TiO₂. **Figure 5.2** shows the XRD patterns of Ru modified TiO₂ support. After impregnation with ruthenium, the XRD peak assigned to RuO was not observed. From the XRD results, no diffraction peaks of RuO or Ru⁰ were observed for the catalyst samples after calcinations suggesting that ruthenium was highly dispersed on the titania surface. After impregnation with the cobalt precursor, the catalysts were dried and calcined. The XRD patterns of the Ru modified

titania supported Co catalysts are shown in **Figure 5.3**. The XRD peaks of the calcined catalysts shown the characteristics of the support as shown in **Figure 5.1**, and also exhibited the XRD peaks at 31° (weak), 36° (strong), 46° (weak), and 65° (weak) which were assigned to Co_3O_4 species. **Figure 5.4** shows the XRD patterns of supported Co catalysts, which were assigned to the characteristics peaks of the TiO_2 and Co_3O_4 .

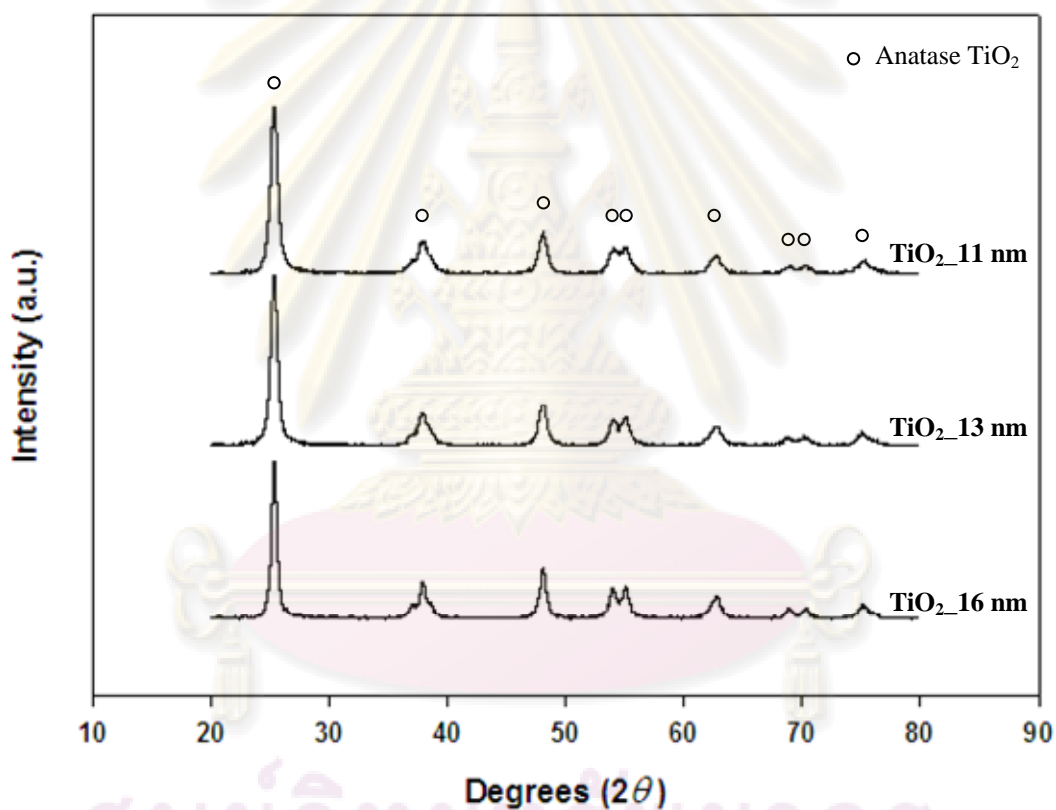


Figure 5.1 XRD patterns of different crystallite size of TiO_2 obtained from various water: alkoxide ratio

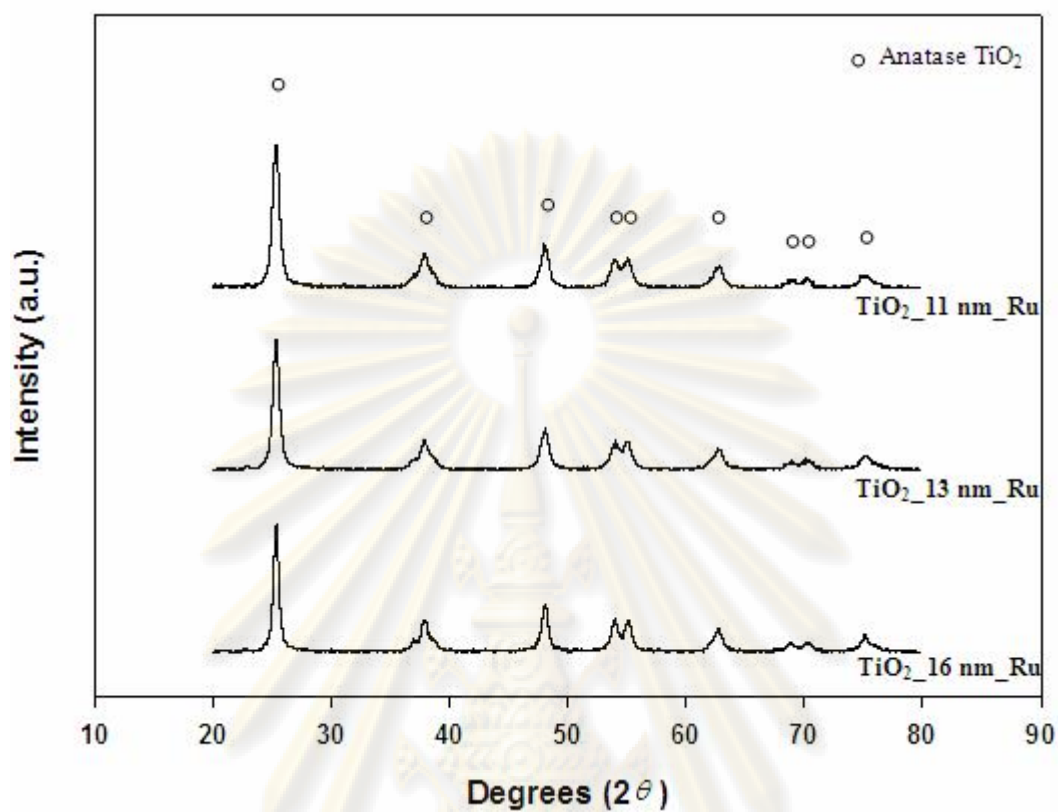


Figure 5.2 XRD patterns of Ru modified titania support

ศูนย์วิจัยทรัพยากร
จุฬาลงกรณ์มหาวิทยาลัย

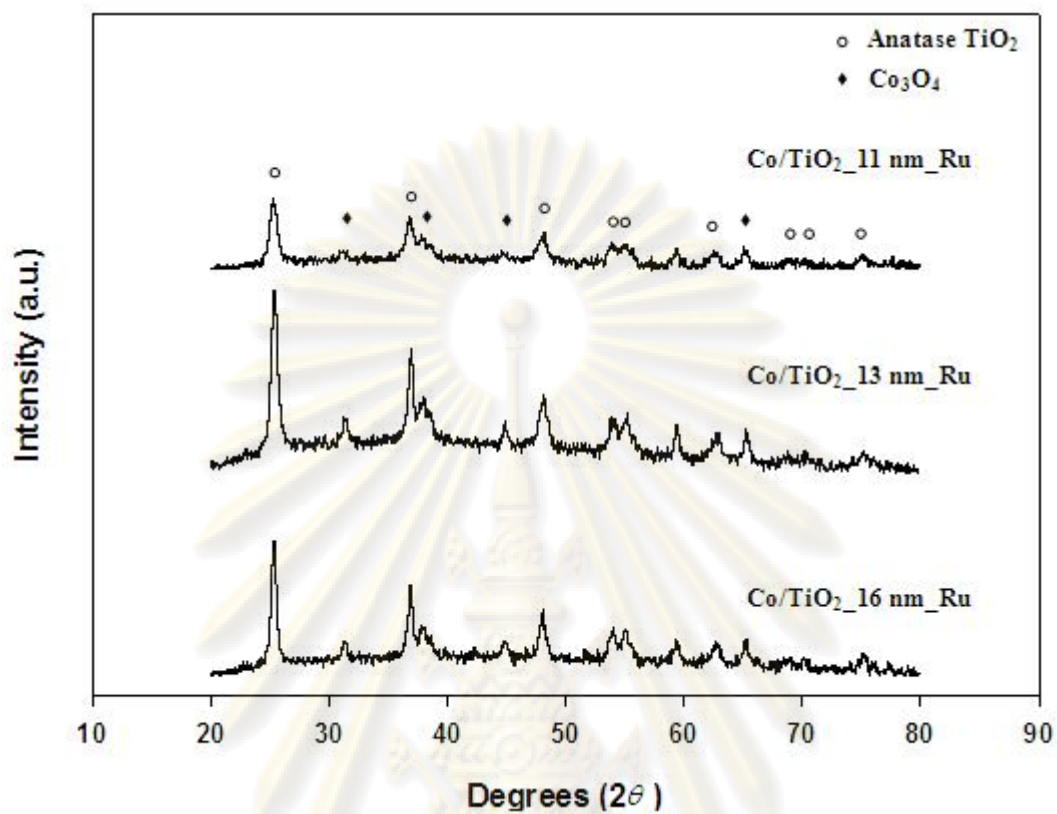


Figure 5.3 XRD patterns of Ru modified titania supported Co catalysts

ศูนย์วิจัยทรัพยากร
จุฬาลงกรณ์มหาวิทยาลัย

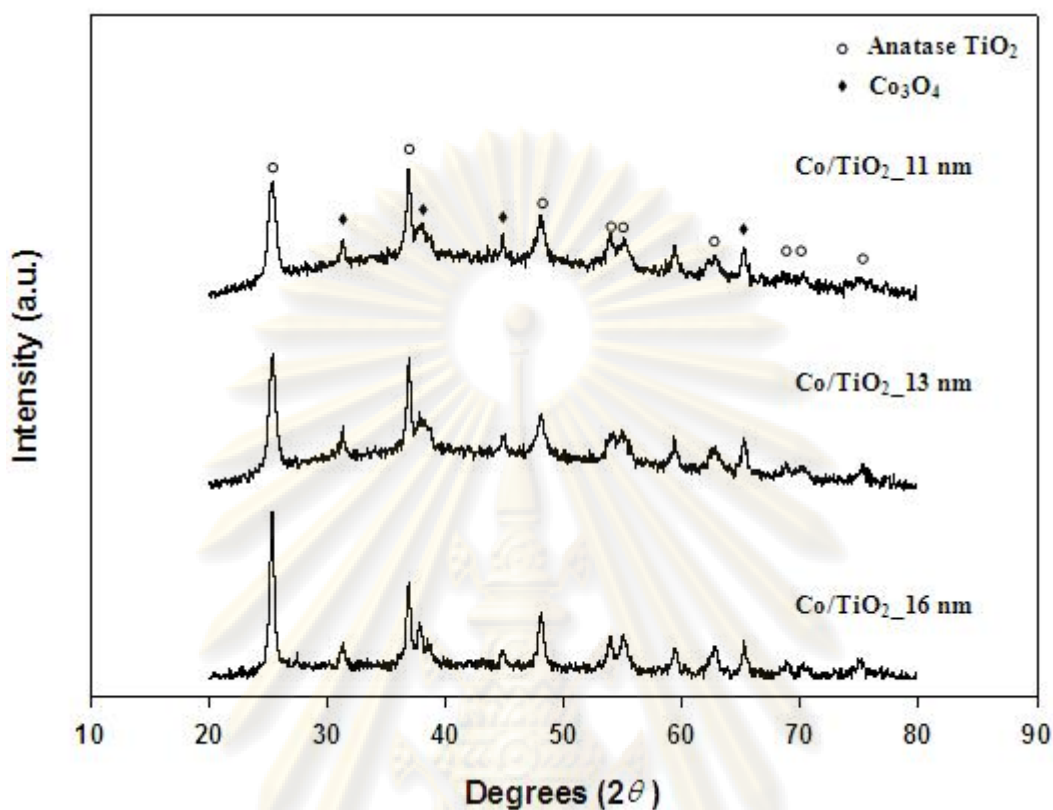


Figure 5.4 XRD patterns of unmodified TiO₂ supported Co catalysts

5.1.1.2 BET surface areas

The most common procedure for determining surface area of a solid is based on adsorption and condensation of nitrogen at liquid nitrogen temperature. This method is also called BET (Brunauer Emmett Teller) method.

BET surface areas, water: alkoxide ratio, and crystallite size of titania supports are shown in **Table 5.1**. An increase in water: alkoxide ratio in the range of 4-165 resulted in smaller crystallite size of TiO₂ and increasing in BET surface area. After calcination, BET surface areas of the TiO₂ samples decreased essentially from 71 for TiO₂_11 nm to 48 m²/g for TiO₂_16 nm.

Table 5.1 Water: alkoxide ratio, average crystallite size, and BET surface areas of titania supports

Sample	Water: alkoxide ratio	BET surface area (m ² /g)	Avg. crystallite size ^a (nm)
TiO ₂ _11 nm	165	71	11
TiO ₂ _13 nm	40	63	13
TiO ₂ _16 nm	4	48	16

^a Determined by XRD

BET surface area of the Ru modified and unmodified titania supported cobalt catalysts determined by N₂ physisorption measurement are shown in **Table 5.2**. BET surface area of the unmodified TiO₂-supported Co catalysts decreased from 52 for Co/TiO₂_11 nm to 10 m²/g for Co/TiO₂_16 nm, and BET surface area of Ru-modified TiO₂-supported Co catalysts also decreased from 47 for Co/TiO₂_11 nm_Ru to 11 m²/g for Co/TiO₂_16 nm_Ru. When compared the BET surface area of the pure titania supports and the titania supported cobalt catalysts, it was found that BET surface areas of the TiO₂-supported Co catalysts were slightly less than that of the original TiO₂ supports suggesting that cobalt was deposited in some of the pores of TiO₂.

ศูนย์วิทยทรัพยากร
จุฬาลงกรณ์มหาวิทยาลัย

Table 5.2 BET surface areas and crystallite size of Co_3O_4 of the catalysts

Catalyst sample	BET surface area (m^2/g)	Crystallite size of $\text{Co}_3\text{O}_4^{\text{a}}$ (nm)
Co/TiO ₂ _11 nm_Ru	47	8.7
Co/TiO ₂ _13 nm_Ru	36	13.9
Co/TiO ₂ _16 nm_Ru	11	15.8
Co/TiO ₂ _11 nm	52	11.0
Co/TiO ₂ _13 nm	40	14.9
Co/TiO ₂ _16 nm	10	19.5

^a Determined by XRD

5.1.1.3 Scanning electron microscopy (SEM) and Energy dispersive X-ray spectroscopy (EDX)

Scanning electron microscopy (SEM) is a powerful tool for observing directly surface texture, morphology and particle granule size of catalyst materials. In the backscattering mode (SEM), the electron beam focused on the sample is scanned by a set of deflection coil. Backscattered electrons or secondary electrons emitted from the sample are detected.

The typical SEM micrographs of various Ru modified and unmodified titania supported Co catalysts are shown in **Figure 5.5**. It was found that there was generally no significant change in elemental distribution for all samples after calcination. The morphology of the titania particles was found to be clearly seen more agglomeration of the particles with Ru modifier especially in Co/TiO₂_16 nm_Ru. The EDX mapping for Co/TiO₂_16 nm are illustrated in **Figure 5.6**. It can be seen that the Co species on the surface were in good distribution.

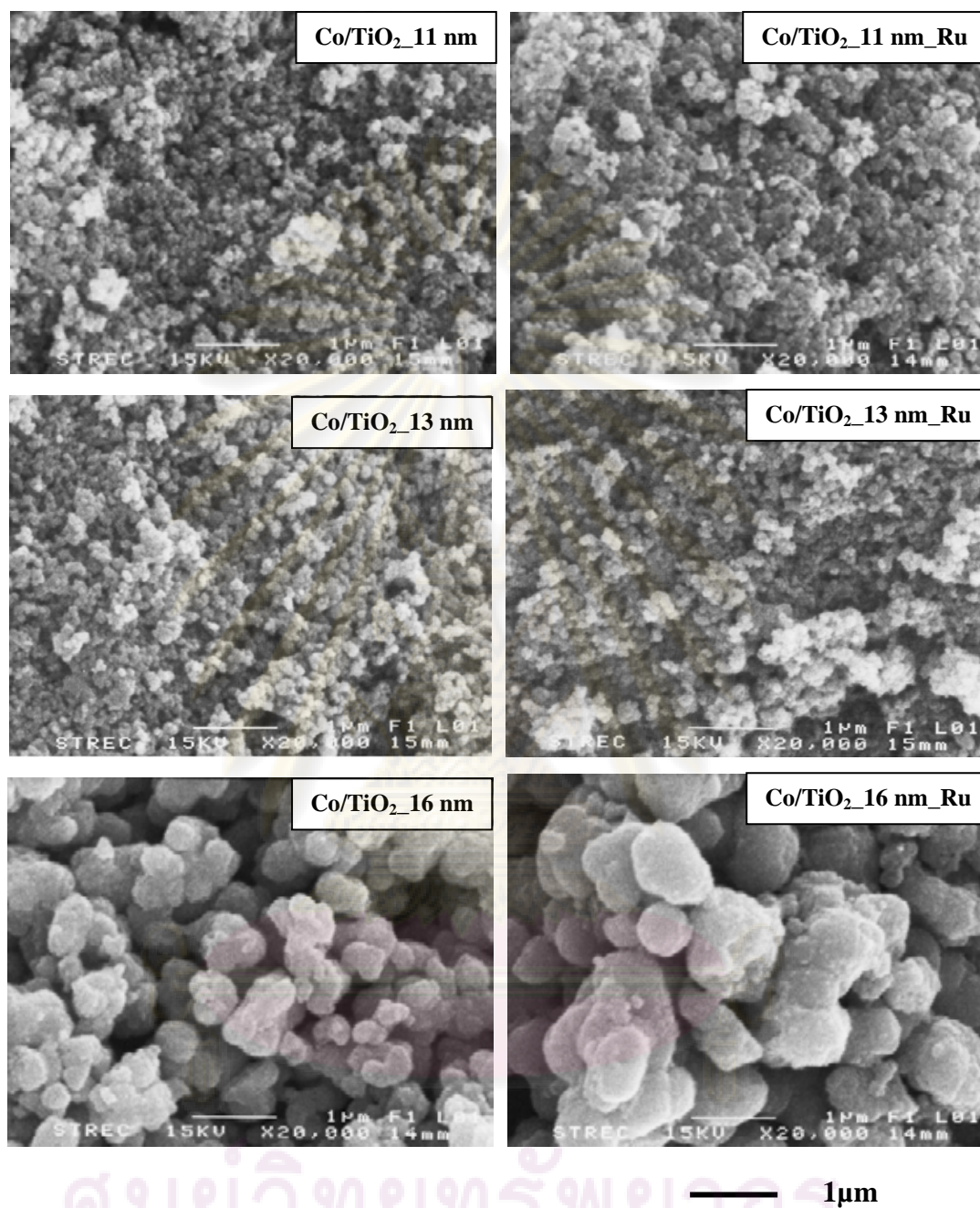


Figure 5.5 SEM micrographs for Ru modified and unmodified TiO₂ supported Co catalysts with different crystallite size

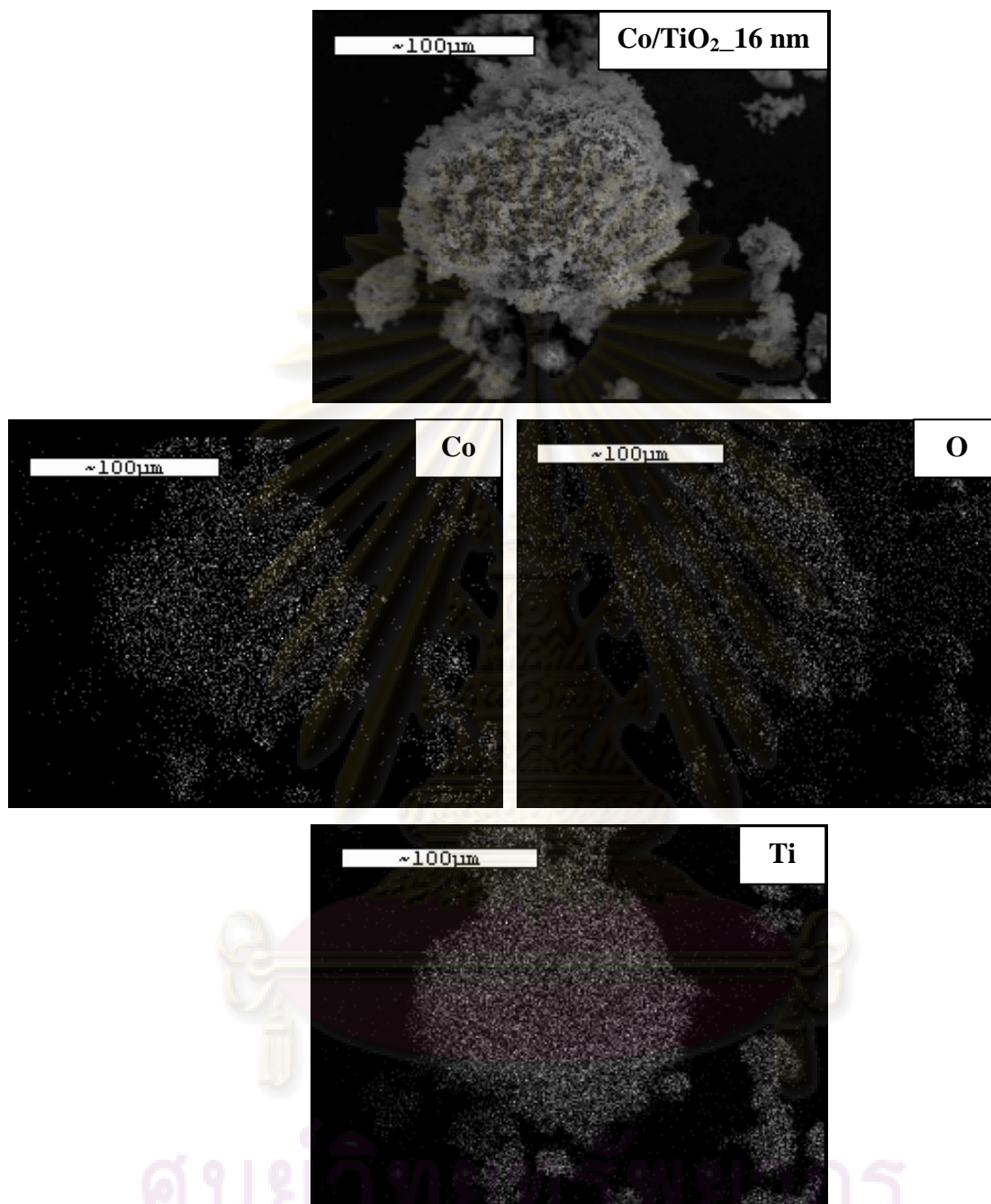


Figure 5.6 EDX mapping for Co/TiO₂_16 nm catalyst granule

ศูนย์วิจัยทรัพยากร
จุฬาลงกรณ์มหาวิทยาลัย

5.1.1.4 Transmission Electron Microscopy (TEM)

TEM is a useful tool for determining crystallite size and size distribution of supported metals. It allows determination of the micro-texture and microstructure of electron transparent samples by transmission of a focused parallel electron beam to a fluorescent screen with a resolution presently better than 0.2 nm.

TEM micrographs for Ru modified and unmodified supported cobalt catalysts are shown in **Figure 5.7**. As seen in this figure, the dark spots represented cobalt oxide species dispersing on the different supports after calcination of samples. The TEM micrographs of the catalyst using smaller crystallite size of TiO₂ exhibited the better dispersion than the larger one. It indicated that the dispersion of cobalt oxide species could be altered by the size of support used as mentioned in Kittiruangrayab et al.'s work [42].

In addition, the Ru modified TiO₂ supported cobalt catalysts showed the similar appearance with those from the unmodified TiO₂-supported cobalt catalysts. In fact, it revealed the similar dispersion of cobalt for all corresponding different size of TiO₂. The crystallite size of cobalt oxide was shown in **Table 5.2**. Although there is no clear difference between modified and unmodified supported cobalt catalysts, the crystallite size of cobalt oxide species determined from XRD was changed. The crystallite size of cobalt oxide on the modified TiO₂ cobalt catalysts were in the range of 9-16 nm, whereas those were in the range of 11-20 nm on the unmodified catalysts. In addition, with the presence of the highly dispersed form of cobalt oxide species, the interaction of those with the specified supports has to be essentially considered. Thus, temperature-programmed reduction on the calcined samples needs to be performed in order to give a better understanding according to such a reduction behavior.

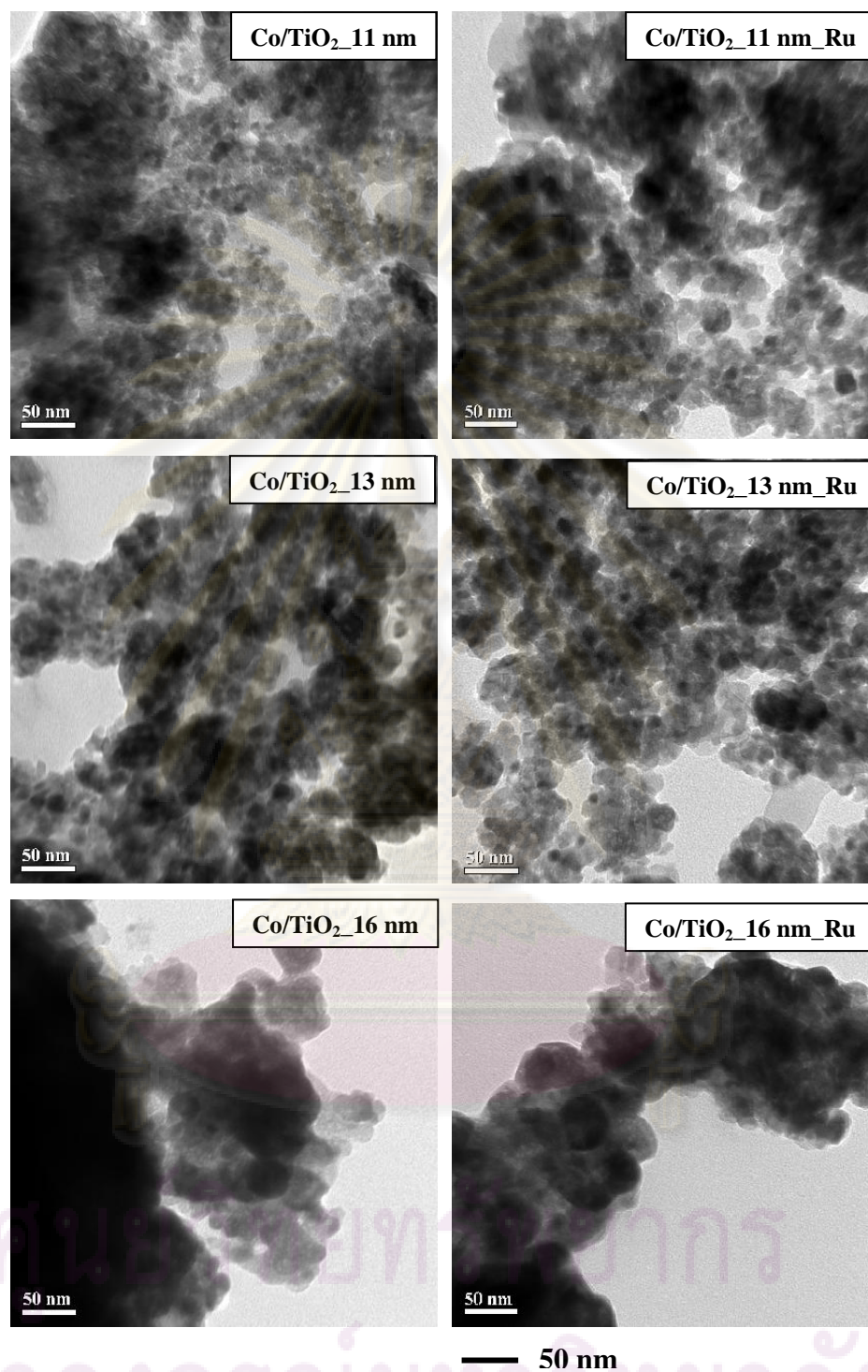


Figure 5.7 TEM micrographs of Ru modified and unmodified supported cobalt catalysts

5.1.1.5 Temperature Programmed Reduction (TPR)

The TPR profiles for all samples are shown in **Figure 5.8**. TPR was performed to determine the reduction behaviors of the samples. Reduction was observed for all catalyst samples to occur in a shoulder and one major peak. The lower reduction temperature shoulder peak of unmodified catalysts was at the 300°C (for TiO₂_16 nm) and 350°C (for TiO₂_11, 13 nm). For Co catalysts on the unmodified-TiO₂, the one broad reduction peak located at 300 to 480°C. The broad peak was related to a two-step reduction of Co₃O₄ to CoO, and then to Co metal [5, 27, 42]. There was also one shoulder and one major peak for the Co catalysts with Ru modification located at 260 and between 350 and 460°C. It would appear that the broad peak was shifted to lower temperature with Ru modification. This indicates that Ru modification caused changes in reduction behavior of the Co catalysts. In some particular case, the peak of the decomposition of the cobalt nitrates, as a cobalt precursor can be observed at the temperature between 200 and 300°C, especially on silica and alumina supports [6]. Prolonged calcination or reduction and recalcination resulted in completed decomposition of any cobalt nitrates present [6]. In addition, it has been often found that, due to interactions between Co₃O₄ and support materials, such as silica or alumina, the highest temperature peak represented the incomplete reduction of Co_xO_y-support. The TPR of supported Co₃O₄ can also manifest a separation of the two reduction steps [3, 6, 31, 42]. A lower temperature shoulder between 200 and 350°C peak was observed due to some possible decomposition of residual Co nitrate. The reduction of Co₃O₄ to CoO and Co⁰ occurred between 300 and 550°C and can be assigned to the reduction of metal oxides with the support [3, 6, 31, 42]. The strong interaction between Co metal and support depends on the size of cobalt and nature of supports [6]. This was suggested that Ru may possibly help in the reduction of Co oxide and the support to make small crystallite size, which would decrease the Co⁰ crystallite size determined from XRD measurement. These results were in accordance with those reported by Hosseini et al. [43]. It was suggested that the use of Ru modified-TiO₂_11 nm and 13 nm supports can result in lower reduction temperature due to the effect of H₂ spillover to Co₃O₄ [3]. Considering the effect of strength of

metal-support interaction, the amount of CO chemisorption which was related to the overall activity during CO hydrogenation, are changed with different interaction.

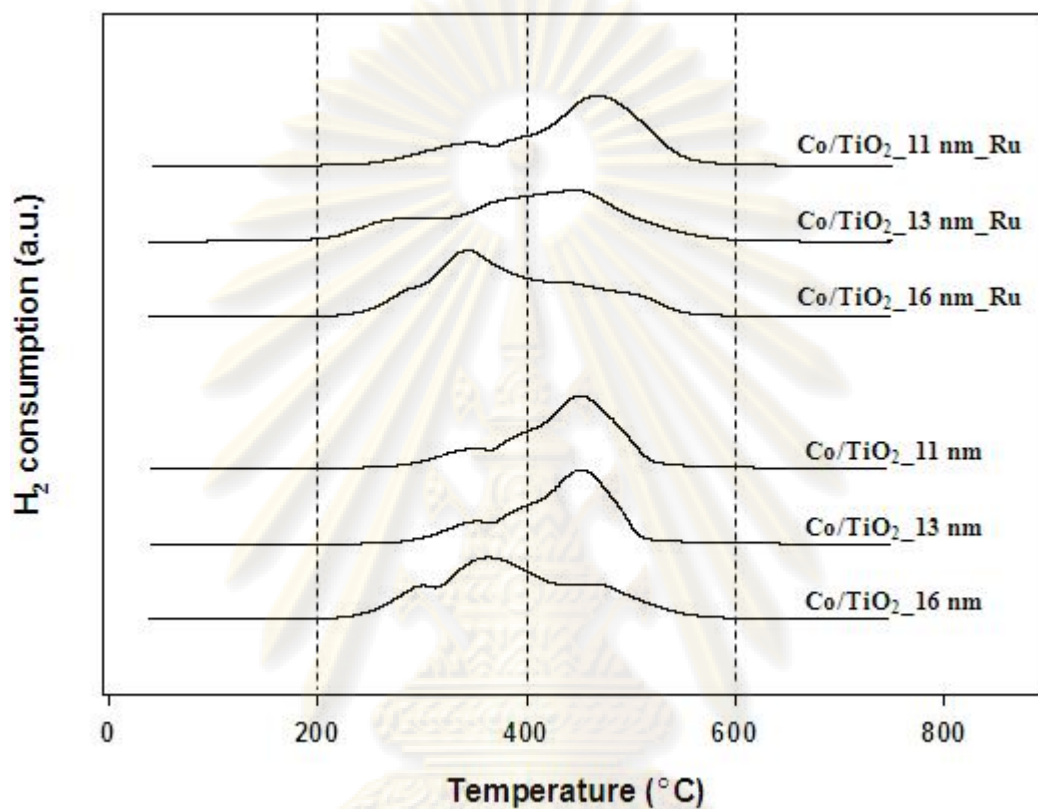


Figure 5.8 TPR profiles of Ru modified and unmodified Co catalysts with different TiO₂ crystallite size

ศูนย์วิทยทรัพยากร
จุฬาลงกรณ์มหาวิทยาลัย

5.1.1.6 CO-Pulse Chemisorption

The characterization results of CO chemisorption for the catalyst sample are illustrated in **Table 5.3**. According to **Table 5.3**, the Ru modified-TiO₂ catalysts exhibited the higher amount of CO uptake on catalytic phase within the range of 31.1 to 11.7 $\mu\text{mol CO/g}$ of catalyst, indicating the higher overall Co dispersion. It was found that the reduced cobalt metal site among three different crystallite sizes of TiO₂ was the largest for the cobalt dispersed on the smallest TiO₂ for both Ru modified and unmodified-support. It seemed that the presence of Ru in the support could result in higher number of Co metal atoms (more active site of Co catalysts). In general, the catalysts with a higher BET surface area exhibits chemisorption and Co dispersion. Consequently, in order to eliminate the effect of BET from the effect of crystallite size, we reported in term of CO chemisorption per unit surface area. It was found that CO chemisorption/BET was increased with increasing crystallite size.

Table 5.3 CO chemisorption results of cobalt catalysts

Sample	CO chemisorption				CO chemisorption/ BET surface area ($\mu\text{mol CO/g.cat/m}^2$)
	Active site ($\times 10^{-18}$ site/g.cat)	Total CO chemisorption ($\mu\text{mol CO/g.cat}$)	% Co Dispersion ^a	Active metal surface area ($\text{m}^2/\text{g.metal}$)	
Co/TiO ₂ _11 nm_Ru	18.7	31.1	4.6	6.9	0.662
Co/TiO ₂ _13 nm_Ru	14.6	24.3	5.1	5.4	0.675
Co/TiO ₂ _16 nm_Ru	7.0	11.7	1.8	2.6	1.064
Co/TiO ₂ _11 nm	13.9	23.1	3.5	5.3	0.444
Co/TiO ₂ _13 nm	12.9	21.4	3.3	4.5	0.535
Co/TiO ₂ _16 nm	4.0	6.7	1.0	1.5	0.670

^a Co metal dispersion (%) = $[1 \times (\text{total CO chemisorption/g.cat})/(\text{no.}\mu\text{mol Co tot./g.cat})] \times 100\%$. [5]

5.1.1.7 X-ray Photoelectron Spectroscopy (XPS)

XPS analysis were carried out to examine the surface species on the cobalt catalysts and also to determine the relative amount of element on the surface. The samples were analyzed in the Co 2p, Ti 2p, O1s, Ru 3d with regards to the binding energy regions. The peaks of Ru 3d would be detected around 280 eV [22, 44-45], but there was no observation of the Ru 3d due to very small amount of Ru loading. The binding energy values corresponding to Co 2p and Ti 2p were hardly affected by the small amount of Ru modification with the values at ~780 eV and ~459.1 eV, respectively. The binding energy, the percentages of atomic concentration, and FWHM of Co 2p_{3/2} and Ti 2p are also given in **Table 5.4**. The atomic concentrations of Co on Ru modified supported catalysts were higher than that on unmodified supported catalysts. The lower surface concentration of cobalt after loaded Ru were in accordance with those reported by Infantes-Molina et al. [44] and Reinikainen et al. [22]. The deconvoluted XPS spectra for the Co 2p_{3/2} core level region of cobalt catalysts on TiO₂_11, 13, and 16 nm are shown in **Figure 5.9-Figure 5.11**.

Table 5.4 Binding energy and surface composition of Ru modified and unmodified Co catalysts

Sample	Co(II) 2p _{3/2}		Ti 2p		Atomic Conc%		
	B.E. (eV)	FWHM	B.E. (eV)	FWHM	Co	Ti	O
Co/TiO ₂ _11 nm_Ru	781.5	2.698	459.9	2.087	1.77	6.41	45.93
Co/TiO ₂ _13 nm_Ru	780.4	3.040	459.1	1.575	1.12	6.50	43.26
Co/TiO ₂ _16 nm_Ru	780.9	2.447	459.1	1.604	4.51	1.88	38.04
Co/TiO ₂ _11 nm	781.5	7.453	459.1	1.688	0.65	3.45	33.37
Co/TiO ₂ _13 nm	780.2	3.078	459.1	1.498	1.25	6.59	41.6
Co/TiO ₂ _16 nm	780.0	2.369	458.9	1.129	1.62	0.36	28.13

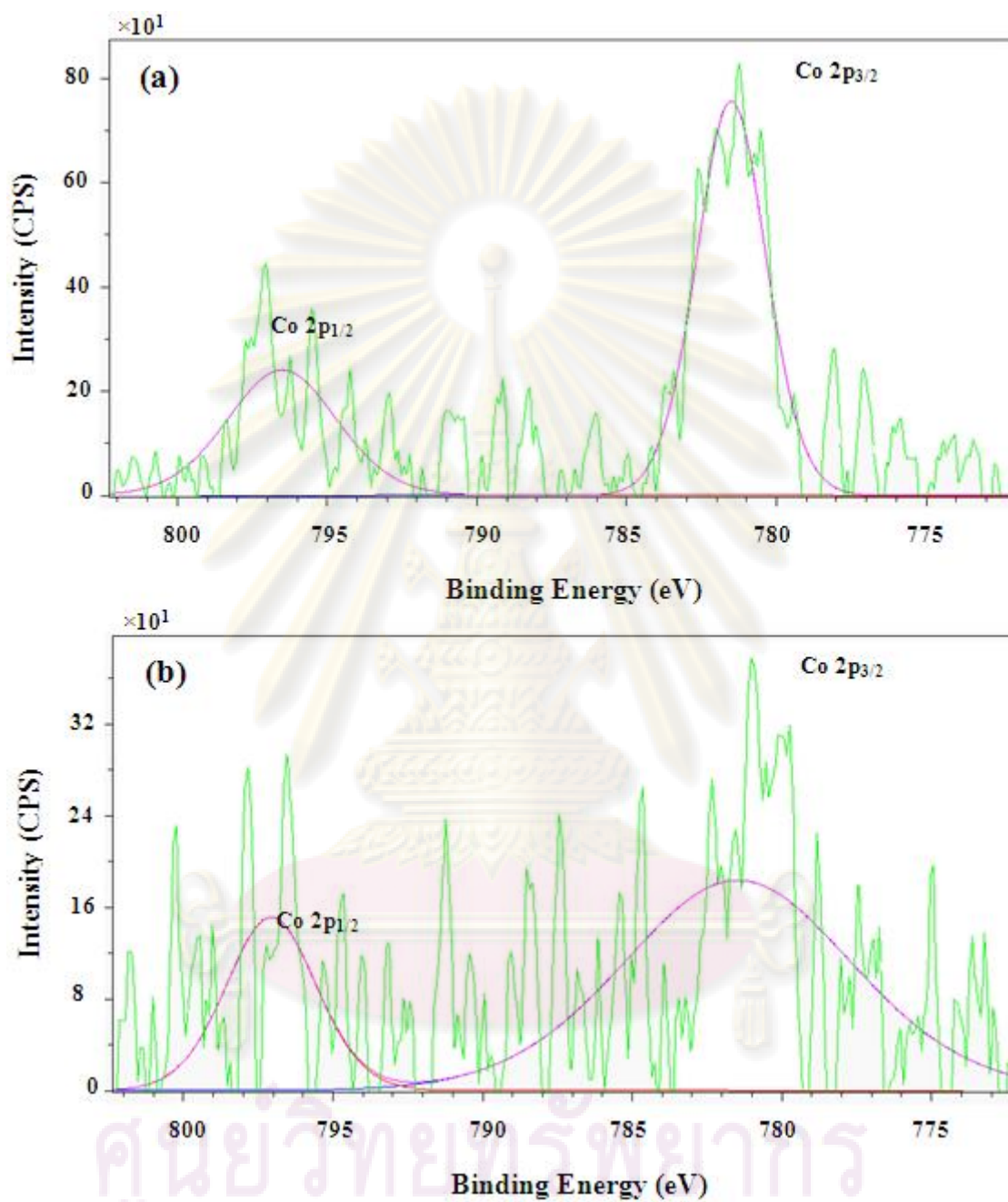


Figure 5.9 The deconvolution of XPS spectra of Ru modified and unmodified supported cobalt catalyst (a) Co/TiO₂_11 nm_Ru (b) Co/TiO₂_11 nm

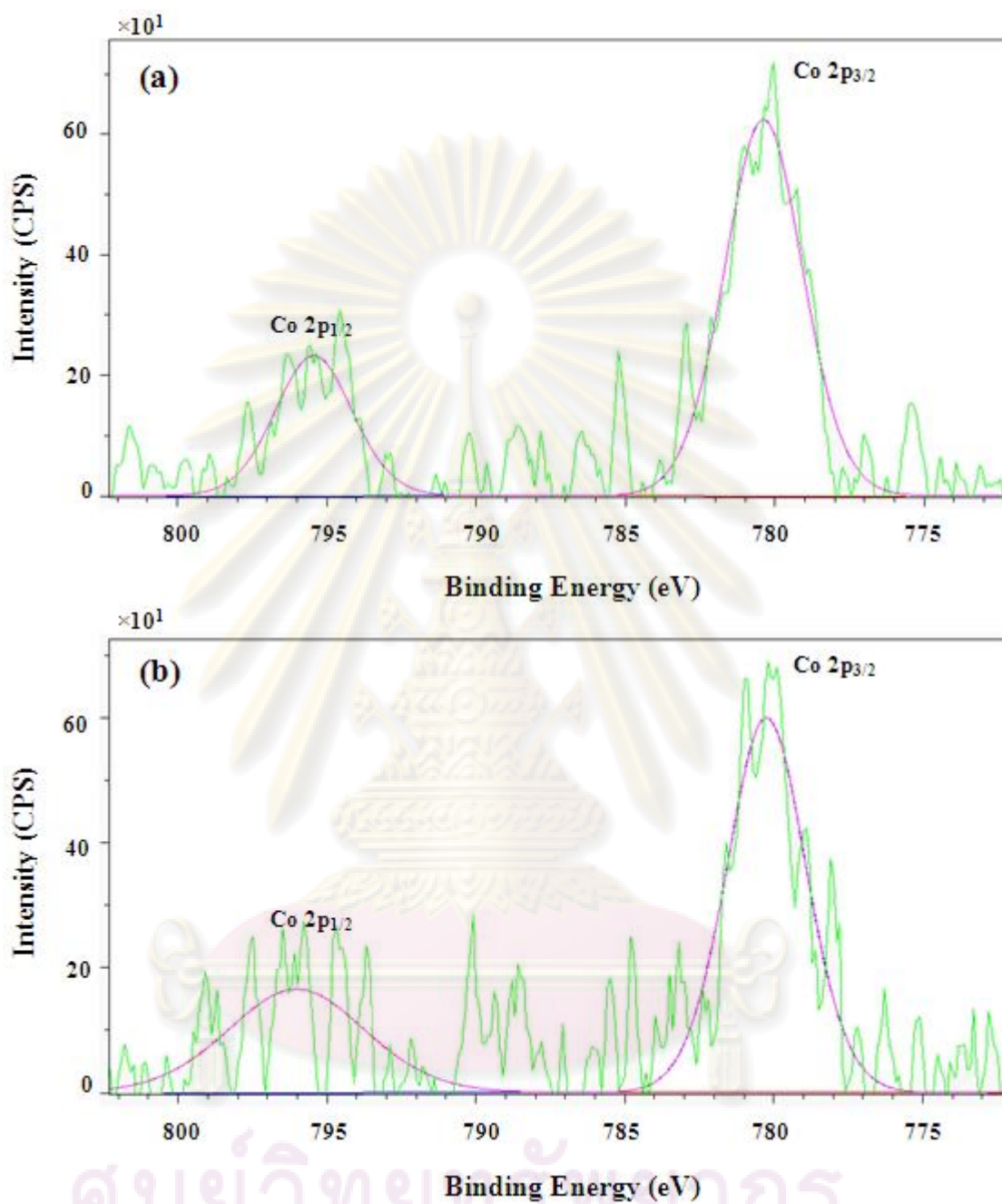


Figure 5.10 The deconvolution of XPS spectra of Ru modified and unmodified supported cobalt catalyst (a) Co/TiO₂_13 nm_Ru (b) Co/TiO₂_13 nm

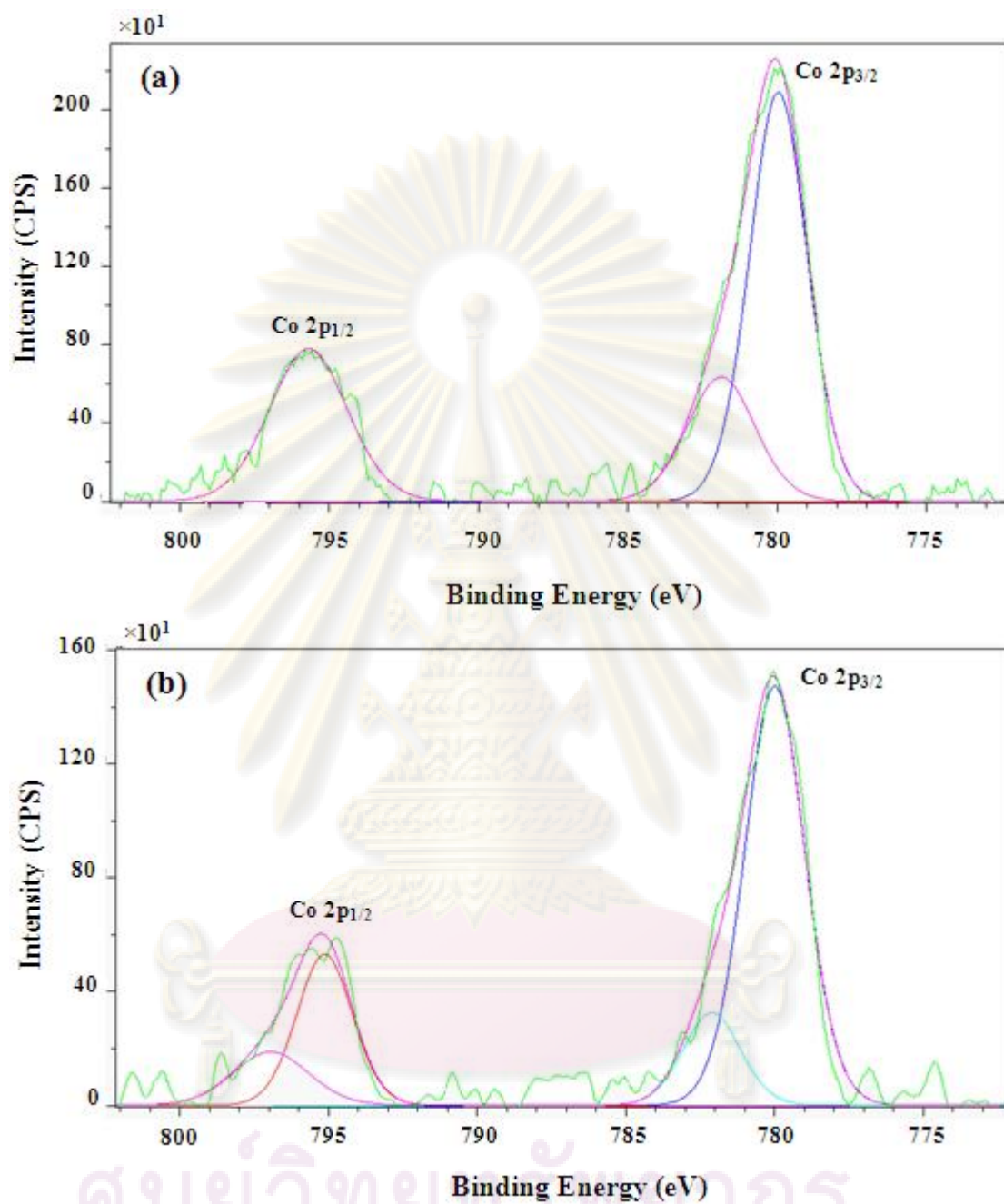


Figure 5.11 The deconvolution of XPS spectra of Ru modified and unmodified supported cobalt catalyst (a) Co/TiO₂_16 nm_Ru (b) Co/TiO₂_16 nm

5.1.2 Reaction study

The reaction study was carried out in CO hydrogenation to determine the overall activity of the catalyst samples. First, the catalysts were reduced in H₂ at 350°C for 3 h in a fixed-bed flow reactor. Then, the reaction test was carried out with flow rate of H₂/CO/Ar = 20/2/8 cm³/min. The conversion, reaction rate, TOF (based on the number of reduced surface cobalt atoms measured from CO chemisorption), and product selectivity during CO hydrogenation at steady-state are given in **Table 5.5**. The conversion of the Co catalysts on unmodified-TiO₂ obviously changed when using different sizes of TiO₂. The rate of these catalysts decreased with larger size of TiO₂, and slightly decreased in C₁ selectivity. Similarly, the cobalt catalyst on the Ru modified support exhibited the higher activity and C₁ selectivity than that on the unmodified support in all crystallite sizes of TiO₂ with slightly change in product selectivity. For the Co catalyst on Ru modified-TiO₂, it can be observed that the size of TiO₂ hardly effected to product selectivity of C₁, but there was moderate change in conversion. The rate vs. time on stream of the modified and unmodified-TiO₂ Co catalysts is illustrated in **Figure 5.10**. The rate of the modified catalysts decreased with increasing of crystallite size of TiO₂. It can be say that the similar trend regarding the activity and product selectivity can be observed in both Ru modified and unmodified support. The increased activity for Ru modified supported cobalt catalysts can be attributed to the dispersion of Co metal on the catalysts as seen from CO chemisorption and TPR results. When considered the difference in rate between the modified and unmodified catalysts of support TiO₂_11 nm, 13 nm, and 16 nm, it was found that the larger crystallite size of TiO₂ showed the distinguish difference in rate of the reaction. The results indicated that Ru modification on support TiO₂ have an effect on the larger crystallite size of TiO₂ more than the smaller ones. Since CO hydrogenation is a structure insensitive reaction, therefore the catalytic activity depends only on the number of reduced Co metal surface atoms available for catalyzing the reaction [42]. The calculated TOFs at steady state of the samples are summarized in **Table 5.5**. They are in the range of 1×10⁻² s⁻¹-typical of Co catalyst under this condition [3, 5, 42]. Considered TOFs calculated based on CO chemisorption of the catalysts, it was found that TOFs of Co catalysts on the Ru

modified and unmodified TiO₂ can be considered essentially similar. Since TOF can be derived from the intrinsic rate by definition, indicating that the intrinsic activity of the samples remain constant. However, there were found that Ru leads to higher specific activities as seen in other studies [3, 10]. The size of TiO₂ also plays an important role on the catalytic activity of the catalysts e.g. the reaction rate decreased when using the larger particle size of TiO₂.

There are many variables that can be effect the kinetic of the reaction such as particle size, support interaction, and the reduction gas composition [42]. There have been found that the particle size of support related to the strength of metal-support interaction [42]. Thus, we may conclude that the particle size of TiO₂ also affected to the size of Co oxide species.

Table 5.5 Activity and product selectivity of Ru modified and unmodified Co catalyst

Sample	Conversion ^a (%)		Rate ^c (×10 ⁻² g CH ₂ /g cat.h)	TOF ^d (× 10 ³ s ⁻¹)	Product selectivity ^c (%)	
	initial ^b	Steady state ^c			C ₁	C ₂ -C ₄
Co/TiO ₂ _11 nm_Ru	94.5	90.9	68	5.8	97.1	2.9
Co/TiO ₂ _13 nm_Ru	79.3	88.9	67	10.4	99.0	1.0
Co/TiO ₂ _16 nm_Ru	91.1	77.0	58	13.1	99.0	1.0
Co/TiO ₂ _11 nm	94.8	76.9	58	6.9	96.9	3.1
Co/TiO ₂ _13 nm	58.2	49.2	37	4.6	93.5	6.5
Co/TiO ₂ _16 nm	66.9	31.7	24	9.6	93.7	6.3

^a CO hydrogenation was carried out at 220 °C, 1 atm, and H₂/CO/Ar = 20/2/8, GSHV= 11400 h⁻¹.

^b After 5 min of reaction.

^c After 5 h of reaction.

^d The TOF calculation was based on CO chemisorption

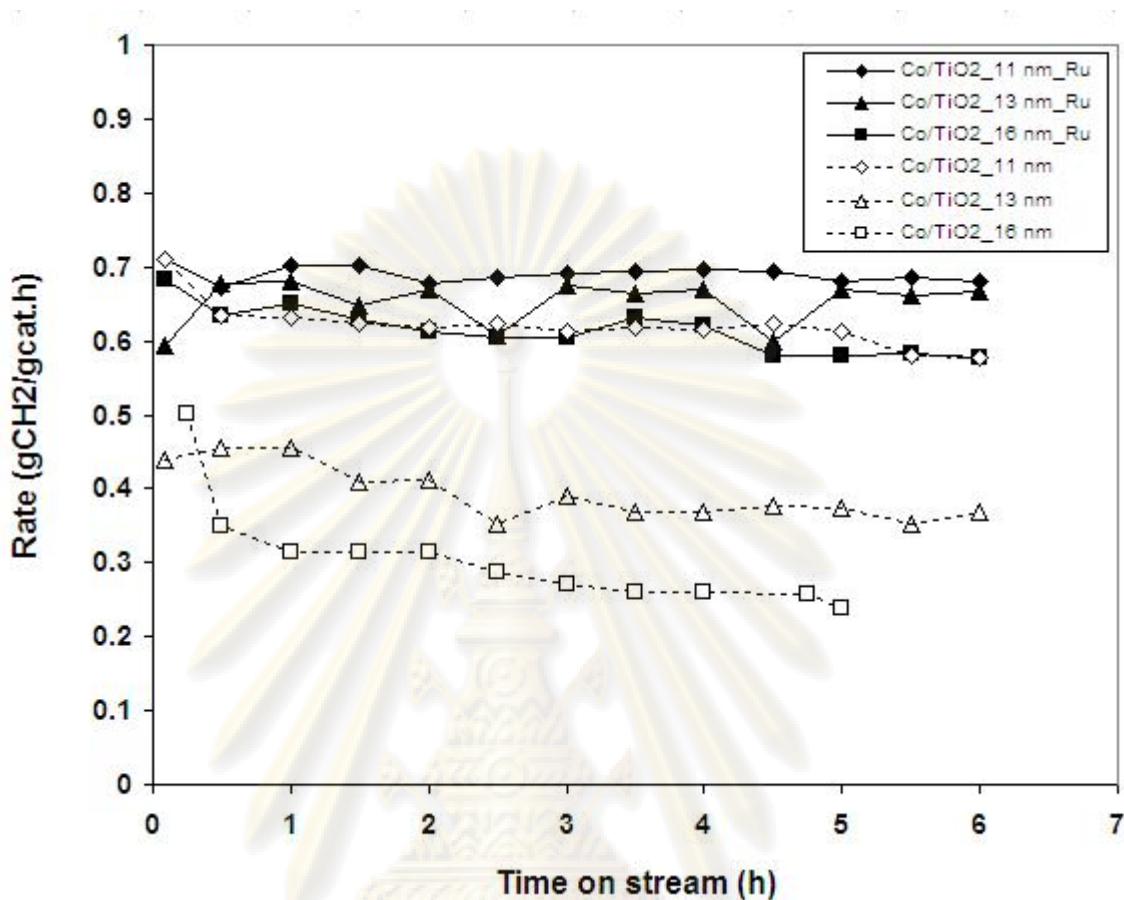


Figure 5.12 Reaction rate vs. time on stream of Ru modified and unmodified Co catalysts with different crystallite size of TiO₂

ศูนย์วิจัยทรัพยากร
จุฬาลงกรณ์มหาวิทยาลัย

5.2 The Study of Zirconium modified different TiO₂ crystallite size

5.2.1 Characterization of the catalysts

5.2.1.1 X-ray Diffraction (XRD)

The XRD patterns of Zr modified TiO₂ supports are shown in **Figure 5.13**. The diffraction peaks of ZrO were not observed for the catalyst samples after calcinations suggesting that zirconia was highly dispersed on the titania surface. After impregnation with the cobalt precursor, the catalysts were dried and calcined. **Figure 5.14** shows the XRD patterns of Zr-modified supported Co catalysts. The XRD peaks of the calcined catalysts shown the characteristics of thTiO₂ support and also exhibited the XRD peaks at 31° (weak), 36° (strong), 46° (weak), and 65° (weak) which were assigned to Co₃O₄ species.

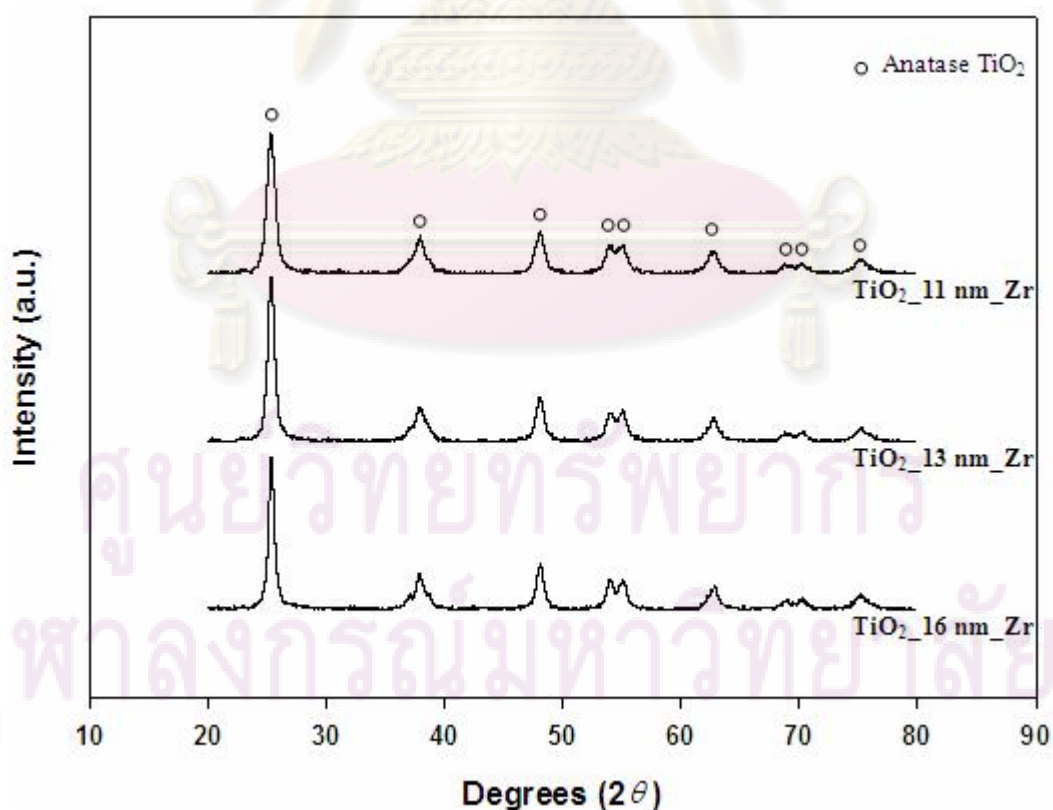


Figure 5.13 XRD patterns of Zr modified titania support

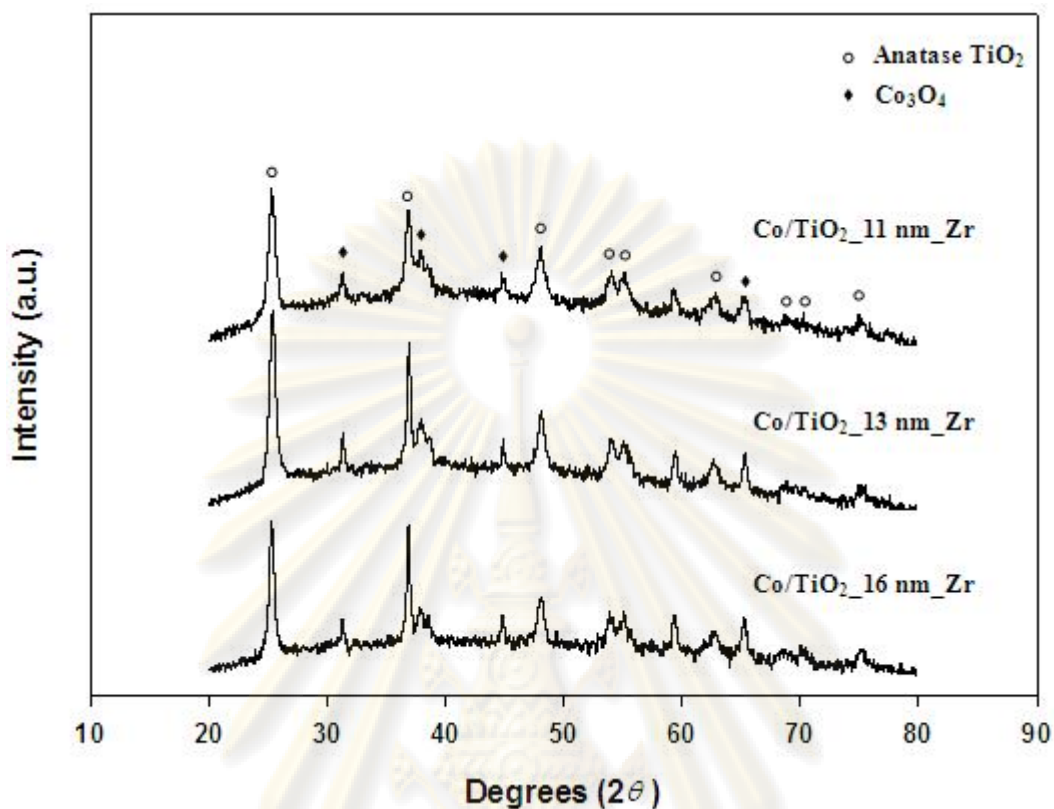


Figure 5.14 XRD patterns of Zr modified titania supported Co catalysts

5.2.1.2 BET surface areas

After modification with 0.3 wt% of Zr, the modified TiO₂ supports were impregnated with 20 wt% of Co. The BET surface areas of the catalyst samples are shown in **Table 5.6**. The zirconium modified cobalt catalysts showed decreases in surface areas. It can be observed that the surface areas of the catalyst samples gradually decreased with increased crystallite size of titania employed.

จุฬาลงกรณ์มหาวิทยาลัย

Table 5.6 BET surface areas and crystallite size of Co_3O_4 of the catalysts

Catalyst sample	BET surface area (m^2/g)	Crystallite size of $\text{Co}_3\text{O}_4^{\text{a}}$ (nm)
Co/TiO ₂ _11 nm_Zr	40	7.3
Co/TiO ₂ _13 nm_Zr	32	20.3
Co/TiO ₂ _16 nm_Zr	12	24.8
Co/TiO ₂ _11 nm	52	11.0
Co/TiO ₂ _13 nm	40	14.9
Co/TiO ₂ _16 nm	10	19.5

^a Determined by XRD

5.2.1.3 Scanning electron microscopy (SEM) and Energy dispersive X-ray spectroscopy (EDX)

A typical SEM micrograph for the Zr modified and unmodified supported cobalt catalyst samples are illustrated in **Figure 5.15**. Although there was generally no significant change in elemental distribution for all samples after calcination, there were some changes in morphologies (i.e. more agglomeration) for the larger crystalline TiO₂ (Co/TiO₂_16 nm_Zr). The EDX mapping for Co/TiO₂_16 nm_Zr are illustrated in **Figure 5.16**. From EDX mapping for all samples, it indicated that the Co oxide species exhibited well distribution throughout the catalyst granules.

จุฬาลงกรณ์มหาวิทยาลัย

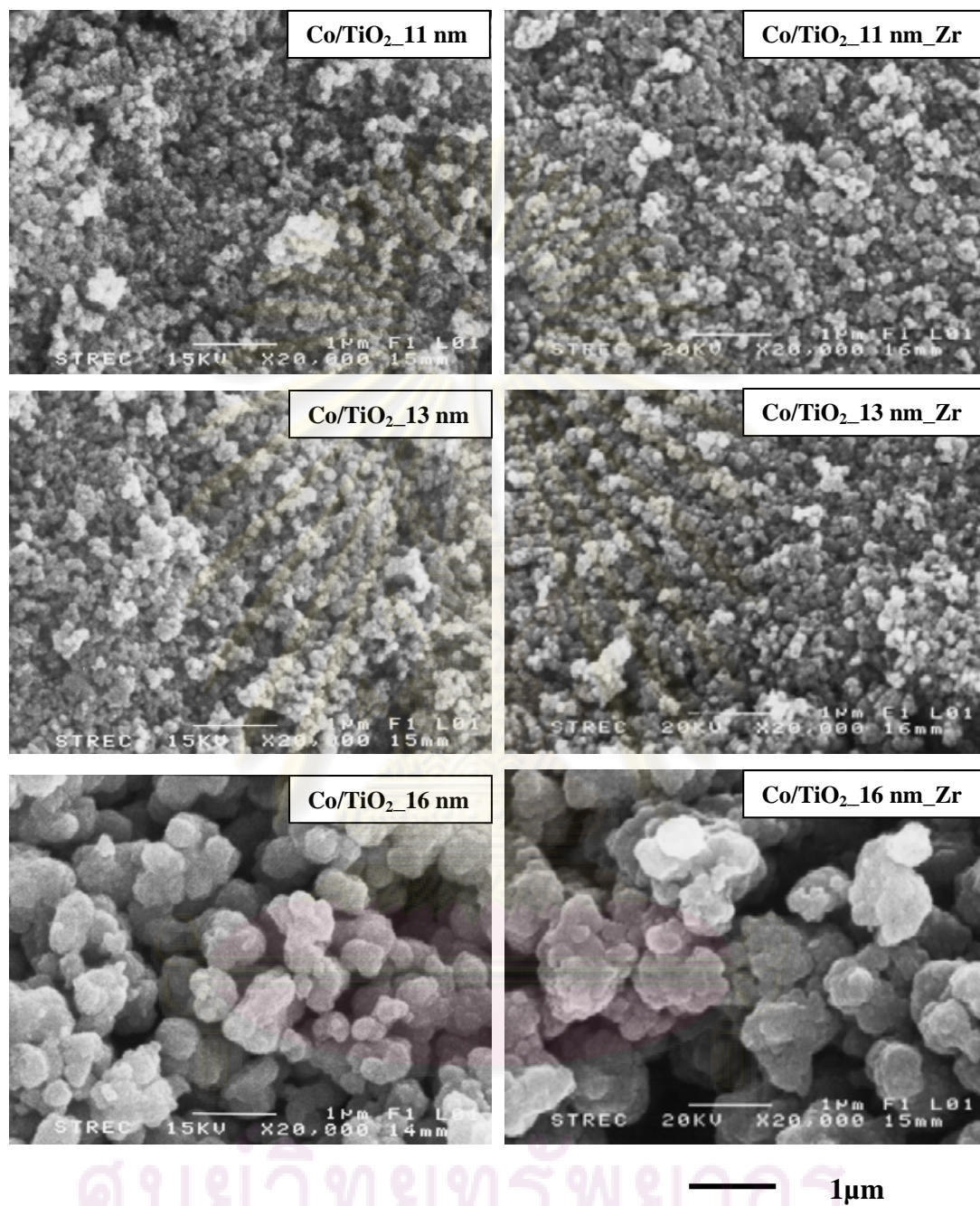


Figure 5.15 SEM micrographs for Zr modified and unmodified TiO₂ supported Co catalysts with different crystallite size

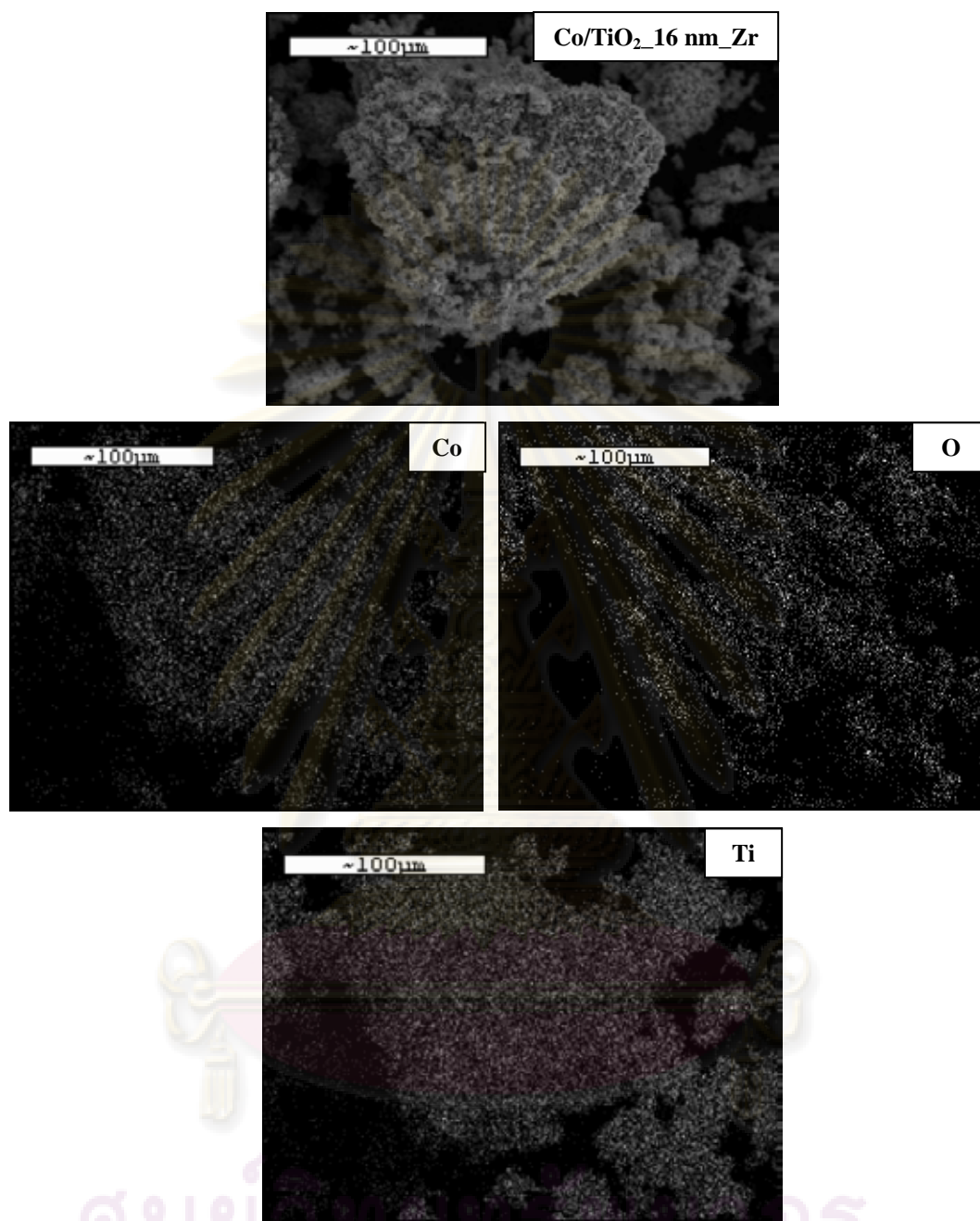


Figure 5.16 EDX mapping for Co/TiO₂_16 nm_Zr catalyst granule

ศูนย์เทคโนโลยีสารสนเทศ
จุฬาลงกรณ์มหาวิทยาลัย

5.2.1.4 Transmission Electron Microscopy (TEM)

The typical TEM micrographs of Zr modified and unmodified cobalt catalysts are shown in **Figure 5.17**. The dark spots represented cobalt oxide species dispersing on the different supports after calcination of samples. The TEM micrographs of the catalyst using smaller crystallite size of TiO₂ exhibited the better dispersion than the larger one. It indicated that the dispersion of cobalt oxide species could be altered by the size of support used. In addition, the Zr modified TiO₂ supported cobalt catalysts showed the similar appearance with those from the unmodified TiO₂-supported cobalt catalysts. In fact, it revealed the similar dispersion of cobalt for all corresponding different size of TiO₂. The crystallite size of cobalt oxide determined from XRD was shown in **Table 5.6**. Although there is no clear difference between modified and unmodified supported cobalt catalysts, the crystallite size of cobalt oxide species was changed. The crystallite size of cobalt oxide on the modified TiO₂ cobalt catalysts were in the range of 7-25 nm, whereas those were in the range of 11-20 nm on the unmodified catalysts. These results are according with those obtained from A. Feller et al. [32], they found that Co crystallite size increased with increasing zirconium content. In addition, with the presence of the highly dispersed form of cobalt oxide species, the interaction of those with the specified supports has to be essentially considered.

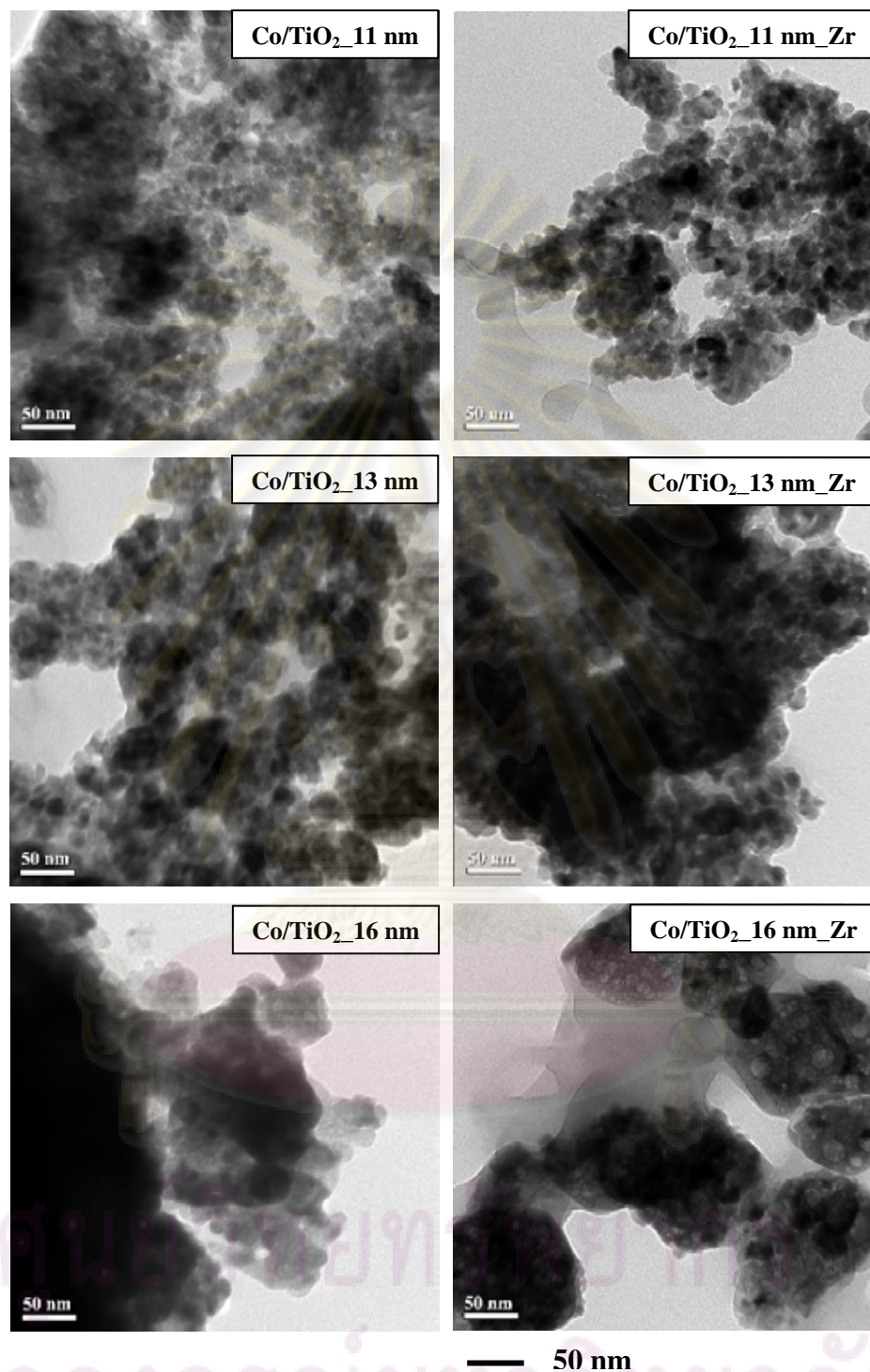


Figure 5.17 TEM micrographs of Zr modified and unmodified supported cobalt catalysts

5.2.1.5 Temperature Programmed Reduction (TPR)

The TPR profiles for all samples are shown in **Figure 5.18**. TPR was performed to determine the reduction behaviors of the samples. Reduction was observed for all catalyst samples to occur in a shoulder and one major peak. The lower reduction temperature shoulder peak of unmodified catalysts was at the 300°C (for TiO₂_16 nm) and 350°C (for TiO₂_11, 13 nm). For Co catalysts on the unmodified-TiO₂, the one broad reduction peak located at 300 to 500°C. The broad peak was related to a two-step reduction of Co₃O₄ to CoO, and then to Co metal [5, 27, 42]. There was also one shoulder and one major peak for the Co catalysts with Zr modification located at 300 and between 400 and 600°C. It would appear that the broad peak was shifted to higher temperature with Zr modification. This indicates that Zr modification caused changes in reduction behavior of the Co catalysts. In some particular case, the peak of the decomposition of the cobalt nitrates, as a cobalt precursor can be observed at the temperature between 200 and 300°C, especially on silica and alumina supports [6]. Prolonged calcination or reduction and recalcination resulted in completed decomposition of any cobalt nitrates present [6]. In addition, it has been often found that, due to interactions between Co₃O₄ and support materials, such as silica or alumina, the highest temperature peak represented the incomplete reduction of Co_xO_y-support. The TPR of supported Co₃O₄ can also manifest a separation of the two reduction steps [3, 6, 31, 42]. A lower temperature shoulder between 200 and 350°C peak was observed due to some possible decomposition of residual Co nitrate. The reduction of Co₃O₄ to CoO and Co⁰ occurred between 400 and 600°C and can be assigned to the reduction of metal oxides with the support [3, 6, 31, 42]. A separation of the two reduction steps has often been found for supported cobalt catalysts due to interactions between cobalt and support materials [5]. The strong interaction between Co metal and support depends on the size of cobalt and nature of supports [6]. Based on the TPR profiles, it indicated that Zr inhibited the reduction of Co oxide species, which accordance with those reported by Wongsalee et al. [33] and Jongsomjit et al. [29]. According to Jongsomjit et al. [29] they found that Zr modification decreased the impact of water vapor during reduction (results in

lower reducibility for an unpromoted Co catalysts), possibly by partially blocking Co ‘aluminate’ form. In this case, it might be possibly that Zr help to produce the Co_xO_y -support. It was suggested that the use of Zr modified- TiO_2 _11 nm and 13 nm supports can result in higher reduction temperature of Co oxides due to the strong metal-support interaction. It was also found that the presence of nano- ZrO_2 in the mixed supports could result in increased reduction temperature of Co oxides due to the strong metal support interaction [46]. Considering the effect of strength of metal-support interaction, the amount of CO chemisorption which was related to the overall activity during CO hydrogenation, are changed with different interaction.

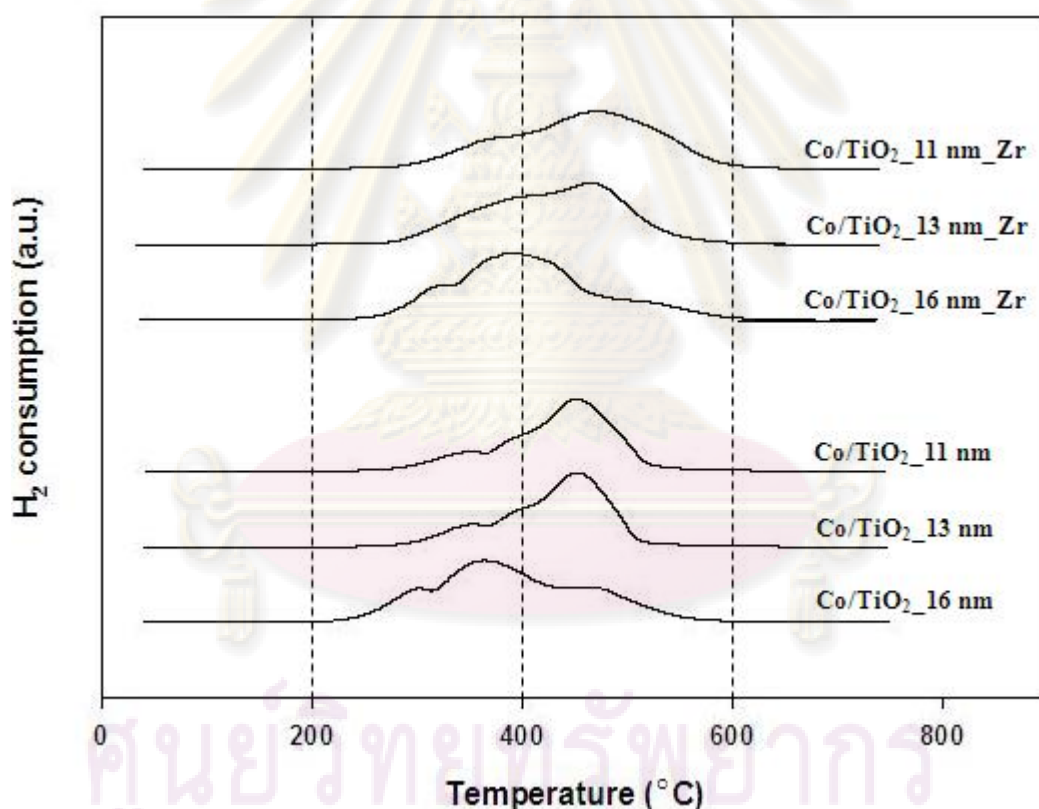


Figure 5.18 TPR profiles of Zr modified and unmodified Co catalysts with different TiO_2 crystallite size

5.2.1.6 CO-Pulse Chemisorption

The characterization results of CO chemisorption for the catalyst sample are illustrated in **Table 5.7**. According to **Table 5.7**, the Zr modified-TiO₂ catalysts exhibited the higher amount of CO uptake on catalytic phase within the range of 29.0 to 9.5 $\mu\text{mol CO/g}$ of catalyst, indicating the higher overall Co dispersion. It was found that the reduced cobalt metal atom was the largest for the cobalt dispersed on the smallest TiO₂ both Zr modified and unmodified-support. It seemed that the presence of Zr in the support could result in more number of Co metal atom (more active site of Co catalysts). In general, the catalysts with a higher BET surface area exhibits chemisorption and Co dispersion. Consequently, in order to eliminate the effect of BET from the effect of crystallite size, we reported in term of CO chemisorption per unit surface area. It was found that CO chemisorption/BET was increased with increasing crystallite size, which this result was accordance with Kongsuebchart et al. [47]. Although the trend of CO chemisorption/BET was similar to Kongsuebchart et al. [47], the Co dispersion was different. The larger crystallite sizes exhibited the lower Co dispersion, but they had amount of CO chemisorption per unit surface area more than the smaller ones.



ศูนย์วิจัยทรัพยากร
จุฬาลงกรณ์มหาวิทยาลัย

Table 5.7 CO chemisorption results of the cobalt catalysts

Sample	CO chemisorption				CO chemisorption/ BET surface area ($\mu\text{mol CO}$ /g.cat/ m^2)
	Active site ($\times 10^{-18}$ site/g.cat)	Total CO chemisorption ($\mu\text{mol CO/g.cat}$)	%Co Dispersion ^a	Active metal surface area ($\text{m}^2/\text{g.metal}$)	
Co/TiO ₂ _11 nm_Zr	17.4	29.0	4.3	6.5	0.725
Co/TiO ₂ _13 nm_Zr	14.1	23.4	3.5	6.1	0.731
Co/TiO ₂ _16 nm_Zr	5.7	9.5	1.4	2.1	0.792
Co/TiO ₂ _11 nm	13.9	23.1	3.5	5.3	0.444
Co/TiO ₂ _13 nm	12.9	21.4	3.3	4.5	0.535
Co/TiO ₂ _16 nm	4.0	6.7	1.0	1.4	0.670

^a Co metal dispersion (%) = $[1 \times (\text{total CO chemisorption/g.cat})/(\text{no.}\mu\text{mol Co tot./g.cat})] \times 100\%$. [5]

5.2.1.7 X-ray Photoelectron Spectroscopy (XPS)

XPS analysis were carried out to examine the surface species on the cobalt catalysts and also to determine the relative amount of element on the surface. The samples were analyzed in the Co 2p, Ti 2p, O1s, Zr 3d with regards to the binding energy regions. The peaks of Zr 3d would be detected around 179.2 eV [48], but there was no observation of the Zr 3d due to very small amount of Zr loading. The binding energy values corresponding to Co 2p and Ti 2p were hardly affected by the small amount of Zr modification with the values at ~780 eV and ~459 eV, respectively. The binding energy, the percentages of atomic concentration, and FWHM of Co 2p_{3/2} and Ti 2p are also given in **Table 5.8**. The deconvoluted XPS spectra for the Co 2p_{3/2} core level region of cobalt catalysts on TiO₂ crystallite size 11, 13, and 16 nm are shown in **Figure 5.19-Figure 5.21**.

Table 5.8 Binding energy and surface composition of Zr modified and unmodified Co catalysts

Sample	Co(II) 2p _{3/2}		Ti 2p		Atomic Conc%		
	B.E. (eV)	FWHM	B.E. (eV)	FWHM	Co	Ti	O
Co/TiO ₂ _11 nm_Zr	781.0	2.908	459.3	1.444	1.98	2.61	47.55
Co/TiO ₂ _13 nm_Zr	780.2	3.019	458.9	1.133	0.53	3.42	39.29
Co/TiO ₂ _16 nm_Zr	781.0	2.957	458.8	1.559	4.29	0.85	35.10
Co/TiO ₂ _11 nm	781.5	7.453	459.1	1.688	0.65	3.45	33.37
Co/TiO ₂ _13 nm	780.2	3.078	459.1	1.498	1.25	6.59	41.60
Co/TiO ₂ _16 nm	780.0	2.369	458.9	1.129	1.62	0.36	28.13

ศูนย์วิทยทรัพยากร
จุฬาลงกรณ์มหาวิทยาลัย

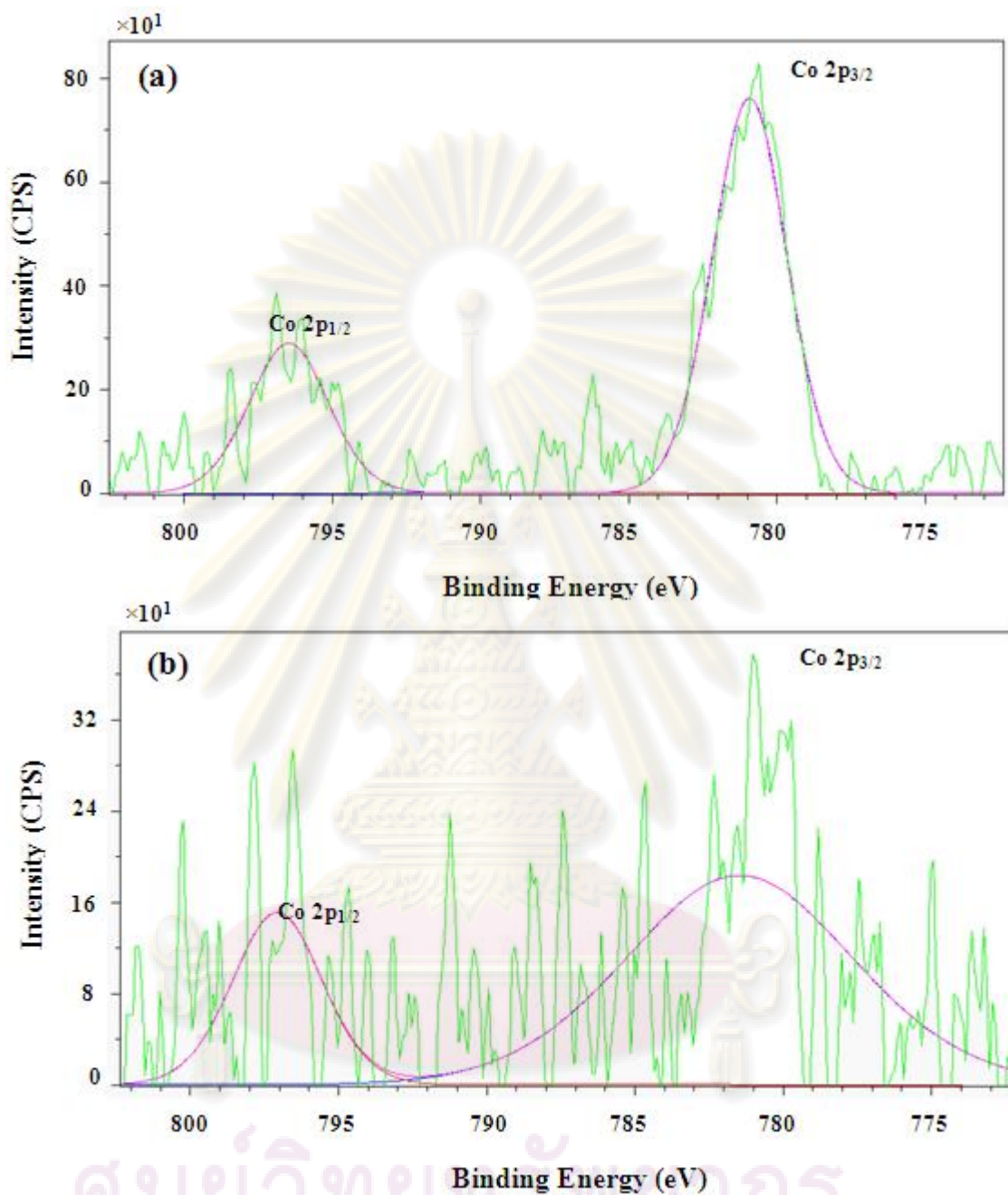


Figure 5.19 The deconvolution of XPS spectra of Zr modified and unmodified supported cobalt catalyst (a) Co/TiO₂_11 nm_Zr (b) Co/TiO₂_11 nm

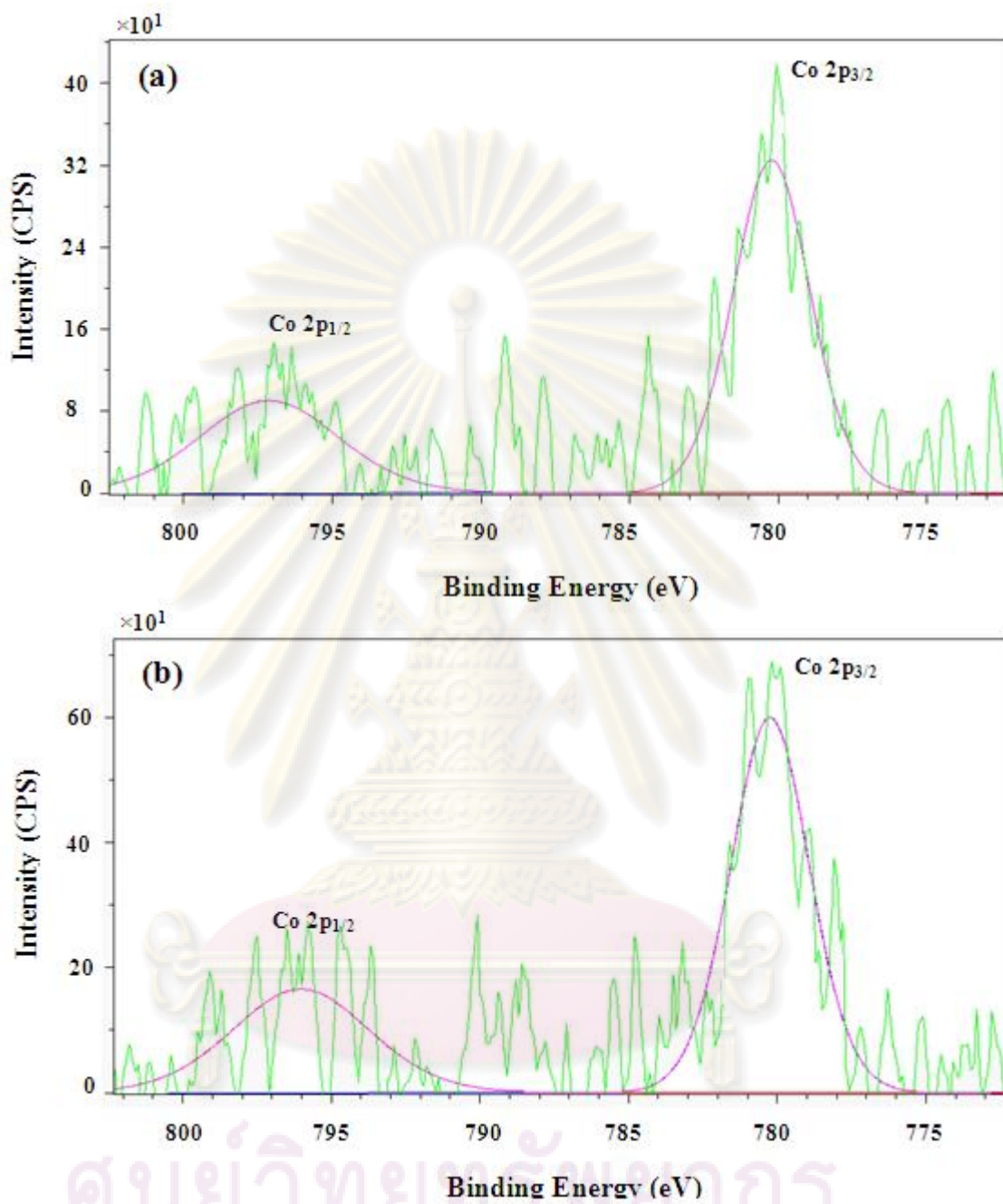


Figure 5.20 The deconvolution of XPS spectra of Zr modified and unmodified supported cobalt catalyst (a) Co/TiO₂_13 nm_Zr (b) Co/TiO₂_13 nm

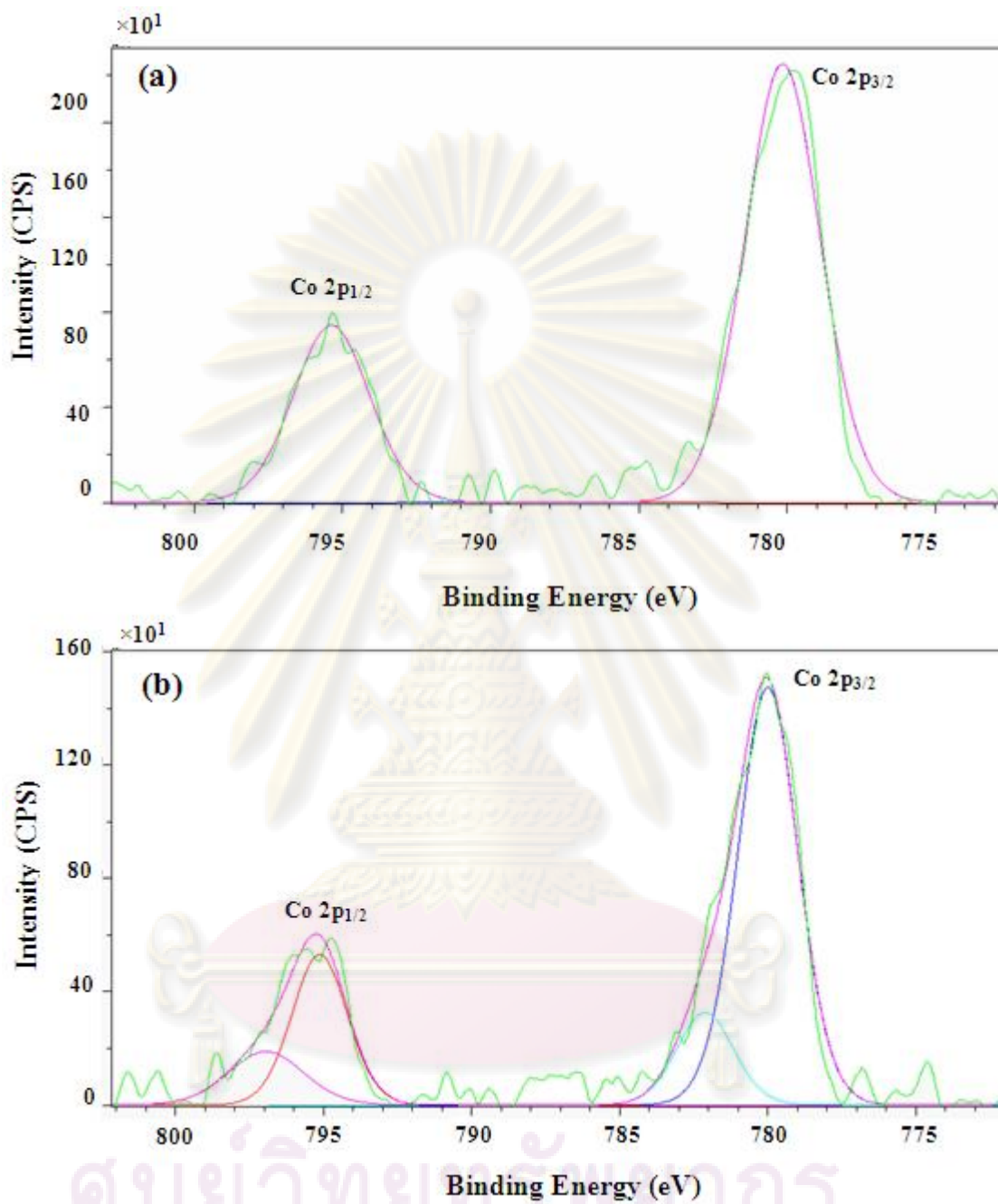


Figure 5.21 The deconvolution of XPS spectra of Zr modified and unmodified supported cobalt catalyst (a) Co/TiO₂_16 nm_Zr (b) Co/TiO₂_16 nm

5.2.2 Reaction study

The conversion, reaction rate, TOF (based on the number of reduced surface cobalt atoms measured from CO chemisorption), and product selectivity during CO hydrogenation at steady-state are given in **Table 5.9**. The conversion of the Co catalysts on unmodified-TiO₂ obviously changed when using of different size of TiO₂. The rate vs. time on stream of the modified and unmodified-TiO₂ Co catalysts is illustrated in **Figure 5.18**. The rate of these catalysts decreased with larger size of TiO₂, and slightly decreased in C₁ selectivity. Similarly, the cobalt catalyst on the Zr modified support exhibited the higher activity and C₁ selectivity than that on the unmodified support in all crystallite sizes of TiO₂ with slightly change in product selectivity. For the Co catalyst on Zr modified-TiO₂, it can be observed that the size of TiO₂ hardly effected to product selectivity of C₁, but there was moderate change in conversion at steady state. The rate of the modified catalysts decreased with increasing of crystallite size of TiO₂ except for TiO₂ size 13 and 16 nm, but there was in the similar value. It can be say that the similar trend regarding the activity and product selectivity can be observed in both Zr modified and unmodified support. The increased activity for Zr modified supported cobalt catalysts can be attributed to the dispersion of Co metal on the catalysts as seen from CO chemisorption results. When considered the difference in rate between the modified and unmodified catalysts of support TiO₂_11 nm, 13 nm, and 16 nm, it found that the larger crystallite size of TiO₂ show the most difference in rate of the reaction. The results indicated that Zr modification on support TiO₂ have an effect on the larger crystallite size of TiO₂ more than the smaller ones. Since CO hydrogenation is a structure insensitive reaction, therefore the catalytic activity depends only on the number of reduced Co metal surface atoms available for catalyzing the reaction [42]. The specific activities (TOFs) of the samples are summarized in Table 4. They are in the range of $1 \times 10^{-2} \text{ s}^{-1}$ -typical of Co catalyst under this condition [3, 5, 42]. Considered TOFs calculated based on CO chemisorption of the catalysts, there found that TOFs of Co catalysts on Zr modified TiO₂ were found to be similar among sample catalysts [except for the Co/TiO₂_16 nm_Zr]. The size of TiO₂ also plays an important role on the catalytic activity of the catalysts e.g. the reaction rate decreased when using the larger particle size of TiO₂.

However, the high TOF of Co/TiO₂_16 nm_Zr sample was probably due to the less active site of the catalyst.

There are many variables that can effect the kinetic of the reaction such as particle size, support interaction, and the reduction gas composition [42]. There have been found that the particle size of support related to the strength of metal-support interaction [47]. Thus, we may conclude that the particle size of TiO₂ also affected to the size of Co oxide species.

Table 5.9 Activity and product selectivity of Zr modified and unmodified Co catalyst

Sample	Conversion ^a		Rate ^c (× 10 ⁻² g CH ₂ /g cat.h)	TOF ^d (× 10 ³ s ⁻¹)	Product selectivity ^c (%)	
	initial ^b	Steady state ^c			C ₁	C ₂ -C ₄
Co/TiO ₂ _11 nm_Zr	97.3	100.0	75	6.9	98.4	1.6
Co/TiO ₂ _13 nm_Zr	95.7	82.6	62	7.1	97.1	2.9
Co/TiO ₂ _16 nm_Zr	96.0	90.4	68	19.1	99.1	0.9
Co/TiO ₂ _11 nm	94.8	76.9	58	6.9	96.9	3.1
Co/TiO ₂ _13 nm	58.2	49.2	37	4.6	93.5	6.5
Co/TiO ₂ _16 nm	66.9	31.7	24	9.6	93.7	6.3

^a CO hydrogenation was carried out at 220 °C, 1 atm, and H₂/CO/Ar = 20/2/8, GSHV= 11400 h⁻¹.

^b After 5 min of reaction.

^c After 5 h of reaction.

^d The TOF calculation was based on CO chemisorption

ศูนย์วิทยทรัพยากร
จุฬาลงกรณ์มหาวิทยาลัย

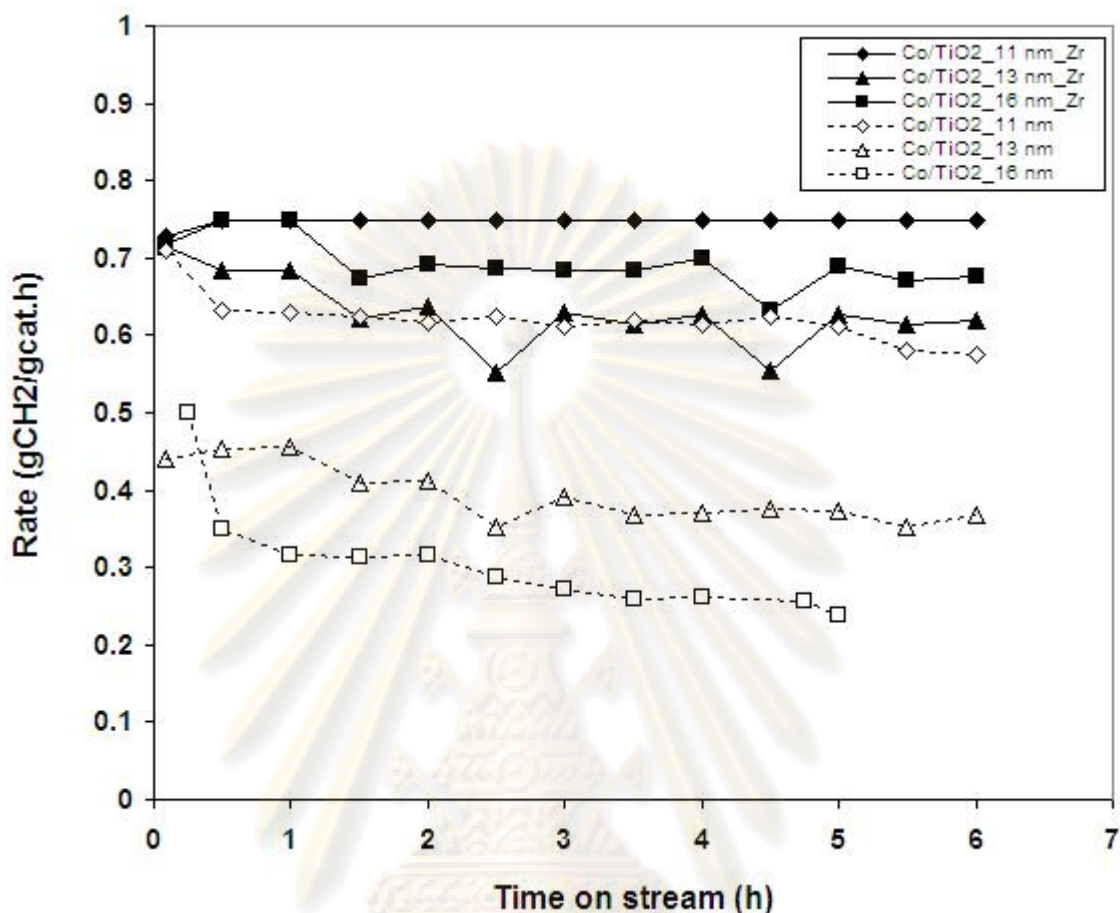


Figure 5.22 Reaction rate vs. time on stream of Zr modified and unmodified Co catalysts with different crystallite size of TiO₂

5.3 Comparison between Ru and Zr-modified TiO₂ support in catalytic activity

The Ru modification on titania support resulted in lower reduction temperature due to the effect of H₂ spillover to Co₃O₄. It has been proposed that noble metal activates H₂ and then becomes a source for H₂ spillover to cobalt oxides [3], whereas Zr, which does not assign to noble metal, caused in different effect to the reduction temperature. The Zr-modified supported catalysts resulted in higher reduction temperature. These results may be explained by the formation between Co oxides and the support. Even though the reduction temperatures were shifted higher, but the

amounts of H₂ consumed were higher than the unmodified ones. These results suggested that Zr may help the inactive cobalt oxides being more reducible.

For better comparison, the activity and product selectivity of Ru-modified, Zr-modified and unmodified cobalt catalysts are shown in **Table 5.10**. The rates at steady state of the Zr-modified supported catalysts were higher than those from the other catalysts. It is considered that Zr modification on TiO₂ supported cobalt catalyst are more active than Ru modification on supported cobalt catalyst under methanation condition.

Table 5.10 Catalytic activity and product selectivity of modified and unmodified-TiO₂ cobalt catalysts

Sample	Conversion ^a		Rate ^c (× 10 ⁻² g CH ₂ /g cat.h)	TOF ^d (× 10 ³ s ⁻¹)	Product selectivity ^c (%)	
	initial ^b	Steady state ^c			C ₁	C ₂ -C ₄
Co/TiO ₂ _11 nm_Ru	94.5	90.9	68	5.8	97.1	2.9
Co/TiO ₂ _13 nm_Ru	79.3	88.9	67	10.4	99.0	1.0
Co/TiO ₂ _16 nm_Ru	91.1	77.0	58	13.1	99.0	1.0
Co/TiO ₂ _11 nm_Zr	97.3	100.0	75	6.9	98.4	1.6
Co/TiO ₂ _13 nm_Zr	95.7	82.6	62	7.1	97.1	2.9
Co/TiO ₂ _16 nm_Zr	96.0	90.4	68	19.1	99.1	0.9
Co/TiO ₂ _11 nm	94.8	76.9	58	6.9	96.9	3.1
Co/TiO ₂ _13 nm	58.2	49.2	37	4.6	93.5	6.5
Co/TiO ₂ _16 nm	66.9	31.7	24	9.6	93.7	6.3

^a CO hydrogenation was carried out at 220 °C, 1 atm, and H₂/CO/Ar = 20/2/8, GSHV= 11400 h⁻¹.

^b After 5 min of reaction.

^c After 5 h of reaction.

^d The TOF calculation was based on CO chemisorption

CHAPTER VI

CONCLUSIONS AND RECOMMENDATIONS

6.1 Conclusions

The present work revealed the physicochemical properties of cobalt on Ru, Zr modified and unmodified-TiO₂ supported catalysts. It can be concluded as follows:

1. Ru and Zr modification of the titania support had a significant impact on the properties of Co/TiO₂ catalysts, especially on the larger crystallite size of TiO₂. It has moderately affected on the catalytic activity, whereas slightly affected on the smaller crystallite size.
2. For both modified and unmodified supports, the catalyst with the smaller crystallite size of TiO₂ (11 nm) exhibited the better catalytic activity than the larger crystallite size (16 nm).
3. Ru and Zr modification on support TiO₂ may help to improved dispersion and gives distribution. Besides Zr modification on support TiO₂ may cause the interaction between cobalt oxide species and the support.
4. For unmodified support, the catalysts with larger crystallite size of TiO₂ exhibited higher C₂-C₄ selectivity than the smaller crystallite size. For modified support, the selectivity of the catalysts was lower for all different crystallite size of TiO₂.

6.2 Recommendations

1. Additional water:alkoxide molar ratio which related to crystallite sizes of TiO_2 synthesized by sol-gel method should be prepared in order to confirm the effect of TiO_2 crystallite size on the properties of Co/TiO_2 catalysts.
2. In order to investigate the effect of Ru or Zr modification on TiO_2 support, the modifier should be loaded in the similar amount for better comparison.
3. Introduce EXAFS (Extended X-ray Absorption Fine Structure) technique to investigate the cobalt coordination number.



ศูนย์วิจัยทรัพยากร
จุฬาลงกรณ์มหาวิทยาลัย

REFERENCES

- [1] Khodakov, A. Y., Chu, W., and Fongarland, P. Advances in the Development of Novel Cobalt Fischer-Tropsch Catalysts for Synthesis of Long-Chain Hydrocarbons and Clean Fuels. Chem. Rev. 107 (2007): 1692-1744.
- [2] Okabe, K., Li, X., Wei, M., and Arakawa, H. Fischer-Tropsch synthesis over Co-SiO₂ catalysts prepared by the sol-gel method. Catal. Today 89 (2004): 431-438.
- [3] Kogelbauer, A., Goodwin Jr., J. G., and Oukaci, R. Ruthenium Promotion of Co/Al₂O₃ Fischer-Tropsch Catalysts. J. Catal. 160 (1996): 125-133.
- [4] Tauster, S. J., Fung, S. C., and Garten, R. L. Strong Metal-Support Interactions. Group 8 Noble Metals Supported on TiO₂. J. Am. Chem. Soc. 100 (1978): 170-175.
- [5] Jongsomjit, B., and Goodwin Jr., J. G. Co-support compound formation in Co/Al₂O₃ catalysts: effect of reduction gas containing CO. Catal. Today 77 (2002): 191-204.
- [6] Jongsomjit, B., Panpranot, J., and Goodwin Jr., J. G. Co-Support Compound Formation in Alumina-Supported Cobalt Catalysts. J. Catal. 204 (2001): 98-109.
- [7] Soled, S. L., Iglesia, E., Fiato, R. A., Baumgartner, J. E., Vromana, H., and Miseoa, S. Control of metal dispersion and structure by changes in the solid-state chemistry of supported cobalt Fischer-Tropsch catalysts. Topics Catal. 26 (2003): 101-109.
- [8] Tsubaki, N., Sun, S., and Fujimoto, K. Different Functions of the Noble Metals Added to Cobalt Catalysts for Fischer-Tropsch Synthesis. J. Catal. 199 (2001): 236-246.
- [9] Jacobs, G., Das, T. K., Zhang, Y., Li, J., Racoillet, G., and Davis, B. H. Fischer-Tropsch synthesis: support, loading, and promoter effects on the reducibility of cobalt catalysts. Appl. Catal. A: General 233 (2002): 263-281.

- [10] Iglesia, E., Soled, S. L., Fiato, R. A., and Via, G. H. Bimetallic Synergy in Cobalt Ruthenium Fischer-Tropsch Synthesis Catalysts. J. Catal. 143 (1993): 345-368.
- [11] Bartholomew, C. H., and Reuel, R. C. Cobalt-Support Interactions: Their Effects on Adsorption and CO Hydrogenation Activity and Selectivity Properties. Ind. Eng. Chem. Prod. Res. Dev. 24 (1985): 56-61.
- [12] Jacobs, G., Das, T. K., Zhang Y., Li, J., Racoillet, G., and Davis, B. H. Fischer-Tropsch synthesis: support, loading, and promoter effects on the reducibility of cobalt catalysts. Appl. Catal. A: General 233 (2002): 263-281.
- [13] Jongsomjit, B., Wongsalee, T., and Prasertdam, P. Characteristics and catalytic properties of Co/TiO₂ for various rutile: anatase ratios. Catal. Comm. 6 (2005): 705-710.
- [14] Wang, C. B., Tang, C. W., Tsai, H. C., and Chien, S. H. Characterization and catalytic oxidation of carbon monoxide over supported cobalt catalysts Catal. Lett. 107 (2006): 223-230.
- [15] Nagaoka, K., Takanabe, K., and Aika, K. Influence of the phase composition of titania on catalytic behavior of Co/TiO₂ for the dry reforming of methane. CHEM. COMMUN (2002): 1006-1007.
- [16] Mohammadi, M. R., Fray, D. J., Mohammadi, A. Sol-gel nanostructured titanium dioxide: Controlling the crystal structure, crystallite size, phase transformation, packing and ordering. Microporous Mesoporous Mater. 112 (2008): 392-402.
- [17] Sirisuk, A., Klansorn, E., and Prasertdam, P. Effects of reaction medium and crystallite size on Ti³⁺ surface defects in titanium dioxide nanoparticles prepared by solvothermal method. Catal. Comm. 9 (2008): 1810-1814.
- [18] Su, C., Hong, B. Y., Tseng, C. M. Sol-gel preparation and photocatalysis of titanium dioxide. Catal. Today 96 (2004): 119-126.
- [19] Kongsuebchart, W., Prasertdam, P., Panpranot, J., Sirisuk, A. Supphasrironngjaroen, P., and Satayaprasert, C. Effect of crystallite size on the surface defect of nano-TiO₂ prepared via solvothermal synthesis. J. Crystal Growth 297 (2006): 234-238.
- [20] Van't Blik, H. F. J., Koningsberger, D. C., Prins, R. Characterization of supported cobalt and cobalt-rhodium catalysts III. Temperature-Programmed

- Reduction (TPR), Oxidation (TPO), and EXAFS of Co---Rh/SiO₂. J. Catal. 97 (1986): 210-218.
- [21] Takeuchi, K., Matsuzaki, T., Arakawa, H., Hanaoka, T., and Sugi, Y. Synthesis of C₂-oxygenates from syngas over cobalt catalysts promoted by ruthenium and alkaline earths. Appl. Catal. 48 (1989): 149-157.
- [22] Reinikainen, M., Niemela, M.K., Kakuta, N., and Suhonen, S. Characterisation and activity evaluation of silica supported cobalt and ruthenium catalysts. Appl. Catal. A: general 174 (1998): 61-75.
- [23] Guzzi, L., Bazin, D., Kovacs, I., Boroko, L., Schay, Z., Lynch, J., Parent, P., Lafon, C., Stefler, G., Koppány, Z., and Sajo, I. Structure of Pt–Co/Al₂O₃ and Pt–Co/NaY bimetallic catalysts: characterization by in situ EXAFS, TPR, XPS and by activity in Co (carbon monoxide) hydrogenation. Top. Catal. 20 (2002): 129-139.
- [24] Jacobs, G., Chaney, J.A., Patterson, P.M., Das, T.K., Maillot, J.C., and Davis, B.H. Fischer-Tropsch synthesis: study of the promotion of Pt on the reduction property of Co/Al₂O₃ catalysts by in situ EXAFS of Co K and Pt L_{III} edges and XPS. J. Synchrotron Radiat. 11 (2004): 414-422.
- [25] Hilmen, A.M., Schanke, D., and Holmen, A. TPR study of the mechanism of rhenium promotion of alumina-supported cobalt Fischer-Tropsch catalysts. Catal. Lett. 38 (1996): 143-147.
- [26] Li, J., Jacobs, G., Yongqing, Z., Das, T., and Davis, B. H. Fischer–Tropsch synthesis: effect of small amounts of boron, ruthenium and rhenium on Co/TiO₂ catalysts. Appl. Catal. A: General 223 (2002): 195-203.
- [27] Jongsomjit, B., Sakdamnusun, C., Goodwin Jr., J.G., and Praserttham, P. Co-support compound formation in titania-supported cobalt catalyst. Catal. Lett. 94 (2004): 209-215.
- [28] Kogelbauer, A., Weber, J. C., and Goodwin Jr., J. G. The formation of cobalt silicates on Co/SiO₂ under hydrothermal conditions. Catal. Lett. 34 (1995): 259-267.

- [29] Jongsomjit, B., Panpranot, J., and Goodwin Jr., J. G. Effect of zirconia-modified alumina on the properties of Co/ γ -Al₂O₃ catalysts. J. Catal. 215 (2003): 66-77.
- [30] Li, J., Zhan, X., Zhang, Y., Jacobs, G., Das, T., and Davis, B. H. Fischer–Tropsch synthesis: effect of water on the deactivation of Pt promoted Co/Al₂O₃ catalysts. Appl. Catal. A: General 228 (2002) 203-212.
- [31] Oukaci, R., Sigleton, A. H., and Goodwin Jr., J. G. Comparison of patented Co F–T catalysts using fixed-bed and slurry bubble column reactors. Appl. Catal. A: General 186 (1999): 129-144.
- [32] Feller, A., Claeys, M., and Steen, E. V. Cobalt Cluster Effects in Zirconium Promoted Co/SiO₂ Fischer–Tropsch Catalysts. J. Catal. 185 (1999): 120-130.
- [33] Wongsalee, T., Jongsomjit, B., and Praserthdam, P. Effect of zirconia-modified titania consisting of different phases on characteristics and catalytic properties of Co/TiO₂ catalysts. Catal. Lett. 108 (2006): 55-61.
- [34] Fujishima, A., Hashimoto, K., and Watanabe, T. Tokyo: Bkc. (1999).
- [35] Carp, O., Huisman, C. L., and Reller, A. Photoinduced reactivity of titanium dioxide. Prog. Solid State Chem. 32 (2004): 33-177.
- [36] Young, R.S. COBALT: Its Chemistry, Metallurgy, and Uses. New York: Reinhold Publishing Corporation, 1960.
- [37] Othmer, K. Encyclopedia of chemical technology. Vol 6. 4th ed. New York: A Wiley Interscience Publication, John Wiley&Son, 1991.
- [38] Kraum, M., and Bearns, M. Fischer–Tropsch synthesis: the influence of various cobalt compounds applied in the preparation of supported cobalt catalysts on their performance. Appl. Catal. A: General 186 (1999): 189-200.
- [39] Wang, C., Ying, J. Y. Sol-Gel Synthesis and Hydrothermal Processing of Anatase and Rutile Titania Nanocrystals. Chem. Mater. 11 (1999): 3113-3120.
- [40] Suriye, K., Praserthdam, P., and Jongsomjit, B. Control of Ti³⁺ surface defect on TiO₂ nanocrystal using various calcination atmospheres as the first step for surface defect creation and its application in photocatalysis. Appl. Surf. Sci. 253 (2007): 3849-3855.

- [41] Suriye, K., Prasertthdam, P., and Jongsomjit, B. Impact of Ti^{3+} Present in Titania on Characteristics and Catalytic Properties of the Co/TiO₂ Catalyst. Ind. Eng. Chem. Res. 44 (2005): 6599-6604.
- [42] Kittiruangrayab, S., Burakorn, T., Jongsomjit, B., and Prasertthdam, P. Characterization of Cobalt Dispersed on Various Micro- and Nanoscale Silica and Zirconia Supports. Catal. Lett. 124 (2008): 376-383.
- [43] Hosseini, S.A., Taeb, A., Feyzi, F., and Yaripour, F. Fischer–Tropsch synthesis over Ru promoted Co/ γ -Al₂O₃ catalysts in a CSTR. Catal. Commun. 5 (2004): 137-143.
- [44] Infantes-Molina, A., Rida-Robles, J.M., Guez-Castello, E.R., Fierro, J. L. G., and Nez-Lopez, A.J. Synthesis, characterization and catalytic activity of ruthenium-doped cobalt catalysts. Appl. Catal. A: General 341 (2008): 35-42.
- [45] Mazzieri, V., Coloma-Pascual, F., Arcoya, A., L'Argentie`re, P. C., Fí`goli, N. S. XPS, FTIR and TPR characterization of Ru/Al₂O₃ catalysts. Appl. Surf. Sci. 210 (2003): 222-230.
- [46] Burakorn, T., Panpranot, J., Mekasuwandumrong, O., Chaisuk, C., Prasertthdam, P., and Jongsomjit, B. Characterization of cobalt dispersed on the mixed nanoscale alumina and zirconia supports. J. Mater. Process. Technol. 206 (2008): 352-358.
- [47] Kongsuebchart, W., Panpranot, J., Satayaprasert, C., and Prasertthdam, P. Effect of TiO₂ crystallite size on the dispersion of Co on nanocrystalline TiO₂. React. Kinet. Catal. Lett. 91 (2007): 119-126.
- [48] Badrinarayanan, S., and Sinha, S. An XPS study of the nitrogen-implanted Zr₇₆Fe₂₄ metglass. J. Phys.: Condens. Matter 2 (1990): 8721-8724.



APPENDICES

ศูนย์วิทยทรัพยากร
จุฬาลงกรณ์มหาวิทยาลัย

APPENDIX A

CALCULATION FOR CATALYST PREPARATION

Preparation of TiO₂ nanocrystal via sol-gel (base precipitation) method and 20%Co/TiO₂ with Ru or Zr modification are shown as follows:

- Reagent:
- Titanium ethoxide, Molecular weight = 284.22
 - Cobalt (II) nitrate hexahydrate (Co(NO₃)₂·6H₂O) 98+%
 - Ruthenium (III) nitrosyl nitrate , solution in dilute nitric acid, 1.5% (Ru(NO)(NO₃)₃)
 - Zirconium (IV) *n*-propoxide 70wt% solution in 1-propanol (Zr(OC₃H₇)₄)

Calculation for the preparation of TiO₂ via sol-gel (base precipitation) method

The preparation by using water:alkoxide molar ratio = X
 = 10 g
 = 10/284.22 mole
 The amount of water used = 10/284.22×18(X)
 The volume of water used = 10/284.22×18(X)
 The volume of ethanol used in the first solution with ethanol= 50 ml
 The volume of ethanol used in the second solution with titanium ethoxide = 50 ml

Calculation for the preparation of cobalt loading catalyst (20%Co/TiO₂)

Example calculation for the preparation of 20%Co/TiO₂

Based on 100 g of catalyst used, the composition of the catalyst will be as follows:

Cobalt = 20 g
 TiO₂ = 100-20 = 80 g

For 5 g of TiO₂

$$\text{Cobalt required} = 5 \times (20/80) = 1.25 \text{ g}$$

Cobalt 1.25 g was prepared from $\text{Co}(\text{NO}_3)_2 \cdot 6\text{H}_2\text{O}$ and molecular weight of Co is 58.93

$$\begin{aligned} \text{Co}(\text{NO}_3)_2 \cdot 6\text{H}_2\text{O} \text{ required} &= \frac{\text{MW of } \text{Co}(\text{NO}_3)_2 \cdot 6\text{H}_2\text{O} \times \text{cobalt required}}{\text{MW of Co}} \\ &= (291.03/58.93) \times 1.25 = 6.17 \text{ g} \end{aligned}$$

Calculation for the preparation of the 0.2% Ru-modified TiO₂ support

Based on 100 g of catalysts used, the composition of the catalyst will be as follow:

$$\begin{aligned} \text{Cobalt} &= 20 \text{ g} \\ \text{Ruthenium} &= 0.2 \text{ g} \\ \text{Titania} &= 100 - (20 + 0.2) = 79.8 \text{ g} \end{aligned}$$

For 5 g of titania

$$\begin{aligned} \text{Cobalt required} &= 5 \times (20/79.8) = 1.25 \text{ g} \\ \text{Ruthenium required} &= 5 \times (0.2/79.8) = 0.0125 \text{ g} \end{aligned}$$

Ruthenium 0.0125 g was prepared from $(\text{Ru}(\text{NO})(\text{NO}_3)_3)$ solution in dilute nitric acid 1.5 wt%

$$\begin{aligned} \text{Ru}(\text{NO})(\text{NO}_3)_3 \text{ required} &= \text{ruthenium required} \times \text{fraction of Ru in nitric sol}^n \\ &= 0.0125 \times (100/1.5) = 0.833 \text{ g} \end{aligned}$$

$$\begin{aligned} \text{Co}(\text{NO}_3)_2 \cdot 6\text{H}_2\text{O} \text{ required} &= \frac{\text{MW of } \text{Co}(\text{NO}_3)_2 \cdot 6\text{H}_2\text{O} \times \text{cobalt required}}{\text{MW of Co}} \\ &= (291.03/58.93) \times 1.25 = 6.17 \text{ g} \end{aligned}$$

Calculation for the preparation of the 0.2% Zr-modified TiO₂ support

Based on 100 g of catalysts used, the composition of the catalyst will be as follow:

$$\begin{aligned} \text{Cobalt} &= 20 \text{ g} \\ \text{Zirconium} &= 0.2 \text{ g} \\ \text{Titania} &= 100 - (20 + 0.2) = 79.8 \text{ g} \end{aligned}$$

For 5 g of titania

$$\begin{aligned} \text{Cobalt required} &= 5 \times (20/79.8) = 1.25 \text{ g} \\ \text{Zirconium required} &= 5 \times (0.2/79.8) = 0.0125 \text{ g} \end{aligned}$$

Ruthenium 0.0125 g was prepared from Zr(OC₃H₇)₄ 70wt% solution in 1-propanol and molecular weight of Zr is 91.224

$$\begin{aligned} \text{Zr(OC}_3\text{H}_7)_4 \text{ required} &= \frac{\text{MW of Zr(OC}_3\text{H}_7)_4 \times \text{zirconium required}}{\text{MW of Zr}} \\ &= (327.88/91.224) \times 0.0125 = 0.045 \text{ g} \end{aligned}$$

Zr(OC₃H₇)₄ 0.045 g was prepared from Zr(OC₃H₇)₄ 70 wt% solution in 1-propanol

As a consequence, Zr(OC₃H₇)₄ 70 wt% solution in 1-propanol required

$$\begin{aligned} &= \frac{\text{percent of solution} \times \text{Zr(OC}_3\text{H}_7)_4 \text{ required}}{\text{percent of Zr(OC}_3\text{H}_7)_4 \text{ in solution}} \\ &= (100/70) \times 0.045 = 0.064 \text{ g} \end{aligned}$$

$$\begin{aligned} \text{Co(NO}_3)_2 \cdot 6\text{H}_2\text{O required} &= \frac{\text{MW of Co(NO}_3)_2 \cdot 6\text{H}_2\text{O} \times \text{cobalt required}}{\text{MW of Co}} \\ &= (291.03/58.93) \times 1.25 = 6.17 \text{ g} \end{aligned}$$

APPENDIX B

CALCULATION FOR TOTAL CO CHEMISSORPTION AND DISPERSION

Calculation of the total CO chemisorption and metal dispersion of the catalyst, a stoichiometry of CO/Co = 1, measured by CO chemisorption is as follows:

Let the weight of catalyst used	=	W	g
Integral area of CO peak after adsorption	=	A	unit
Integral area of 86 μ l of standard CO peak	=	B	unit
Amounts of CO adsorbed on catalyst	=	B-A	unit
Concentration of Co	=	C	% wt
Volume of H ₂ adsorbed on catalyst	=	$86 \times [(B - A) / B]$	μ l
Volume of 1 mole of CO at 100°C	=	24.86	μ l
Mole of CO adsorbed on catalyst	=	$[(B - A) / B] \times [86 / 24.86]$	μ mole
Molecule of CO adsorbed on catalysts	=	$[(B - A) / B] \times [86 / 24.86] \times [6.02 \times 10^{23}]$	μ mole
Total CO chemisorption (Metal active site)	=	$[(B - A) / B] \times [2.08 \times 10^{24}] \times [1 / W]$	μ mole/g cat
Molecular weight of cobalt	=	58.93	
Metal dispersion (%)	=	$\frac{1 \times CO_{tot} / g \text{ of catalyst} \times 100}{No \mu mole Co_{tot} / g \text{ of catalyst}}$	
	=	$\frac{1 \times N \times 100}{No \mu mole Co_{tot}}$	
	=	$\frac{1 \times N \times 58.93 \times 100 \times 100}{C \times 10^6}$	
	=	$\frac{0.59 \times N}{C}$	

Note: N = $[(B - A) / B] \times [86 / 24.86] \times [1 / W]$ μ mole/g cat

APPENDIX C

CALIBRATION CURVES

This appendix showed the calibration curves for calculation of composition of reactant and products in CO hydrogenation reaction. The reactant is CO and the main product is methane. The other products are linear hydrocarbons of heavier molecular weight that are C₂-C₄ such as ethane, ethylene, propane, propylene and butane.

The thermal conductivity detector, gas chromatography Shimadzu model 8A was used to analyze the concentration of CO by using Molecular sieve 5A column.

The VZ10 column are used with a gas chromatography equipped with a flame ionization detector, Shimadzu model 14B, to analyze the concentration of products including of methane, ethane, ethylene, propane, propylene and butane. Conditions uses in both GC are illustrated in Table C.1.

Mole of reagent in y-axis and area reported by gas chromatography in x-axis are exhibited in the curves. The calibration curves of CO, methane, ethane, ethylene, propane, propylene and butane are illustrated in the following figures.

Table C.1 Conditions use in Shimadzu modal GC-8A and GC-14B.

Parameters	Condition	
	Shimadzu GC-8A	Shimadzu GC-14B
Width	5	5
Slope	50	50
Drift	0	0
Min. area	10	10
T.DBL	0	0
Stop time	8	20
Atten	2	2
Speed	10	3
Method	1	1
Format	1	1
SPL.WT	100	100
IS.WT	1	1

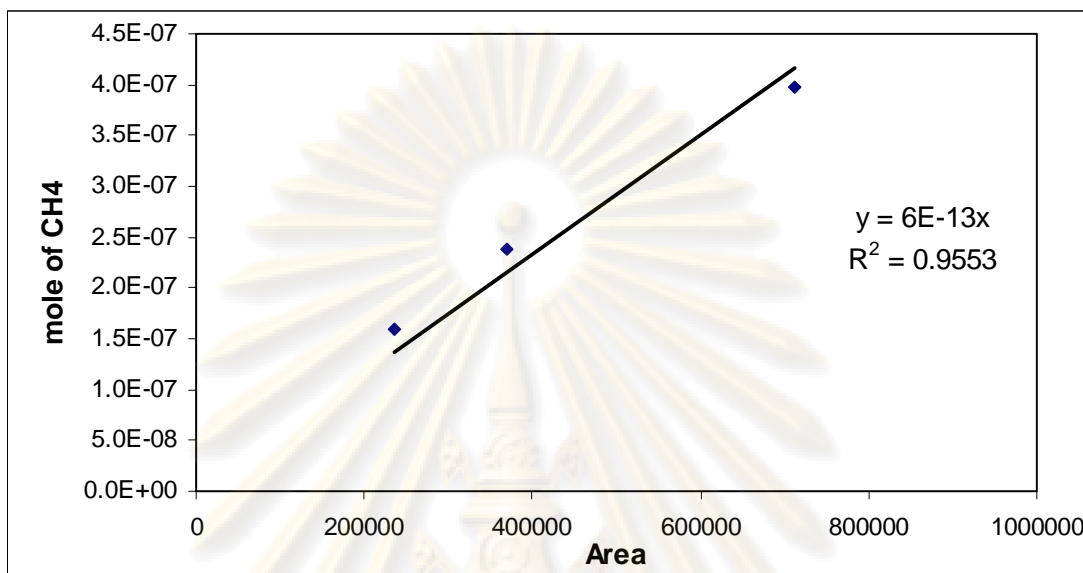


Figure C.1 The calibration curve of methane

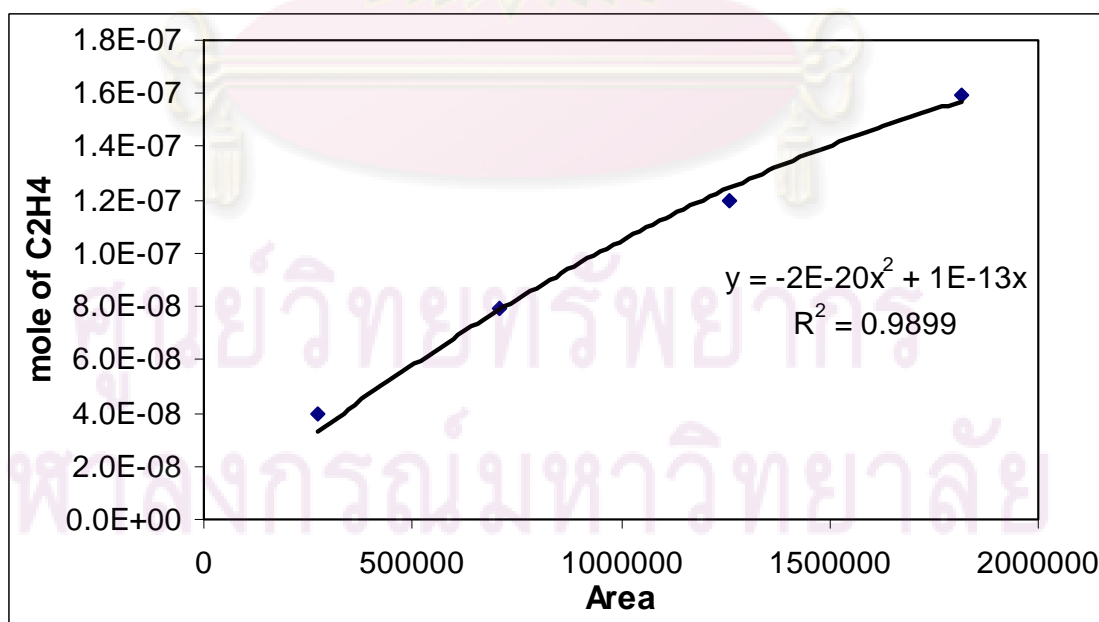


Figure C.2 The calibration curve of ethylene

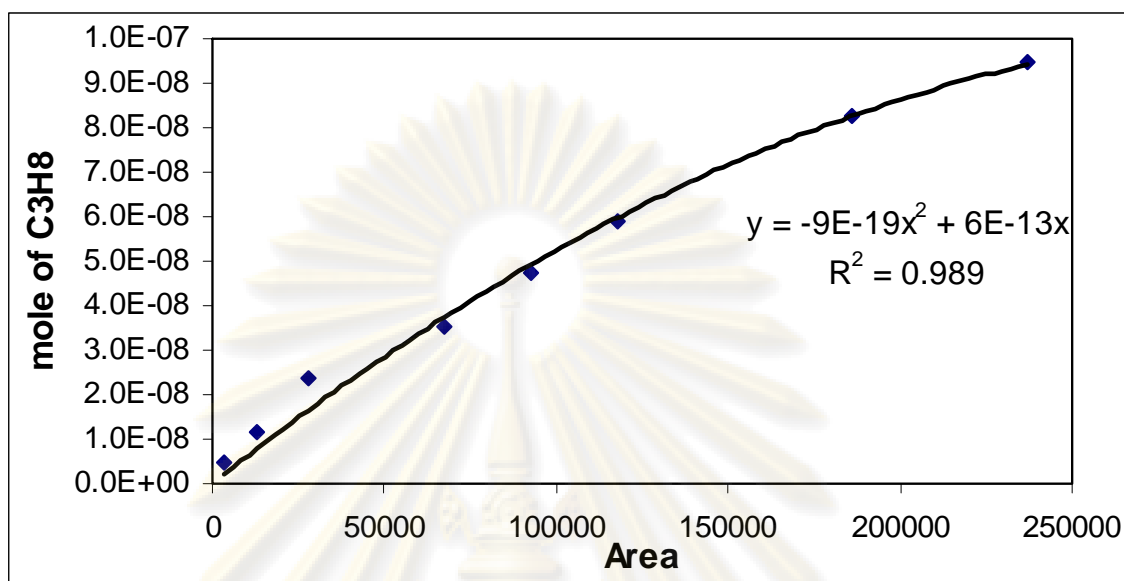


Figure C.3 The calibration curve of propane

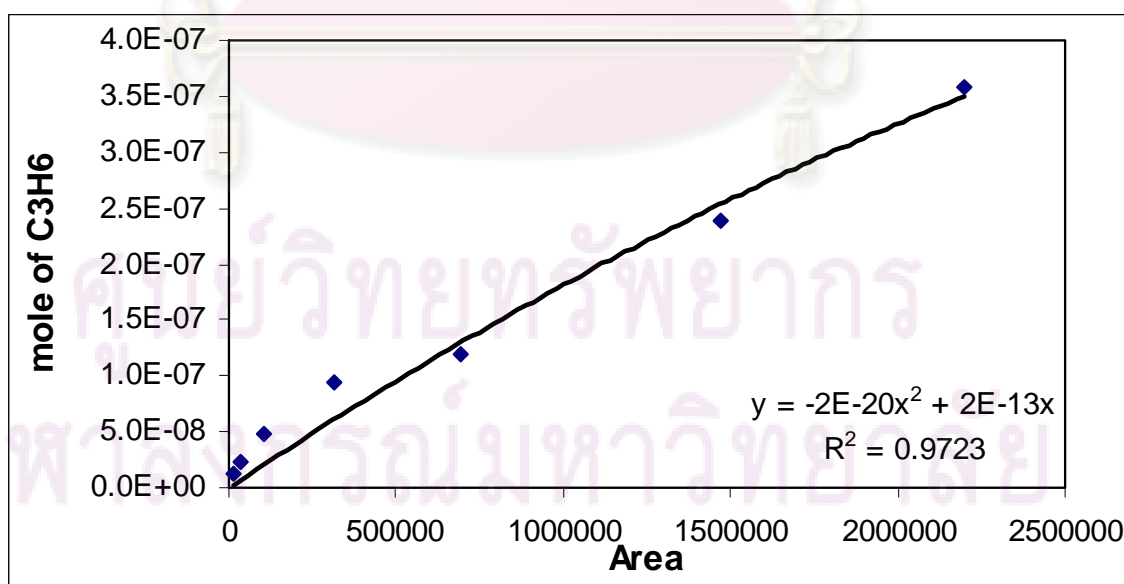


Figure C.4 The calibration curve of propene

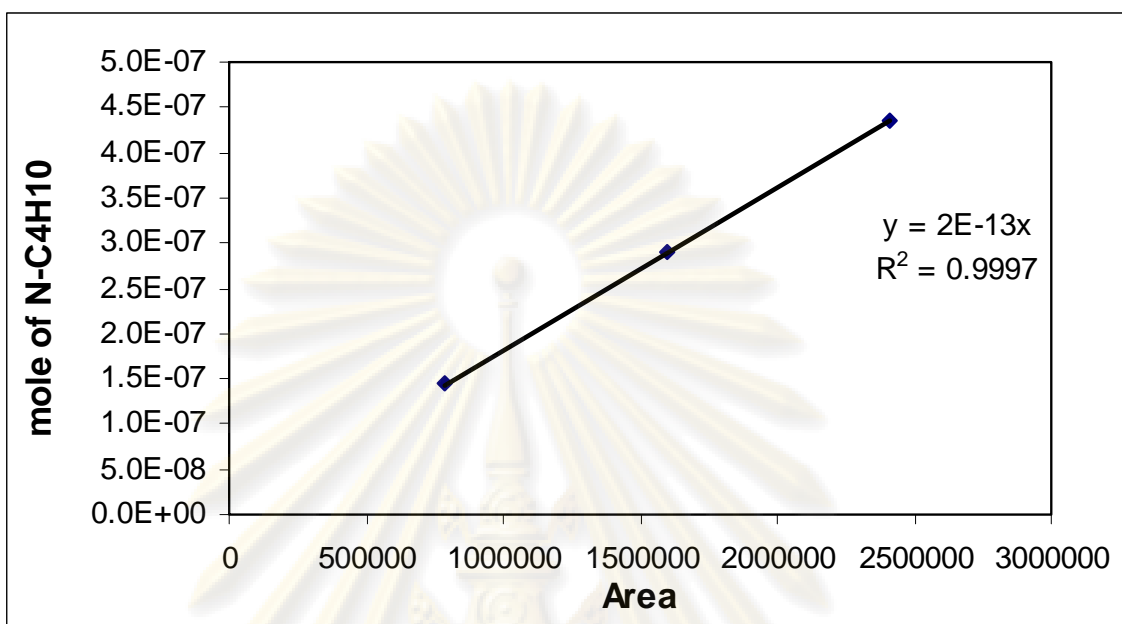


Figure C.5 The calibration curve of butane

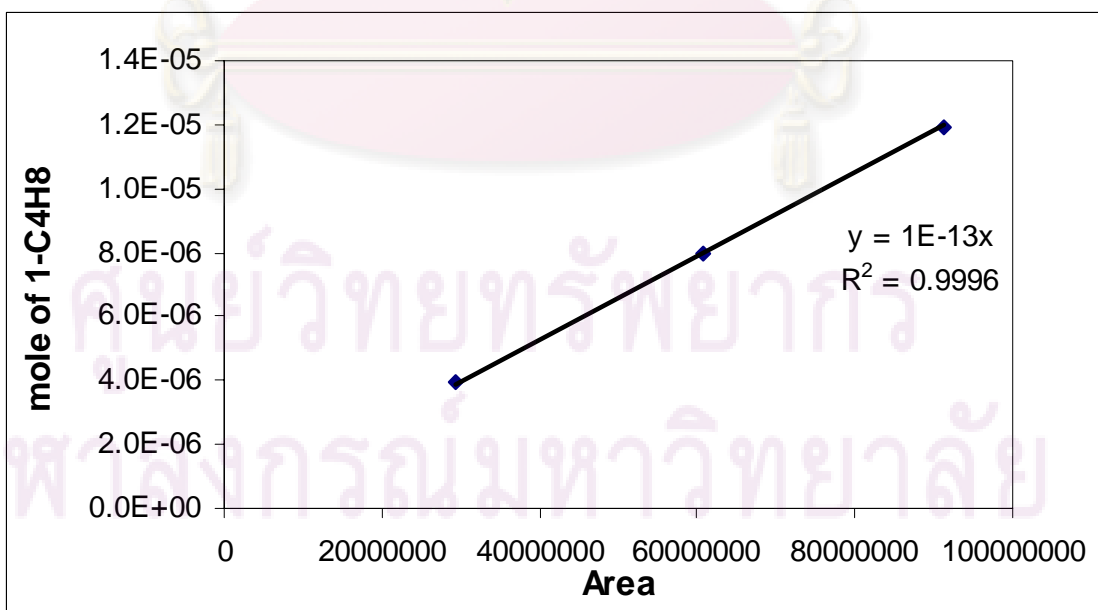


Figure C.6 The calibration curve of butene

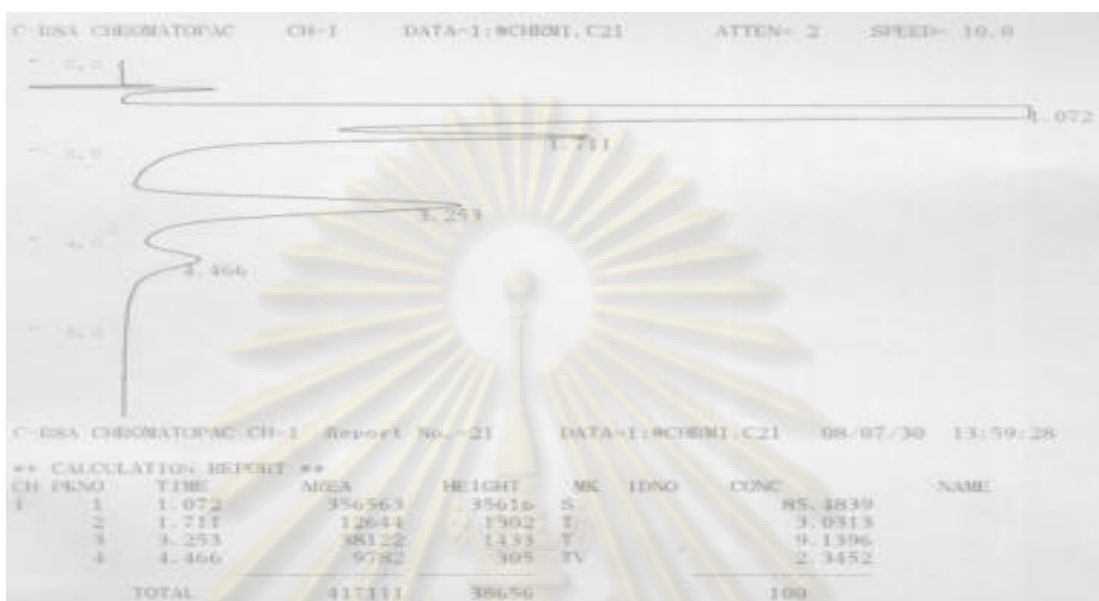


Figure C.7 The chromatograms of catalyst sample from thermal conductivity detector, gas chromatography Shimadzu model 8A (Molecular sieve 5A column)



Figure C.8 The chromatograms of catalyst sample from flame ionization detector, gas chromatography Shimadzu model 14B (VZ10 column)

APPENDIX D

CALCULATION OF CO CONVERSION, REACTION RATE AND SELECTIVITY

The catalyst performance for the CO hydrogenation was evaluated in terms of activity for CO conversion rate and selectivity.

Activity of the catalyst performed in term of carbon monoxide conversion and reaction rate. Carbon monoxide conversion is defined as moles of CO converted with respect to CO in feed:

$$\text{CO conversion (\%)} = \frac{100 \times [\text{mole of CO in feed} - \text{mole of CO in product}]}{\text{mole of CO in feed}} \quad (\text{i})$$

Reaction rate was calculated from CO conversion that is as follows:

Let the weight of catalyst used	=	W	g
Flow rate of CO	=	2	cc/min
Reaction time	=	60	min
Weight of CH ₂	=	14	g
Volume of 1 mole of gas at 1 atm	=	22400	cc

$$\text{Reaction rate (g CH}_2\text{/g of catalyst)} = \frac{[\% \text{ conversion of CO} / 100] \times 60 \times 14 \times 2}{W \times 22400} \quad (\text{ii})$$

Selectivity of product is defined as mole of product (B) formed with respect to mole of CO converted:

$$\text{Selectivity of B (\%)} = 100 \times [\text{mole of B formed} / \text{mole of total products}] \quad (\text{iii})$$

Where B is product, mole of B can be measured employing the calibration curve of products such as methane, ethane, ethylene, propane, propylene and butane

$$\text{mole of CH}_4 = (\text{area of CH}_4 \text{ peak from integrator plot on GC} - 14B) \times 8 \times 10^{12} \quad (\text{iv})$$

APPENDIX E

CALCULATION OF TURNOVER OF FREQUENCY

$$\text{Metal active site} = y \quad \text{molecule/g catalysts}$$

$$\text{TOF} = \frac{\text{rate}}{(\text{number of active site})}$$

$$= \frac{[\text{molecule substrate converted}]}{[\text{g cat.}][\text{min}]} \bigg| \frac{[\text{g cat.}]}{y [\text{active site}]} \bigg| \frac{[\text{min}]}{[\text{s}]}$$

$$= [\text{s}^{-1}]$$

ศูนย์วิทยทรัพยากร
จุฬาลงกรณ์มหาวิทยาลัย

APPENDIX F

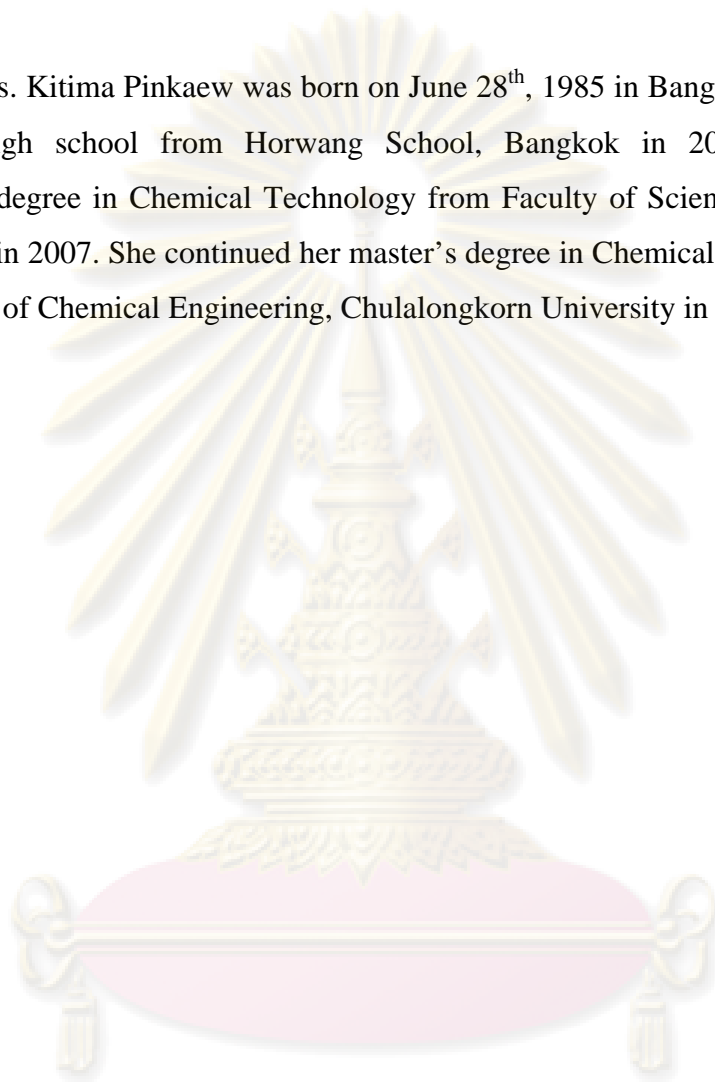
LIST OF PUBLICATIONS

1. Kitima Pinkaew, Bunjerd Jongsonjit, “Carbonmonoxide hydrogenation over Co/TiO₂-Ru catalysts”, Proceedings of the 18th Thailand Chemical Engineering and Applied Chemical Conference, Pattaya, Thailand, Oct. 20-21, 2008.
2. Kitima Pinkaew, Bunjerd Jongsonjit, “Ruthenium modification on nanocrystalline TiO₂-supported cobalt catalysts on methanation”, will be submits to Catalysis Communications, 2009
3. Kitima Pinkaew, Bunjerd Jongsonjit, “Zirconium modification on nanocrystalline TiO₂-supported cobalt catalysts on methanation”, will be submits to Catalysis Communications, 2009

ศูนย์วิทยทรัพยากร
จุฬาลงกรณ์มหาวิทยาลัย

VITA

Miss. Kitima Pinkaew was born on June 28th, 1985 in Bangkok, Thailand. She finished high school from Horwang School, Bangkok in 2003, and received bachelor's degree in Chemical Technology from Faculty of Science, Chulalongkorn University in 2007. She continued her master's degree in Chemical Engineering at the department of Chemical Engineering, Chulalongkorn University in 2008.



ศูนย์วิทยทรัพยากร
จุฬาลงกรณ์มหาวิทยาลัย